AN ABSTRACT OF THE THESIS OF

Deborah Lynn Goard for the degree of Master of Science in Forest Engineering presented on November 24, 2003.
Title: Characterizing the Spatial Distribution of Short Duration, High Intensity Rainfall in the Central Oregon Coast Range.

Abstract approved

Arne E. Skaugset III

Shallow, translational landslides occur naturally and are the dominant form of erosion in the Pacific Northwest and the Oregon Coast Range. These landslides are triggered during large, infrequent storms. Forest management activities, such as timber harvesting, can exacerbate the occurrence of these landslides. Understanding the relationship between the occurrence of shallow, translational landslides and the temporal and spatial variability of short duration, high intensity rainfall is an important step to understanding how to manage landslide-prone forested terrain. Rainfall intensity data collected during the last 14 years from a network of 13 tipping bucket rain gauges were analyzed to characterize the rainfall regime of the central Oregon Coast Range. Partial duration analysis was carried out to determine the 2-, 5-, 10-, 25-, 50-, and 100-year return period antecedent precipitation index (API) and rainfall intensities for the 30-minute, 1-, 2-, 6-, 12-, and 24-hour rainfall durations. The Spearman Rank Correlation method was used to determine if patterns existed in the relative

rank of rainfall intensities across the study area. Isohyetal maps of rainfall intensity for each unique combination of rainfall duration and return period were also developed. Analysis of the rainfall intensity data showed that rainfall intensity was highly variable across the study area, although the variability across the study area was fairly constant. The coefficient of variation in average rainfall intensity across the study area was approximately 20 percent. The Spearman Rank Correlation method showed that patterns in rainfall occurred across the study area and that these patterns were consistent for all rainfall durations and return periods. In other words, the rain gauge locations that got the most rainfall were the wettest regardless of rainfall duration or return period and the same is true for the rain gauge locations that received the least amount of rainfall. Examination of the isohyetal maps showed that all of the variability in rainfall intensity occurred within the minimum distances between rain gauge locations, which is 10 to 15 km. Analysis of the API data showed similar trends.

Characterizing the Spatial Distribution of Short Duration, High Intensity Rainfall in the Central Oregon Coast Range

by
Deborah Lynn Goard

A THESIS

submitted to

Oregon State University

In partial fulfillment of
the requirements for the
degree of

Master of Science

Presented November 24, 2003
Commencement June 2004

Master of Science thesis of Deborah Lynn Goard
Presented on November 24, 2003

APPROVED:

Major Professor, representing Forest Engineering

Head of the Department of Forest Engineering

Dean of the Graduate School

I understand that my thesis will become part of the permanent collection of Oregon State University libraries. My signature below authorizes release of my thesis to any reader upon request.

Deborah Lynn Goard, Author

TABLE OF CONTENTS

TABLE OF CONTENTS (Continued)

Page

TABLE OF CONTENTS (Continued)

Page

LIST OF FIGURES

LIST OF FIGURES (Continued)

LIST OF FIGURES (Continued)

LIST OF TABLES

LIST OF TABLES (Continued)

Table Page

LIST OF APPENDIX TABLES

LIST OF APPENDIX TABLES (Continued)

LIST OF APPENDIX FIGURES

LIST OF APPENDIX FIGURES (Continued)

LIST OF APPENDIX FIGURES (Continued)

Figure Page

LIST OF APPENDIX FIGURES (Continued)

Figure Page

Characterizing the Spatial Distribution of Short Duration, High Intensity Rainfall in the Central Oregon Coast Range

INTRODUCTION

In the Pacific Northwest, landslides occur naturally, are very common, and are the dominant form of erosion. The debris flows that result from landslides can scour stream channels and impact aquatic resources in the short and long term (Swanson et al. 1987). They can also result in damage to property, such as homes and other dwellings, and loss of human life.

Forest management can exacerbate the occurrence of landslides (Sidle et al. 1985). To understand how forest management can exacerbate the occurrence of landslides and how to mitigate this effect, forest managers must understand the processes that cause landslides to occur. Landslides usually occur during large storms (Caine 1980). In the H.J. Andrews Experimental Forest in the Cascade Mountains of Oregon debris flows in forested areas appeared to be initiated by storms with a return period of seven or more years (Swanston and Swanson 1976). However, not all large storms are landslide producing storms. Landslides appear to be triggered when localized cells of short duration, high intensity rainfall are embedded within large storms (Caine 1980).

Understanding how localized cells of high intensity rainfall correlate with the occurrence of landslides is difficult due to a lack of precipitation

intensity data available for forested, landslide prone terrain. For example, in the central Oregon Coast Range the preponderance of precipitation intensity data comes from low elevation locations along the coast or in the valleys. Data from a network of 13 tipping bucket rain gauges located in the central Oregon Coast Range were used to fill the gap in this database. The rain gauges are located on ridges and at higher elevations in the central Oregon Coast Range and rainfall data was collected for 14 years.

Traditionally, investigations of landslide occurrence across a landscape have been correlated with spatially lumped values of total precipitation and short duration precipitation intensity. For this thesis, the temporal and spatial variability of short duration precipitation intensity data from the 13 rain gauges will be investigated. This will allow insight into how precipitation intensity is distributed spatially during a large storm. Knowledge of the temporal variability of short duration, high intensity rainfall should be helpful to forest managers that use these data to design roads and drainage structures. Knowledge of the spatial variability of short duration, high intensity rainfall in landslide prone terrain will allow the development of a relationship between short duration, high intensity rainfall and the occurrence of landslides. Once this relationship is found it may be useful to forest land managers in the prediction of landslides.

OBJECTIVES

The overall goal of this project is to investigate the temporal and spatial variability of short duration, high intensity rainfall. To realize this goal, rainfall intensity data from 13 tipping bucket rain gauges located on ridges and at higher elevations in the central Oregon Coast Range will be analyzed. The study area represented by the rain gauge network is quintessentially landslide-prone terrain (Robison et al. 1999). Specific objectives are:

1. To calculate the temporal variability of short duration, high intensity rainfall in the central Oregon Coast Range.
2. To characterize and describe the spatial variability of short duration, high intensity rainfall in the central Oregon Coast Range.

LITERATURE REVIEW

Introduction

Landslides occur naturally in the Oregon Coast Range and the Pacific Northwest. There are many types of landslides that occur in the Pacific Northwest, however the type of landslide that causes the most concern are shallow, translational landslides. The initiation sites of shallow, translational landslides are, in general, small (~20 m^3); however, this type of landslide can travel considerable distances (thousands of meters) in a very short time (seconds to minutes) and landslide deposits can be very large (thousands of m^3). Further, potential initiation sites for shallow, translational landslides are ubiquitous across the landscape.

When a landslide will occur depends primarily on rainfall and parameters such as amount and intensity of precipitation and antecedent precipitation. Where a landslide will occur depends on geology, topography, slope, vegetation, and the type and intensity of forest land management. The knowledge of how natural processes and management affect the occurrence of shallow, translational landslides is important when managing landslide-prone terrain.

Characteristics of Landslides

Landslides or “mass movements” that occur in the Oregon Coast Range or the Pacific Northwest can take many forms. An abbreviated list of landslides would include soil creep, earth flows, rotational slumps, and shallow, translational landslides of a form generally called debris flows (Swanson et al. 1987).

Soil creep is a nondiscrete failure where the entire soil profile moves downslope. The soil profile moves downslope at rates of millimeters to centimeters per century. It is characterized by physical indicators such as tipped trees, hummocky terrain, and moved fence lines along roads. Soil creep occurs along with other forms of surface transport of sediment such as root throw and dry ravel (Sidle et al. 1985).

Rotational slumps and earth flows are discrete failures that move at the rate of centimeters to meters per year and are characterized by a headscarp and a nick point with a runout zone characterized by hummocky terrain and jack-strawed trees. Rotational slumps and earth flows have the potential to contribute large amounts of sediment to streams at a local scale (Sidle et al. 1985).

Rotational failures occur at a rate of hours to days. These discrete failures involve an arcuate failure surface with steep scarps on the upslope and a pile of debris downslope. There is a lack of drainage in the soil and tension cracks may develop at the top of the failure.

Shallow, translational landslides, or debris flows, are the most common form of landslide on steep, forested land (Sidle et al. 1985). Debris flows are also the most common type of landslide that occurs in the Oregon Coast Range (Robison et al. 1999). Shallow, translational landslides are wider and longer than they are deep. They can occur within seconds to minutes and although debris flows begin as a solid mass, they ultimately turn into a liquid and flow at high speeds. Debris flows can have significant impacts at sites that are far away from their initiation site (Sidle et al. 1985). These characteristics make the debris flow the landslide that elicits the most concern. Because of their ubiquity, they have the most potential to be affected by management including road construction and timber harvesting.

The occurrence of shallow, translational landslides in forested landslide prone terrain is associated with physical characteristics that include bedrock geology, slope, topography, and vegetation. Shallow, translational landslides occur on slopes greater than 50 percent (Robison et al. 1999, Gresswell et al. 1979). They also tend to occur in steep, concave “hollows” or depressions (Robison et al. 1999, Dietrich 1989). However, Robison et al. (1999) found as many debris flow initiation sites on planer slopes as on concave slopes. In the Oregon Coast Range, debris flows initiate in shallow, noncohesive soil located above bedrock or glacial till surfaces (Swanston and Swanson 1976).

Harvesting and Landslides

Timber harvesting can exacerbate the occurrence of landslides. Determining the magnitude of the actual impact of harvesting can be quite difficult. Part of the problem comes from the difficulty of locating small landslides under a forest canopy using aerial photographs (Robison et al 1999). Also, it is difficult to separate the affects of timber harvest from concurrent activities such as road construction, skid trails, and prescribed burning (Brown and Krygier 1971).

The frequency of occurrence and the size of landslides may be changed by management practices (Montgomery et al. 2000, Swanson et al. 1989, May 1999). Studies have found an increase in the occurrence of landslides associated with clearcuts ranging from two to four fold up to twenty-one fold (Johnson et al. 2000, Bishop and Stevens 1964). May (1999) studied 53 landslides that resulted in debris flow deposits in 3rd order streams in the Oregon Coast Range as a result of the February 1996 storm. Eleven of these debris flows went through areas that were clearcut, fourteen went through areas of forest and clearcut. Eight debris flows began at roads and ran through both clearcut and mixed forested and clearcut areas. The remaining debris flows went through areas of mature forests, originating at either roads associated with mature forests, or the forests themselves.

In Alaska, Johnson et al. (2000) looked at 15 randomly chosen landslides in three forest ages; clearcut, second growth, and old growth. Landslide deposits from clearcuts were composed of sediment, woody debris fragments, and stumps with rootwads. Landslides from second growth resembled either that of the clearcut areas or the old growth depending on which area it was closer to (Johnson et al. 2000). The landslides in old growth were composed of sediment, entire trees, and woody debris fragments. All landslides that began in clearcuts had more erosion per unit area than landslides that began in old growth. The landslides from the old growth were larger than the landslides from second growth and clearcut areas (Johnson et al. 2000). This data is supported by Robison et al. (1999) who reported a forty-two percent average increase in landslide density in clearcut areas in the Oregon Coast Range.

Debris flows in the Oregon Coast Range from clearcut areas traveled further and had larger deposits than debris flows from forested areas (Robison et al. 1999). All debris flows from steep clearcuts in Southeast Alaska flowed into first and second order channels (Johnson et al. 2000). Swanston (1968) found that the most frequent and damaging mass movements in Alaska occurred in recently logged as well as undisturbed areas. On Prince of Wales Island in Southeast Alaska, out of over three hundred debris flows, eighty-nine percent had decayed roots at

the initiation site, convergent topography, blowdown, and wetland vegetation that were there before any timber harvest (Johnson et al. 2000).

Landslide occurrence decreases with the time after harvest. Montgomery et al. (2000) observed that over half of the thirty-five landslides that occurred between the years of 1987 and 1996 on Mettman Ridge in the Oregon Coast Range, happened between three to five years after harvest. Robison et al. (1999) and Bishop and Stevens (1964) conclude that the first ten years after clearcutting is the time period with the highest increase in landslide occurrence. This lag time may be due to time it takes for root deterioration to occur (Bishop and Stevens 1964).

Rain and Landslides

Landslides in the Pacific Northwest are triggered during large, infrequent storms (Swanson et al. 1987). The conditions that lead to debris slides include antecedent soil moisture and the amount and intensity of rainfall and/or snowmelt (Sidle et al. 1985).

Most landslides occur during periods of high intensity rainfall (Bishop and Stevens 1964). Shallow, translational landslides are triggered during regional, wet mantle storms accompanied by bursts of high intensity rainfall (Montgomery et al. 2000). A general relationship to predict the combined minimum intensities and durations of rainfall that will trigger shallow, translational landslides was developed by Caine (1980). The

threshold line was developed by finding the lower boundary of plotted intensities and durations at which landslides occurred at seventy-three sites around the world. The general lower threshold is shown in Figure 1 and is defined by the equation

$$I = 14.82 * D^{-0.39} \qquad \text{Equation 1}$$

where

$I =$ intensity of rainfall
$D =$ duration of rainfall

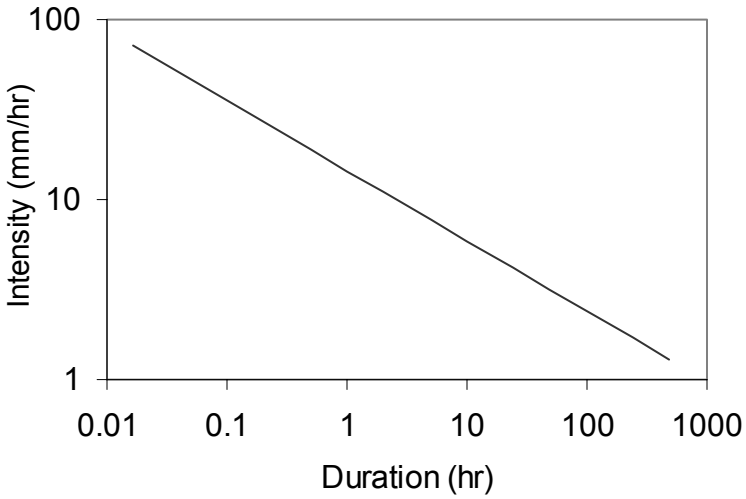

Figure 1. Caine's lower boundary threshold line for triggering shallow, translational landslides. This relationship was created from the relationship between rainfall duration (hr) and intensity values (mm/hr) found to trigger landslides around the world (Caine 1980).

This relationship is reported to be valid for rainfall durations ranging from 10 minutes to 10 days (Caine 1980).

Finding the critical rainfall is important to predict landslides and give warnings (Kobashi and Suzuki 1987). Keefer et al. (1987) put together a real-time regional landslide warning system for the San Francisco Bay Region in order to predict the occurrence of landslides during storms. Both the Cannon-Ellen threshold and the Wieczorek threshold use one formula that predicts the rainfall intensity threshold written as

$$Q_c = (I_r - I_o) * D \qquad \text{Equation 2}$$

where

$D =$ duration of rainfall
$I_r =$ rainfall intensity
$I_o =$ average drainage rate
$Q_c =$ critical volume of water

Values for the variables differ among locations. These estimates can be general for regions that are broad and highly variable. For the Cannon-Ellen and the Wieczorek thresholds the values are:

Cannon-Ellen I_o = 6.86 mm/hr, Q_c = 38.1 mm
Wieczorek I_o = 1.52 mm/hr, Q_c = 9 mm

The above formula may also be used for the Caine threshold using the variables I_o = 4.49 mm/hr and Q_c = 13.65 mm. This formula is valid for durations between 1 hour and 24 hours (Keefer et al. 1987). This is valid for a hillslope where storms have an average rainfall with approximately constant intensity, as well as a combination of the intensity and duration of

the rain that is needed for the critical volume of needed water for debris flow initiation. For San Francisco this is usually 300 – 400 mm of rain. The suggested threshold value is 250 mm or more that is at least 30% of the mean annual precipitation (Keefer et al. 1987). The above equation for the critical volume of water was tested. Out of ten slides that were witnessed visually, and therefore had the exact time of initiation known, eight of the landslides, using both the Cannon-Ellen and the Wieczorek thresholds, were predicted (Keefer et al. 1987).

Antecedent Precipitation Index

The amount of rainfall as well as the manner that the rain falls is important in the occurrence of landslides (Sidle and Swanston 1982, Wong 1991). One way to quantify this pattern and to quantify antecedent soil moisture conditions is with the Antecedent Precipitation Index (API).

API has been used as a model for the prediction of storm runoff and the initiation of landslides in the central Oregon Coast Range (Fedora and Beschta 1989, Wong 1991). API has a memory of rainfall that has occurred prior to the present time. All rainfall occurring prior to the present time is decayed using a recession coefficient. The recession coefficient is affected by the local geology, soil properties and topography of the area (Fedora 1987). In addition, evapotranspiration affects the recession coefficient although to what amount is unknown (Wong 1991). Wong

(1991) states that due to the low summer rainfall amounts in the central Oregon Coast range, the value of API from the previous water year has little effect on the value of API at the beginning of the next soil movement season with the use of a recession coefficient of 0.87. Additionally in the central Oregon Coast Range, the use of rainfall data seventy-two hours before a runoff event was found to be sufficient for the calculation of API (Fedora and Beschta 1989).

The amount of rainfall that leads to failure should be a function of the amount of water in the soil when it fails (Kobashi and Suzuki 1987). In New Zealand, Crozier (1999) developed the Antecedent Water Status Model (AWSM) to predict landslide occurrence within the next 24 hours in New Zealand. The model assumes that in order for a slope to fail there must be a critical amount of water stored in the soil called the critical water content. Most landslides result from soil water content in excess of the capacity of the soil to store water. This causes positive pore pressures that cause failure (Crozier 1999). The critical water content includes the water already stored in the soil, the antecedent soil water, and the rainfall throughout the storm (Crozier 1999).

In the central Oregon Coast Range at the Condon landslide, a threshold API of 160 mm was estimated as a result of 16 soil movement events between the years of 1984 and 1990 (Wong 1991). On a daily scale, high API values were associated with large amounts of soil

movement (Wong 1991). Finlay et al. (1997) found antecedent rainfall to cause slides only during short duration, high intensity events. In addition, most slides occurred during large storms at the time of the peak hourly rainfall. Antecedent precipitation may be of special importance in mid to upslope hollows that are more susceptible to mass movements because of accumulated ground water (Sidle and Swanston 1982).

Spatial Variation of Rainfall for Mountainous Regions

Where climate systems interact with differences in elevation, such as in the Oregon Coast Range, it is important to understand how rainfall is distributed across the landscape. Many factors influence the amount of rainfall that occurs at a particular site. When topography is taken into account there may be confounding variables that decrease the correlation of altitude to rainfall amounts, especially with higher elevations and shorter durations (Wotling et al. 2000.) Loukas and Quick (1996) found, for the Seymour watershed just north of Vancouver, Canada, that rainfall amounts increased from valley floor to mid-elevation areas. Rainfall amounts then decreased between the mid-elevation areas and the higher-elevation areas. They suggest this is caused by a two-cloud system otherwise known as the seeder-feeder effect. The upper cloud (seeder) is not influenced by the terrain and dries out the higher air while moistening the lower air. The lower moist air is then lifted orographically and quickly

saturates. The location of this second cloud (feeder), usually in the mid-elevation range, determines where the most rainfall occurs. This seeder-feeder effect has also been observed on Norfolk Island (Bradley et al. 1998) and in the middle Himalayan range during the winter and pre-monsoon seasons (Singh and Kumar 1997). In contrast to this, Singh and Kumar (1997) found the expected positive linear relationship between rainfall amount and elevation for the outer Himalayan range and for the post-monsoon and monsoon seasons in the middle Himalayan range.

Models for predicting the distribution of rainfall often do not incorporate the effects of local orography. These include the Kriging technique and the Gumbel logistic model. The Kriging technique allows for interpolation of rainfall amounts from known amounts of rainfall in the surrounding area. The Gumbel logistic model is also a statistical model, which is an approximation of the normal distribution. This has been used to correlate variables such as total rainfall amount of a storm and the maximum rainfall intensity of a storm (Yue 2001.) The need to include local orography into these models has been recognized and put into use by Corradini (1985) and Andrieu et al. (1996.) The addition of the effect of orography on rainfall allowed both models to be represented by two components. One ties in the mesoscale of the area, assuming it is flat, and the other ties in the orographic effect, which uses the slope and the wind velocity of the local area researched. The use of both these components in

the model for how orography affects rainfall allows for a more complete and accurate view of what actually occurs within a given area.

Parameter-elevation Regression on Independent Slopes Model

The Parameter-elevation Regressions on Independent Slopes Model (PRISM) uses point data, a digital elevation model (DEM) as well as other spatial data sets to get gridded estimates of annual, monthly and single event climatic parameters (Daly et al. 1998). Datasets are obtained through the National Weather Service network. When compared to other procedures, PRISM has a lower bias and a lower mean absolute error (Daly et al. 1994).

PRISM is able to account for differences in elevation present in the Oregon Coast Range and can be used to obtain values for the spatial distribution of rainfall intensities. This allows for vertical extrapolation of data beyond the lowest gauge and the highest gauge by assuming linearity (Daly et al. 1998). The effects of terrain on rainfall are modeled as gradients such as rain shadows, coastal effects, and orographic effects.

PRISM has also gone one step further and produced Landslide Potential Mapping. The primary information needed for this modeling is rainfall and the slope of the landscape (Taylor et al. 2003). By combining slope information with rainfall intensities previously obtained from PRISM, maps of potential landslide locations are produced which could potentially be used as a management tool.

Previous work from the rain gauge network

Values of rainfall intensity for different durations and return periods have been estimated for the Oregon Coast Range using a small number of low elevation rain gauge locations (Arkell and Richards 1986). The rainfall data, which was collected as a part of the NOAA (National Oceanic and Atmospheric Administration) system of weather stations, is available for the central Oregon Coast Range from the Western Regional Climate Center (2003). The rainfall intensity values for the 6- and 24-hour durations and the 2-, 5-, 1-, 25-, 50-, and 100-year return periods in mm/hr for the central Oregon Coast Range are listed in Table 1.

Table 1. Range of values of rainfall intensities (mm/hr) for the central Oregon Coast Range estimated by NOAA using low elevation rainfall data.

	Duration	
Return Period	6 hour	24 hour
2-year	8-11	5-6
5-year	10-12	6-7
10-year	11-14	6-8
25-year	13-16	7-8
50-year	15-17	7-10
100-year	15-19	8-11

The rainfall data from the Forest Engineering rain gauge network from 1988 through 1995 was analyzed by Surfleet (1997). Partial series analysis was used to determine 5- and 30-minutes, 1-, 2-, and 6-hour

durations, and 2-, 5-, 10-, and 25-year return periods. API values were also determined for the return periods.

The values of rainfall intensity were highly variable across the study area, especially in the central section. The average rainfall intensities for the 13 rain gauges for all durations and return periods are shown in Table 2. For the 2-year return period for durations of 2-hours and less, the Thompson and South Creek rain gauges had the highest rainfall intensities. For durations greater than 6 hours, the Indian and South Creek rain gauges had the highest rainfall intensities. For the six hour duration, the Indian, South, Thompson, and Panther Creek rain gauges had the highest rainfall intensities.

Table 2. Average rainfall intensities (mm/hr) for all 13 rain gauges obtained from previous analysis of rainfall data from the rain gauge network (Surfleet 1997).

	5 minutes	30 minutes	1 hour	2 hour	6 hour
1 year	4	10	15	23	47
2 year	5	11	17	27	53
3 year	5	12	18	28	56
4 year	5	13	19	30	58
5 year	6	13	20	31	60
10 year	6	15	22	34	65
25 year	7	16	25	37	72

A linear regression was developed between rainfall intensities for the 2-year return period and elevation. No significant relationships were found. Also, no significant relationships were determined between API and the rainfall intensities.

METHODS

Study Area

The thirteen tipping bucket rain gauges used to collect data for this study are located in the central Oregon Coast Range (see Figure 2). The study area represented by the rain gauge network is bordered by the Umpqua River on the south and the Alsea River on the north. The town of Mapleton is the approximate geographic center of the study area. The study area is approximately 81 km (50 miles) long from the north to the south, 32 km (20 miles) wide from the east to the west, and covers approximately 2,590 square kilometers (1000 square miles) of forest land.

The central Oregon Coast Range has a mean annual precipitation (MAP) between 2,032 and 4,318 mm with snow a rare occurrence (Ketcheson and Froehlich 1978). Rainfall occurs primarily in response to regional fronts that come off the Pacific Ocean. In addition to regional fronts, MAP shows an increasing trend with elevation illustrating the effect of topography by orographic lifting (Daly et al. 1994). Most rainfall falls between November and March and falls with low to moderate intensity relative to other regions of the country.

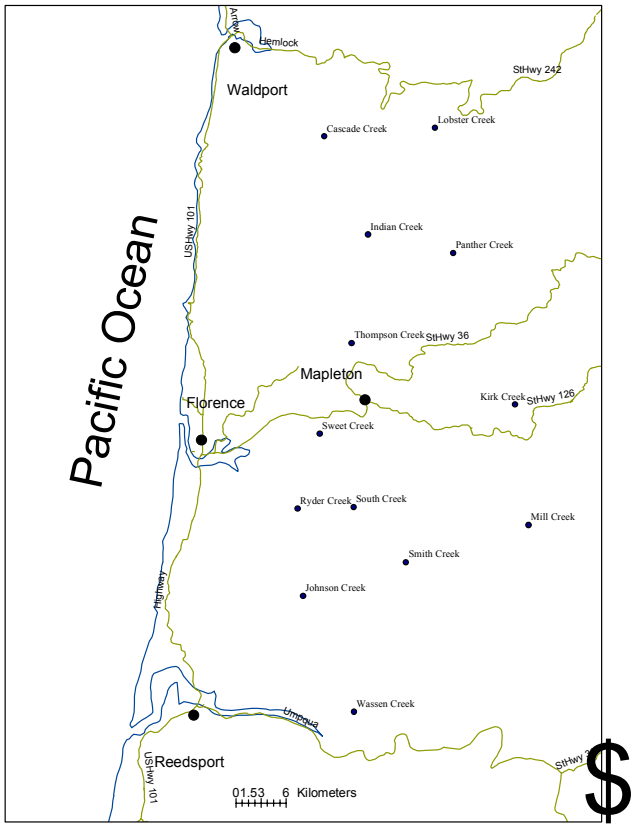

Figure 2. Map of rain gauge network.

The soils of the study area are in the Digger-Bohannon-Preacher soil associations. Digger soils are well-drained and moderately deep with sandstone and siltstone as parent material. Bohannon and Preacher soils are well drained, deep soils derived from sedimentary rock. The major underlying geology of the area is Tyee and Flourney sandstone and siltstone (Ketcheson and Froehlich 1978). The Tyee and Flourney

formations are marine sandstones with rhythmically bedded siltstones on mudstones.

The topography of the Oregon Coast Range is composed of steep hillslopes with narrow ridges and deeply-incised valleys (Dietrich 1989). Elevations in the study area range from 30 m at the town of Mapleton to over 700 m at the top of Saddle Mountain.

The primary overstory vegetation is Douglas-fir (*Pseudotsuga menziesii*) with some western hemlock (*Tsuga heterophylla*) and western redcedar (*Thuja plicata*). Red alder (*Alnus rubra*) and big-leaf maple (*Acer macrophyllum*) are present along streams. Understory vegetation consists of salal (*Gaultheria shallon*), huckleberry (*Vaccinium spp*), vine maple (*Acer cirinatum*), swordfern (*Polystichum munitum*), salmonberry (*Rubus spectabilis*), and rhododendron (*Rhododendron spp*).

Installation

Installation of the rain gauges was a joint effort between the Coastal Oregon Productivity Enhancement (COPE) program and the Department of Forest Engineering at Oregon State University. The purpose of the rain gauge network is to collect rainfall data, especially rainfall intensity, in the landslide-prone portion of the central Oregon Coast Range. Tipping bucket rain gauges were installed during the years 1988 to 1990. The rain gauges

were installed on or near ridge tops in recent clearcuts at that time at elevations that range from 232 to 500 meters (Table 3).

Table 3. Elevation (m) of rain gauges in the central Oregon Coast Range.

Gauge	Elevation (m)
Indian Creek	317
Thompson Creek	238
Sweet Creek	317
South Creek	500
Smith Creek	372
Johnson Creek	232
Wassen Creek	427
Kirk Creek	427
Mill Creek	305
Panther Creek	341
Ryder Creek	244
Lobster Creek	366
Cascade Creek	305

Data Collection

The tipping bucket rain gauges have a 20.3 cm (8 inch) diameter orifice. Each gauge has two screens located within each funnel to catch debris and minimize the chance of clogging. Rainfall data are stored on a HOBO event recorder. The event recorder records the date and time to the nearest second for each tip, nominally 0.254 mm (0.01 inch) of rain. Originally, Omniloggers were used to collect data that recorded the date and time to the nearest minute for each 1 mm (0.04 inches) of rain (Surfleet 1997). Then, from 1995 to 1998 Starloggers were used that recorded the date and time to the nearest minute for each 0.254 mm (0.01

inches) of rain. All of the rain gauges are visited approximately once every two months for maintenance and to download data. The data are downloaded to a laptop computer using BoxCar 4.2 with a HOBO shuttle.

Equipment maintenance

During each site visit the area around the rain gauge is cleared and the rain gauges are cleaned and leveled. Vegetation surrounding each rain gauge is kept cleared to approximately a 45-degree angle to minimize the effect of wind on gauge catch. Rain gauges are calibrated in the field by pouring a known volume of water into the rain gauge orifice that will produce a predetermined number of tips. When properly calibrated, all rain gauges will record +/- 5 percent of the known volume of water. This is the acceptable level of error in these rain gauges and is the error inherent in the instrument when delivered from the factory (Surfleet 1997). Batteries are replaced in the HOBO event recorders once a year.

Data Analysis

Mean Annual and Average Monthly Rainfall

The rainfall data downloaded from the rain gauges is stored in personal computers and analyzed in a spreadsheet that contains raw data of date, time, and amount of rain for each tip. The initial step of reduction and analysis of the rainfall data is to sum and average the data for mean

annual and average monthly rainfall. The first step to determine mean annual and average monthly rainfall is to fill in the periods of missing rainfall.

Missing rainfall data occurred due to problems such as failure of the HOBO event recorders, rain gauge clogging, and tampering by humans and animals. Missing data were filled in at the monthly level in order to obtain values for mean annual precipitation. For each rain gauge for each month a simple linear regression relationship was developed for that rain gauge and all the rain gauges directly adjacent to it. The linear regression was based on months in the database when the two rain gauges had common data. Missing data were calculated using the best relationship between the rain gauge with missing data and all the rain gauges that were adjacent.

In this manner, missing data could be generated for all the months at all the rain gauges that had missing data. Once the monthly data were generated, the average monthly and mean annual rainfall could be summed for each year and averaged over the years of record.

Separating Storms

Once the annual and monthly data had been calculated, the raw rainfall data was further reduced by dividing it into storms. A storm is defined as a 12-hour period of time when more than 12 mm (0.5 inches) of

rain fell. Thus, the raw rainfall data was divided up into a series of discrete storms. Missing data was not filled in for analysis of data at the individual storm level. Then for each storm the maximum intensity for the 30-minute, 1-, 2-, 6-, 12-, and 24-hour duration, if appropriate, was determined. This was done by finding the predetermined duration of time in which the greatest volume of rain fell during that storm. These values were determined and stored to a separate spreadsheet.

Antecedent Precipitation Index

Conditions of antecedent precipitation were determined through the calculation of API. Calculation of API for the study site may be used as an index of soil moisture at the 13 rain gauge locations, and may be used to estimate values over the entire study area (Fedora 1987). To determine values for API a regression coefficient, C, was used to define the decay of the residual effects of precipitation through time (Fedora 1987). The formula used for calculation of API is taken from Fedora (1987) and is

$$API_t = API_{t-\Delta t} * C + P_t \qquad \text{Equation 3}$$

where

$API_t =$ Antecedent precipitation index at time t (inches)
$API_{t-\Delta t} =$ Antecedent precipitation index at time $t - \Delta t$ (inches)
$C =$ Recession coefficient based on the time interval of Δt
$P_t =$ Precipitation that occurs during Δt (inches)

The value chosen for the regression coefficient used for this study was 0.985. This value is based on hourly data of between 0.995 and 0.985 obtained from observations of three piezometric wells on a headwall site located in the Oregon Coast Range (Bransom 1997). This value was used because it is a conservative estimate and was previously used in analysis of API for this rain gauge network (Surfleet 1997).

Because the chosen recession coefficient is only appropriate when the time interval of precipitation observations and the time interval used to calculate the recession coefficient are the same, C must be adjusted due to the varying intervals of time that occurred during the rainfall collection (Fedora 1987). The equation used to calculate the adjusted decay rate is

$$C(a) = C(b)^{\left[\frac{\Delta t(a)}{\Delta t(b)}\right]} \qquad \text{Equation 4}$$

where

$C(a) =$ Recession coefficient based on time interval $\Delta t(a)$
$C(b) =$ Recession coefficient based on time interval $\Delta t(b)$
$\Delta t(a) =$ Time interval of precipitation observations
$\Delta t(b) =$ Time interval used to derive recession coefficient $C(b)$

Substituting the new recession coefficient based on the time interval of the precipitation observations Equation 1 becomes

$$API_t = API_{t-\Delta t} * C(a) + P_t \qquad \text{Equation 5}$$

API values were also calculated for each storm. For each storm that is identified in the rainfall data the maximum value of API is generated.

API is calculated by starting at the beginning of the year and calculating a running API value using the equation described above. Because the API value requires knowledge of the rainfall that occurred antecedent or prior to the storm of interest, storms that occurred and were adjacent to blocks of missing data had to be removed from the data set because a value of API could not be calculated.

Partial Series

The frequency analysis for the 13 rain gauge locations and the six durations was carried out using partial duration series (Chow 1964). A partial duration series differs from an annual series by using all data of interest above a predetermined threshold instead of just maximum annual values (Kite 1977). Once the raw rainfall data is reduced and maximum rainfall intensities are known for all of the storms, durations, and rain gauges, the next step is to determine the threshold value for partial duration series. The method used in this thesis to establish the threshold value is the minimum of the annual maximum values. Thus, from the dataset, the annual maximum values for all the durations and all the years of data are obtained and the annual series of maximum values is established. The minimum of these annual maximum values becomes the threshold value for the partial duration series. Once the threshold value has been established, the partial duration series values can be determined by selecting all values in the database greater than the threshold value.

Once the partial duration series data have been selected, the analysis is straightforward. The analysis is the same as for an annual series except the resulting return periods must be corrected for the number of data points. The first step in the analysis process is to sort the data in descending order from the highest to the lowest value and then rank the data with the largest value having a rank of $m = 1$ and the smallest value having a rank of $m = n$ where n is the sample size. When data points have the same numeric values they are arbitrarily assigned different and successive ranks. Once the rank has been established, the return period is calculated using the Gringorton plotting position (Bedient and Huber 1992), which takes the form:

$$Tr = \frac{[(n+1) - 2a]}{m - a} \qquad \text{Equation 6}$$

where

$m =$ rank,
$n =$ number of events,
$a = 0.4$
$Tr =$ return period.

The calculated return periods must be corrected by a correction factor. The correction factor is the number of years of record divided by the number of data points. The correction factor becomes the fractional component of a year that each data point represents. For example, if there are 30 storms or data points and 10 years of record then the correction factor is 10/30 or 1/3. Each return period is multiplied by 1/3 to get the

actual return period. The correction factor also means that each data point represents 1/3 of a year. Once the values of the return period have been corrected, the data is plotted as log/log or log/probability graphs. Figure 3 shows a graph of rainfall intensity versus return period for the 24-hour data for the Lobster Creek rain gauge.

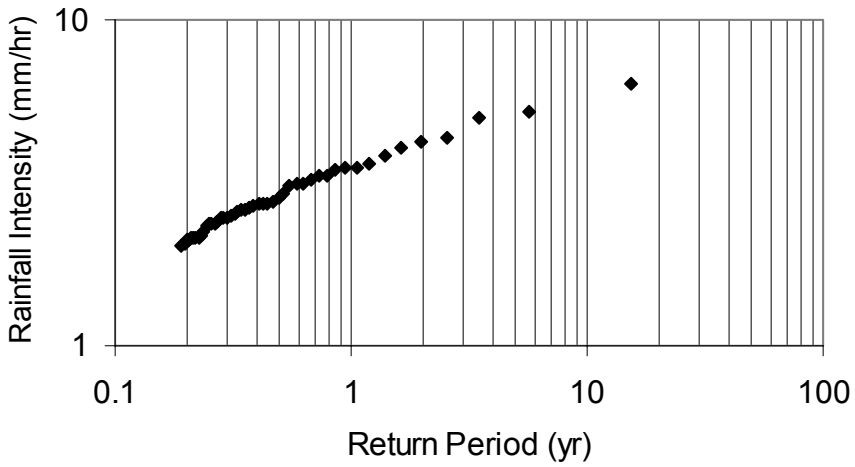

Figure 3. Cumulative frequency distribution for the raw data for rainfall intensities (mm/hr) and their associated return period of the 24-hour duration at the Lobster Creek rain gauge.

The data is then fit to the Extreme Value Type I or the Gumbel cumulative probability distribution. The Gumbel distribution was used because the frequency factor can be determined as a closed form equation, thus analysis of a large amount of data is simplified in a spreadsheet environment, and because the Gumbel distribution was previously shown to fit these data well (Surfleet 1997). For a given data

set, rainfall intensities for the different durations were determined using the Chow equation (Chow 1964).

$$Ppt_{Tr} = Ppt + \sigma * K \qquad \text{Equation 7}$$

where

Ppt_{Tr} = amount of rainfall for the return period;
Ppt = mean of the normalized rainfall for each duration;
σ = standard deviation of the normalized rainfall for each duration;
K = frequency factor for the Gumbel distribution.

K is calculated for a return period of 2-, 5-, 10-, 25-, 50-, and 100-years using the formula from Bedient and Huber (1992).

$$K = -0.7797 * \left[0.5772 + \ln\left(\ln\left(\frac{Tr}{Tr-1} \right) \right) \right] \qquad \text{Equation 8}$$

Once the rainfall intensity values have been calculated for a given return period, it must also be corrected by the same correction factor discussed above. To do this each return period was divided by the individual correction factor previously determined for each of the six durations for each rain gauge. Once this new return period was calculated a new value for K was determined by inserting the new return period into Equation 8. The new value for K was then inserted into Equation 7 to determine the rainfall intensity for the corrected return period. The cumulative frequency distribution can then be plotted with the raw data on rainfall intensity versus return period plot (Figure 4). Partial series analysis

in this manner was carried out for all six durations at all 13 rain gauge locations.

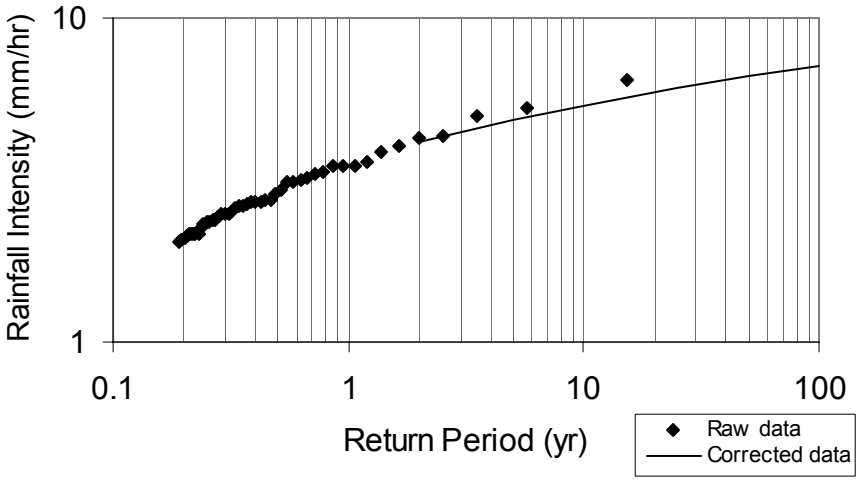

Figure 4. A graph showing the raw data and the Gumbel cumulative frequency distribution for the rainfall intensities (mm/hr) for the 24-hour duration at the Lobster Creek rain gauge.

Once the values of the rainfall intensities for the different durations and return periods for each rain gauge have been estimated, that data is presented in several ways. Tabular values of the rainfall intensities for each unique combination of duration and return period for each rain gauge are listed in Appendix A. These same data are presented in graphical form. One form is Intensity-Duration-Frequency (IDF) curves where rainfall intensity is graphed against duration for a series of curves representing a return period. One graph is prepared for each rain gauge location. These graphs are shown in Appendix B. Finally, the graphs of the frequency analysis are prepared where rainfall intensity is graphed versus return

period. Each graph represents one duration and data from all the rain gauges is shown on each graph (Figures 13 to 18).

Spearman Rank Correlation

The Spearman Rank Correlation Coefficient was used to investigate patterns in rainfall intensity among rain gauges with regard to rainfall duration and return period. This technique investigates patterns nonparametrically by using relative ranking instead of numerical values (Moroney 1951).

The total value of all the ranks are found using the equation

$$\frac{m * n(n+1)}{2} \qquad \text{Equation 9}$$

where

$m =$ the number of return periods or durations
$n =$ the number of rain gauges.

For the rain gauge data, there are six return periods and durations and 13 rain gauges thus $m = 6$, $n = 13$, and the total possible rank is 546. If no difference in the relative rank between rain gauges exists then each rain gauge would have the same rank, which in this case is 42. If there is a difference and complete agreement in rank the ranks should form a series of m, $2m$,…, nm.

In order to discern if there is agreement in relative rank the Coefficient of Concordance (W) is calculated. W is the ratio between the

maximum sum of squares ($S_{\max}$) and the sum of squares differences between the observed and expected rank totals (S). It is found using the equation

$$W = \frac{S}{S_{\max}} \qquad \text{Equation 10}$$

The formulas to obtain S and $S_{\max}$ are

$$S = (y - x)^2 + (y_1 - x_1)^2 + \ldots + (y_i - x_i)^2 \qquad \text{Equation 11}$$

$$S_{\max} = \frac{m^2(n^3 - 1)}{12} \qquad \text{Equation 12}$$

The value for W is between 0 and 1. The closer the value is to 1 the more agreement in ranks there is. Once the value for W has been determined, it can be tested for significance using Snedecor's F distribution. To do this, a correction factor is added to the original value for W. This is done by subtracting a unity value from the numerator, S, and by adding 2 to the denominator, $S_{\max}$. An F_{SN} value is calculated with the formula

$$F_{SN} = \frac{(m-1)*W}{1-W} \qquad \text{Equation 13}$$

The greater and lesser estimates of the degrees of freedom are then found by

$$DF_g = (n-1) - \frac{2}{m} \qquad \text{Equation 14}$$

$$DF_l = (m-1)\left[(n-1)-\frac{2}{m}\right] \qquad \text{Equation 15}$$

These values for the degrees of freedom are then used to find the tabular values of F at the 1 and 5 percent level of significance. The calculated and tabular values of F are compared to determine if the relative rank of the rainfall intensity data is statistically significant.

Isohyetal Maps of Rainfall Intensity

Isohyetal maps that show how rainfall intensity is distributed spatially at different durations and for each return period were developed for the study area. Isohyetal maps were also developed for API over all return periods. The process described by Daly and Taylor (2002) was used to construct these maps.

The required data to make the isohyetal maps were values for rainfall intensities for each duration and return period, API for each return period, and gridded values for MAP over the study area. The gridded values for MAP were obtained from Chris Daly of the Oregon Climate Service and were generated using PRISM. The values of MAP were on a 4 km grid and did not include data generated by this study.

Values of MAP obtained by this study were used as a basis for a grid. However, the range in elevations from this study area is not very robust and no rain gauges are present that have either very high or very

low elevations. The relationship between MAP and elevation for this study showed a negative relationship with MAP decreasing as elevation increased. Thus gridded values of MAP generated by PRISM for Oregon were used as a base map.

The first step in constructing isohyetal maps of rainfall intensity was to develop a relationship between the different values of rainfall intensity and MAP. Linear regression was used to develop a relationship for each unique combination of return period, duration, and MAP. The MAP value used was for the grid cell where each rain gauge was located in the PRISM grid (Figure 5). The adjusted values for MAP are listed in Table 4.

Table 4. Adjusted values for mean annual precipitation (mm) for all 13 rain gauges using the PRISM grid.

Gauge	Mean Annual Precipitation (mm)
Indian Creek	2278
Thompson Creek	2140
Sweet Creek	2047
South Creek	2205
Smith Creek	2144
Johnson Creek	2051
Wassen Creek	2140
Kirk Creek	1687
Mill Creek	1389
Panther Creek	2295
Ryder Creek	2156
Lobster Creek	2283
Cascade Creek	2273

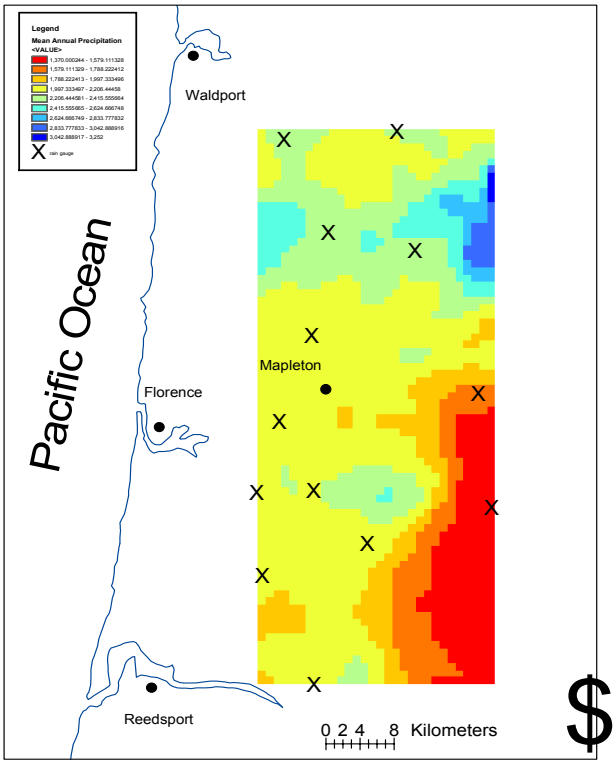

Figure 5. Isohyetal map of mean annual precipitation (mm) obtained from PRISM.

The value of rainfall intensity came from the IDF-curves and is the unique value of rainfall for each duration and return period for each rain gauge. A graph of the relationship that was developed for the 30-minute, 2-year return period data is shown in Figure 6. Notice that the relationship is developed in log-log space. Thus the linear regression takes the form:

$$\log P_{Tr,D} = a(\log MAP) + b$$

Equation 16

where

$P_{Tr,D} =$ rainfall value for a given return period and duration
$MAP =$ Mean Annual Precipitation
a and $b =$ regression coefficients

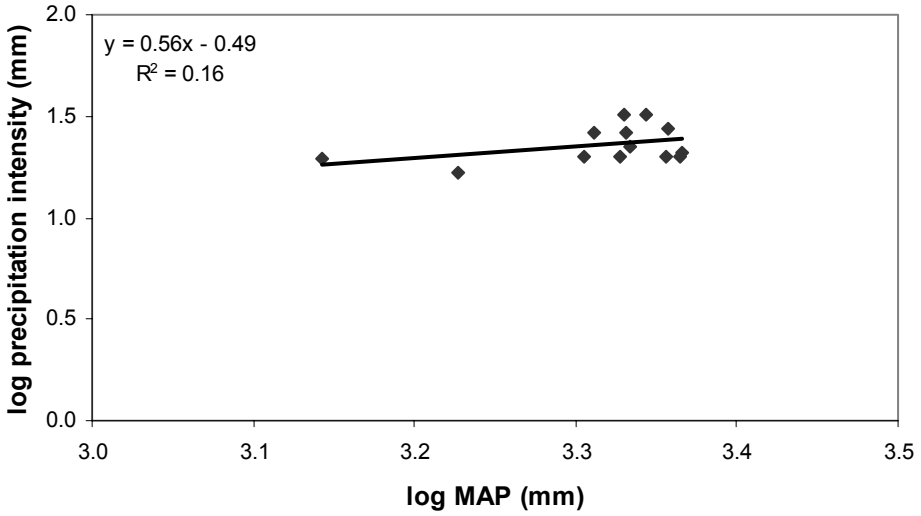

Figure 6. Relationship between the log 30-minute, 2-year rainfall intensity (mm/hr) and the log MAP (m) obtained from PRISM. The regression equation is used to determine the grid of the predicted values for rainfall intensity.

Once the regression equations had been developed, the residuals (R_1) were calculated using the equation

$$R_1 = \log P_{Tr,D} - \left[a(\log MAP) + b\right] \qquad \text{Equation 17}$$

The residuals can be expressed as standardized residuals (SR_1) for the purpose of further computation using the equation

$$SR_1 = \frac{R_1}{\left[a \log_{10}(MAP) + b\right]} \qquad \text{Equation 18}$$

The standardized residuals for each rain gauge and each unique combination of rainfall duration and return period were imported into GIS (ArcMap) and a gridded map of standardized residuals was made using inverse distance squared weighting. A gridded map of predicted rainfall intensities was also prepared using the linear regressions developed and the gridded map of MAP. Once the two values are known, a gridded map of actual predicted rainfall intensities can be calculated by adding the gridded rainfall values to the gridded standardized residuals.

$$GP_2 = (GRS_1 * GP_1) + GP_1 \qquad \text{Equation 19}$$

where

GP_1 = grid of the log of actual values for rainfall intensity for any given duration and return period
$GSR =_1$ grid of the standard residuals for the same duration and Tr
$GP_2 =$ grid of the log of predicted values for the same duration and Tr

These operations all take place in log space so it is necessary to back transform all predicted values. The maps shown in Appendix E (Figures E1 to E36) are the result of this process at every unique combination of rainfall duration and return period. Maps in Appendix F (Figures F1 to F6) are the result of this process at every unique combination of API and return period.

RESULTS AND DISCUSSION

Analysis of the rainfall data collected from the 13 rain gauges in the central Oregon Coast Range shows rainfall characteristics that are variable across the landscape. The general rainfall pattern of the study was determined through the characterization of the major storms, mean annual precipitation, and average monthly rainfall. To determine the temporal and spatial distribution of rainfall intensity, intensity-duration-frequency graphs, frequency analysis, and isohyetal maps were generated and the Spearman Rank Correlation method was used as a non-parametric statistical package. In addition, the relationship between rainfall intensity and elevation was examined to see if there was a pattern. Finally, the antecedent precipitation index for the area was analyzed in the same manner as rainfall intensity to determine the spatial pattern across the landscape.

Individual Storms

Based on the definition of a storm explained in the Methods, on average each rain gauge measured 37 storms per year. The average rainfall for each storm was 54 mm (2.1 inches) and lasted 49 hours.

There have been three large, multi-year return period storms during the 14 years of data collection for the rain gauge network. The biggest storm occurred between February 3rd and 9th, 1996. The storm lasted a

little over five days (128 hours) and, on average, 368 mm (14.5 inches) of rain fell with a high amount of 646 mm (25.4 inches) at the Indian Creek rain gauge and a low of 150 mm (5.9 inches) at the Mill Creek rain gauge. A second large storm occurred between November 17th and December 3rd, 1998. The storm lasted over nine days (228 hours) and rainfall averaged 389 mm (15.3 inches) across the network with a high of 503 mm (19.8 inches) at the Indian Creek rain gauge and a low of 284 mm (11.2 inches) at the Mill Creek rain gauge. Finally, a third large storm occurred between November 23rd and December 5th, 1995. This storm also lasted a little over nine days (226 hours) and rainfall averaged 289 mm (11.4 inches) with a high of 503 mm (19.8 inches) at the Indian Creek rain gauge and a low of 129 mm (5.1 inches) at the Wassen Creek rain gauge.

Mean Annual Precipitation

Mean Annual Precipitation for the rain gauge network was calculated to help describe the spatial variability of the rainfall data. The methods used to calculate MAP, including missing values, are described in the Methods. Values for MAP for all of the rain gauges as well as the average values of MAP are listed in Table 5. The average MAP is 2049 mm (80.7 inches) and ranges from a high of 2826 mm (111.3 inches) at the Indian Creek rain gauge to a low MAP of 1668 mm (65.7 inches) at the Kirk Creek rain gauge. A bar graph showing values for MAP for each rain

gauge along with the overall average of MAP for all gauges is shown in Figure 7.

Table 5. Mean annual precipitation (mm) of all 13 rain gauges.

Gauge	Mean Annual Precipitation (mm)
Indian Creek	2826
Thompson Creek	2039
Sweet Creek	2048
South Creek	2600
Smith Creek	1762
Johnson Creek	2091
Wassen Creek	1764
Kirk Creek	1668
Mill Creek	1755
Panther Creek	2292
Ryder Creek	2089
Lobster Creek	1722
Cascade Creek	1986

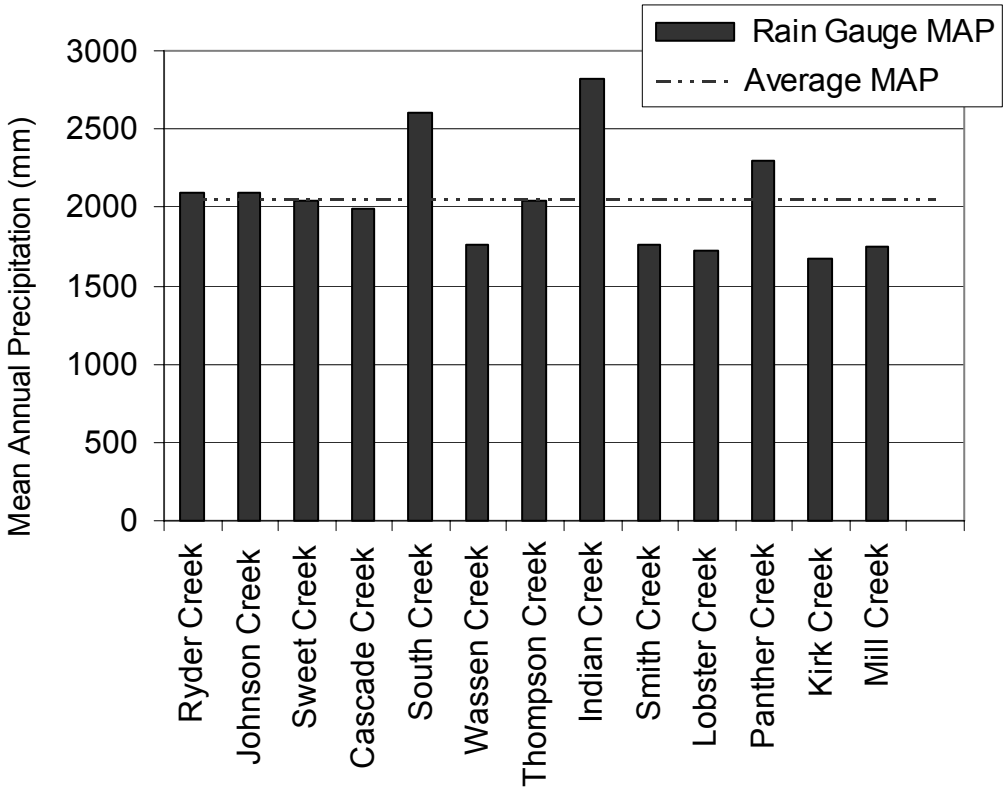

Figure 7. Mean annual precipitation (mm) of all 13 rain gauges and average mean annual precipitation (mm) arranged from westernmost to easternmost position.

In areas of mountainous terrain, most of the variability in rainfall that occurs for long durations, such as MAP, can be explained by differences in elevation. This was found by Singh and Kumar (1997) in the Satluj and Beas basins in the outer Himalayas. Using rainfall data in the Satluj basin from five rain gauge stations between the elevations of 600 to 700 m they found rainfall to increase linearly with altitude between approximately 1000 mm and 1300 mm on the leeward side. For the Beas basin, rain gauges

were located between the elevations of 400 and 800 m and annual rainfall was between 1300 and 1500 mm on the leeward side.

Another example of MAP increasing with increasing elevation was found in various locations throughout the Wasatch Front area outside of Salt Lake City, Utah (Peck and Brown 1962). Relationships were derived during two periods, the winter months (October-April) and the summer months (May-September). For the winter months elevations ranged from 2,000 to 11,000 feet with normal rainfall beginning at approximately 6 inches and increasing to approximately 34 inches. For the same elevations during the summer months the normal rainfall began at approximately 2.5 inches and increased to approximately 12 inches.

To analyze the spatial variability of rainfall intensity, a basemap of MAP was needed. For this basemap, values of MAP were assigned to the study area on a 4 km^2 grid. To determine the values for MAP, a relationship between elevation and MAP was developed using data from rain gauges at known locations. Through this relationship, MAP can be used as a surrogate for elevation.

The relationship between elevation and MAP was determined for the 13 rain gauges in the study area. This relationship is shown in Figure 8.

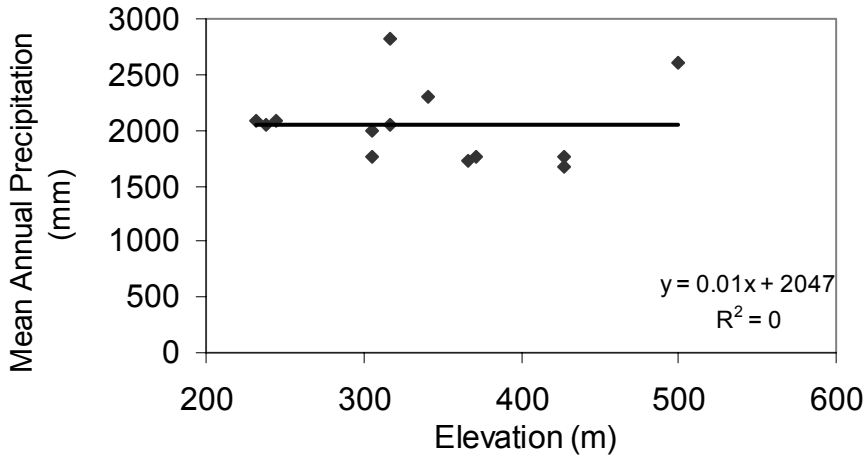

Figure 8. Relationship between elevation (m) and mean annual precipitation (mm) for all 13 rain gauges.

The raw data and the resulting relationship show that there is not a significant relationship between elevation and MAP for rain gauges in the study area. This means that elevation does not explain the variability in MAP for the 13 rain gauges. Examples of this are the Indian Creek rain gauge, which has the highest MAP of 2826 mm but is in the lower one third in elevations at 317 m and the Kirk Creek rain gauge which has the lowest MAP but is at the second highest elevation at 427 m. One reason for the lack of correlation between MAP and elevation for the study rain gauges is the low range of elevations represented by the rain gauge locations. While the area of land that the rain gauges represent is actually quite large, approximately 2590 square kilometers, the range of elevations is not. The highest and lowest elevations at which the rain gauges are located are 500

m and 232 m, however seven, or over half of them, are located between 300 and 375 meters.

An additional reason for the non-significant relationship between elevation and MAP for the 13 rain gauges in the study area is the rainshadow effect caused by the Coast Range. Mean annual precipitation on the coastal side of the crest of the Coast Range should be greater than for the inland side of the Coast Range. These differences in MAP are caused by orographic lifting on the coastal side versus downward air flow on the inland side of the Coast Range. Orographic lifting would result in a lower MAP on the inland side of the crest of the Coast Range than at a location at the same elevation on the coastal side of the crest. This is observed for the rain gauges used for this study. For example, the westernmost rain gauge, Ryder Creek, is located at 244 m elevation and has a MAP of 2089 mm (82.2 inches). In contrast, the easternmost rain gauge, Kirk Creek, is at an elevation of 427 m yet only has a MAP of 1668 mm (65.7 inches), approximately 400 mm less rainfall per year. Another example is the difference between the Mill Creek rain gauge on the inland side of the crest of the Coast Range and both the Cascade Creek and Sweet Creek rain gauges on the coastal side of the crest. Both the Mill Creek and the Cascade Creek rain gauges are located at an elevation of 305 m while the Sweet Creek rain gauge is at a similar elevation of 317 m. Despite the similarities in elevation the Mill Creek rain gauge has a MAP of

1755 mm (69.1 inches) while the Cascade Creek and Sweet Creek rain gauges have a MAP of 1986 (78.2 inches) and 2048 mm (80.6 inches), respectively.

In order to supplement the relationship between elevation and MAP, MAP from four additional locations was added. These data come from three communities located along the Oregon coast and one community in the Umpqua Valley adjacent to the Umpqua River (Oregon Climate Service 2003, NOAA 2003, Desert Research Institute 2003). These communities are Gardiner, Newport, Reedsport, and Elkton, Oregon. All of the communities are located at low elevations and are adjacent to the study area. The elevations and MAP for these communities are listed in Table 6.

Table 6. Elevation (m) and mean annual precipitation (mm) of four lower elevation weather stations within and adjacent to the study area.

Station	Elevation (m)	Mean Annual Precipitation (mm)
Gardiner	9	1761
Newport	46	1767
Reedsport	18	1940
Elkton	37	1334

These data were added to the 13 rain gauges and a linear regression was developed. The data and the regression are shown in Figure 9.
It is interesting to note that the addition of lower elevation data to the data of the 13 rain gauges elevation explained only 14 percent of the variability

in MAP, meaning that something other than elevation must explain over 85 percent of the variability of MAP. In addition, the slope of the regression line in Figure 9 indicates the total effect attributed to elevation between the coast and the highest elevation rain gauge is less than the variability among the 13 rain gauges used for this study.

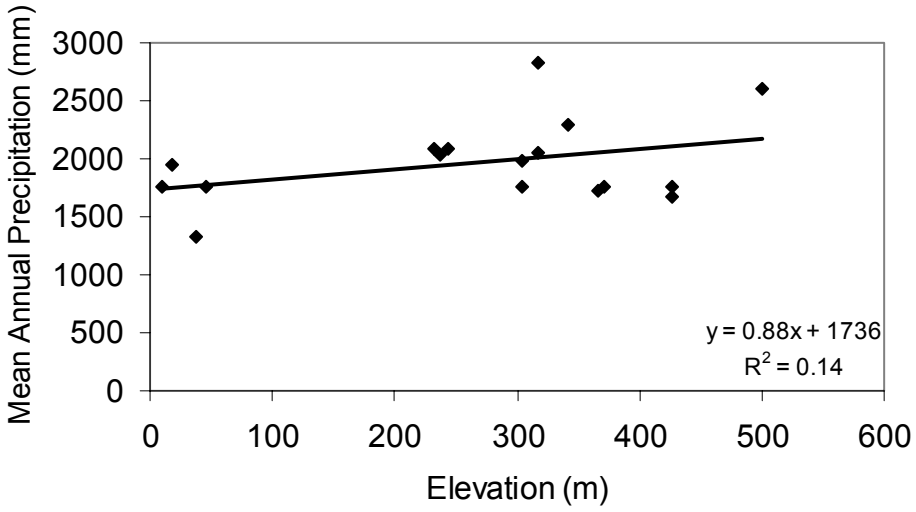

Figure 9. Relationship between elevation (m) and mean annual precipitation (mm). Data includes all 13 rain gauges and 4 additional lower elevation stations (Gardiner, Newport, Reedsport, and Elkton, OR).

Average Monthly Rainfall

Average monthly rainfall for all 13 rain gauges was calculated. Missing values were estimated using the methods described previously. Values for the average and overall monthly rainfall for all the rain gauges are shown in Table 7. The overall average monthly rainfall for the entire

rain gauge network is shown graphically in Figure 10. The month with the highest average rainfall is November with 375 mm (14.8 inches) followed closely, as expected, by January and December with 351 mm (13.8 inches) and 314 mm (12.4 inches), respectively. In those months, the Indian Creek rain gauge had the highest average monthly rainfall with 557 mm (21.9 inches) 523 mm (20.6 inches), and 443 mm (17.4 inches) for November, January, and December, respectively. The lowest average monthly rainfall for November and January was 275 mm (10.8 inches) and 273 mm (10.7 inches), respectively, at the Lobster Creek rain gauge and 234 mm (9.2 inches) for December at the Smith Creek rain gauge.

Table 7. Average monthly rainfall (mm), for all 13 rain gauges.

Gauge	January	February	March	April	May	June	July	August	September	October	November	December
Indian Creek	523	371	302	254	147	87	23	44	69	221	557	443
Thompson Creek	350	262	202	190	114	49	24	36	56	178	406	295
Sweet Creek	319	291	199	178	132	72	13	32	36	151	345	290
South Creek	435	310	276	247	158	100	32	32	71	221	492	379
Smith Creek	303	232	183	148	102	44	18	22	40	147	361	234
Johnson Creek	360	248	221	185	127	66	32	30	42	175	345	329
Wassen Creek	297	193	187	155	127	61	17	31	42	114	306	241
Kirk Creek	289	202	175	137	101	44	12	27	43	136	289	289
Mill Creek	317	225	193	137	97	45	18	27	37	134	327	295
Panther Creek	381	294	218	197	126	65	20	34	54	199	437	378
Ryder Creek	389	244	213	195	123	71	28	30	43	170	392	296
Lobster Creek	273	232	194	144	98	44	15	27	48	144	275	291
Cascade Creek	328	268	234	163	102	53	24	29	63	173	345	318
Average	351	259	215	179	120	62	21	31	50	166	375	314

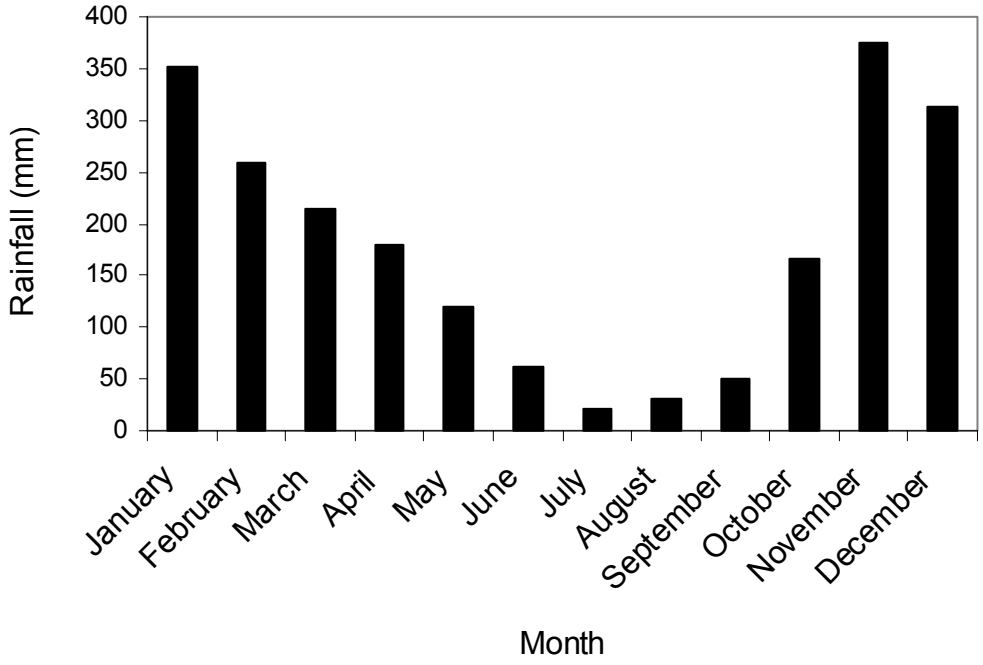

Figure 10. Average monthly rainfall (mm) for all 13 rain gauges.

The average monthly rainfall data shows that the central Oregon Coast Range has a Mediterranean climate. During the 14 years that rainfall data has been collected, on average 83 percent of the rain falls between November and April. Approximately half of the rain, or 51 percent, falls in the three winter months of December, January, and February.

The month with the lowest average monthly rainfall was July with 21 mm (0.8 inches). For July, the Johnson Creek and the South Creek rain gauge had the highest average rainfall of 32 mm (1.3 inches) and the Kirk Creek rain gauge had the lowest average rainfall at 12 mm (0.5 inches).

The highest average monthly rainfall occurred at the Indian Creek rain gauge the months of January through April, August, November, and December. The months of July and October both had two rain gauges with the highest average monthly rainfall. They were the South Creek and Thompson Creek rain gauges and the Indian Creek and South Creek rain gauges respectively. During the remaining months of May, June, and September, the highest mean monthly rainfall occurred at the South Creek rain gauge.

Rainfall intensities

Rainfall intensity values were determined for each combination of return period and duration of rainfall. The return periods used were 2-, 5-, 10-, 25-, 50-, and 100-years. The durations that were used were 30-minute, 1-, 2-, 6-, 12-, and 24-hour. All rainfall intensity values for each of the 13 study rain gauges were calculated using partial series analysis. The value of rainfall intensity for each unique combination of rain gauge, return period, and duration is listed in Appendix A (Figures A1 to A13).

In addition to tabular values, these results can be presented graphically. These graphs are called Intensity-Duration-Frequency (IDF) curves, and they show the relationship between rainfall intensity and duration for the six return periods for each rain gauge. The individual IDF-curves for each rain gauge are shown in Appendix B (Figures B1 to B13).

Values of rainfall intensities were averaged over the network of 13 rain gauges for each unique combination of duration and return period. These results along with the coefficient of variation for each of the average rainfall intensities are listed in Table 8. These data are presented graphically in an IDF-curve of average rainfall intensities in Figure 11.

Table 8. Average rainfall intensity (mm/hr) and coefficient of variation (%) for the six return periods and six durations. Data is from all 13 rain gauges in the network.

		0.5 hour	1 hour	2 hour	6 hour	12 hour	24 hour
2 year	Avg (mm/hr)	25	17	13	9	7	5
	CV (%)	29	22	20	20	20	20
5 year	Avg (mm/hr)	29	20	15	10	8	6
	CV (%)	33	24	21	21	20	20
10 year	Avg (mm/hr)	32	22	17	11	9	6
	CV (%)	35	25	22	22	21	21
25 year	Avg (mm/hr)	37	25	19	13	10	7
	CV (%)	37	26	23	23	21	21
50 year	Avg (mm/hr)	40	27	20	14	10	8
	CV (%)	39	27	24	23	21	21
100 year	Avg (mm/hr)	44	30	22	15	11	8
	CV (%)	40	28	24	24	21	21

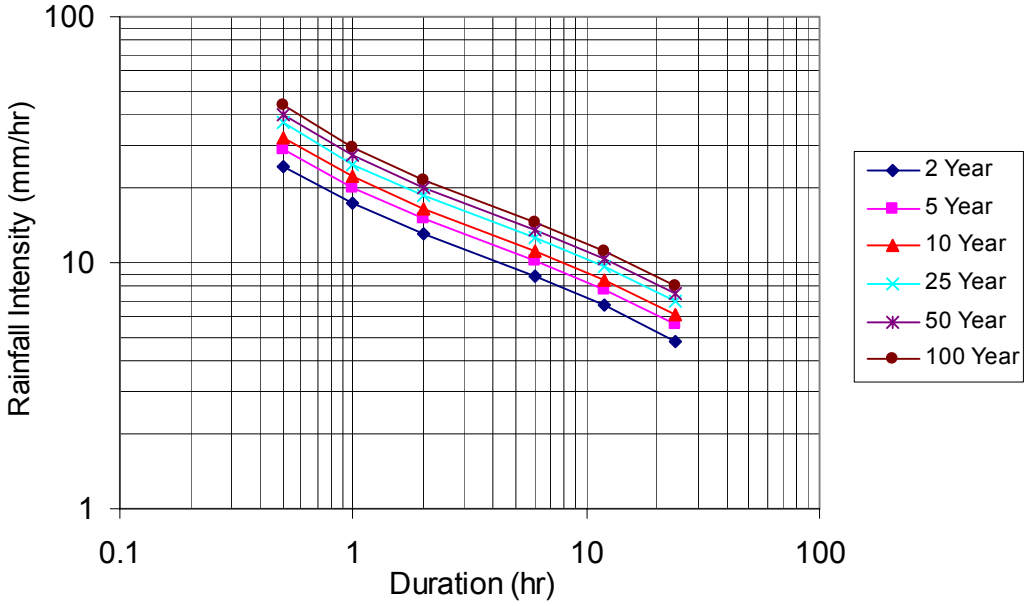

Figure 11. Average rainfall intensity (mm/yr) versus duration (hr) for the six return periods. Rainfall intensity is averaged over all 13 rain gauges in the network.

The rainfall intensity values for each rain gauge and the average rainfall intensities across the network were as expected. Rainfall intensity increases with increasing return period and decreasing duration. Thus, the highest rainfall intensities are for short durations and long return periods while the lowest rainfall intensities are for long durations and short return periods. The highest estimated rainfall intensity is 61 mm/hour for the 30-minute duration, 100-year return period at Thompson Creek. The lowest estimated rainfall intensity is 4 mm/hour for the 2-year return period, 24-hour duration period at six rain gauges. On average, the highest estimated rainfall intensity is 44 mm/hour for the 30-minute duration, 100-year return

period and the lowest is 5 mm/hour for a 2-year return period, 24-hour duration.

The rainfall intensity values in Table 8 can be used to estimate the magnitude of rainfall intensity that can be expected for short and long durations and for frequent and infrequent return periods. For example, a 24-hour duration, or daily rainfall, is a common length of time to compare rainfall intensities or amounts. The 24-hour rainfall intensity for a 2-year return periods is 5 mm/hour and increases to 7 mm/hour for a 25-year return period. This means that for the central Oregon Coast Range there is a 50 percent chance that 120 mm (4.7 inches) of rain will fall in a 24-hour period in any given year but only a 4 percent chance that 168 mm (6.6 inches) will fall in any 24-hour period.

Hourly rainfall is often used for comparisons of short duration rainfall intensities. For the data from the central Oregon Coast Range the 2-year, 1-hour rainfall intensity is 17 mm/hour and the 25-year, 1-hour duration intensity is 25 mm/hour. This means that there is a 50 percent chance of seeing 17 mm (0.7 inches) of rain in one hour in any given year but only a 4 percent chance of seeing 25 mm (1 inch) in one hour.

The variability of the rainfall intensities across the rain gauge network is remarkably stable. The coefficient of variation ranges from a low of 20 percent at the low return period, longer durations to a high of 40 percent at the high return period, shorter durations (Table 8). The

coefficient of variation is 20-25 percent for 75 percent of the data. The coefficient of variation is greater than 25 percent only for the 30-minute duration data and the 25, 50, and 100-year return periods for the 1-hour data. Other than these short duration and/or high return period data, the variability in rainfall intensity across the network is stable.

In addition to the average rainfall intensity values, the maximum values of rainfall intensity are also of interest. The maximum rainfall intensity values range from a high of 61 mm/hour for the 100-year return period, 30 minute duration to a low of 8 mm/hour for the 2-year return period, 24-hour duration. The 24-hour duration goes up to 11 mm/hour for the 25-year return period. The 1-hour duration rainfall intensities range from 23 mm/hour for the 2-year return period to 33 mm/hour for the 25-year return period. This means that the maximum 24-hour rainfall amount that has a 50 percent chance of occurring in any given year is 192 mm (7.7 inches) and the maximum 24-hour rainfall amount that has a 4 percent chance of occurring in any given year is 246 mm (15.6 inches). For the shorter durations, the maximum 1-hour rainfall amount that has a 50 percent chance of occurring in any given year is 23 mm (0.9 inches) and the maximum 1-hour rainfall amount that has a 4 percent chance of occurring in any given year is 33 mm (1.3 inches). Maximum rainfall intensities are listed in Table 9 and the IDF-curve is shown in Figure 12.

Table 9. Maximum rainfall intensity (mm/hr) estimated for the six return periods and six durations for all 13 rain gauges in the network.

	30 minute	1 hour	2 hour	6 hour	12 hour	24 hour
2 year	32	23	17	13	10	8
5 year	39	26	20	15	12	9
10 year	44	29	22	17	13	10
25 year	51	33	25	19	15	11
50 year	56	36	27	20	16	12
100 year	61	38	29	22	17	13

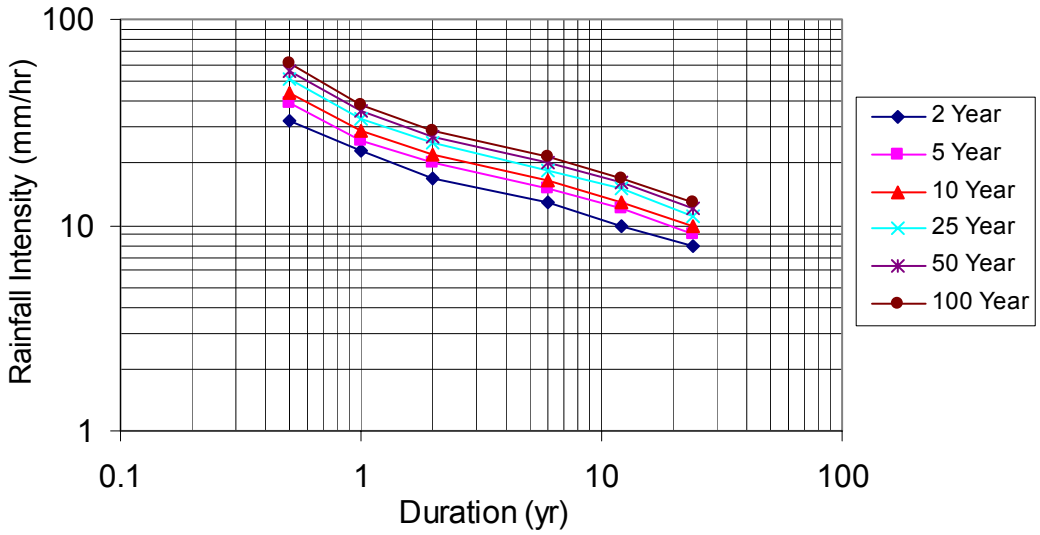

Figure 12. A graph of maximum rainfall intensity (mm/hr) versus duration for the six return periods for all 13 rain gauges in the network.

Spearman Rank Correlation

The Spearman Rank Correlation method was used to determine if there were statistically significant patterns in the relative rank of rainfall

intensities estimated for each duration and return period. This method was used because it is a nonparametric method and only tests the relative rank and not the numeric values of the rainfall intensities.

The original and adjusted Coefficient of Concordance (W), the calculated F_{SN} and the tabular F values at $\alpha = 0.05$ and 0.01 for the durations of rainfall intensities are listed in Table 10.

Table 10. Values of Coefficient of Concordance (W), and F-statistics as a result of the Spearman Rank Correlation method for durations for all 13 rain gauges.

Duration	W	Wadj	F_{Sn}	$F_{1\%}$	$F_{5\%}$
0.5 hour	0.937	0.937	73.77	2.55	1.95
1 hour	0.974	0.974	187.20	2.55	1.95
2 hour	0.968	0.967	148.49	2.55	1.95
6 hour	0.863	0.863	31.41	2.55	1.95
12 hour	0.825	0.825	23.56	2.55	1.95
24 hour	0.697	0.697	11.48	2.55	1.95

The test statistics shows that among the different return periods, the relative rank of rainfall intensity for a given duration and rain gauge was highly statistically significant. In other words, the rain gauge location that had the highest rainfall intensity for the 1-hour duration and the 2-year return period would also have the highest rainfall for the 1-hour duration and the 100-year return period. The tabular values of the relative rank of

individual rain gauges by return period for the six durations are listed in Appendix C (Tables C1 to C6).

In addition to durations, the original and adjusted Coefficient of Concordance (W), and the calculated and tabular F values for $\alpha = 0.05$ and 0.01 for the rainfall intensity data by return period are shown in Table 11.

Table 11. Values of Coefficient of Concordance (W), and F-statistics as a result of the Spearman Rank Correlation method for return period for all 13 rain gauges.

Return Period	W	W_{adj}	F_{Sn}	$F_{1\%}$	$F_{5\%}$
2 year	0.752	0.752	15.14	2.55	1.95
5 year	0.703	0.702	11.80	2.55	1.95
10 year	0.741	0.741	14.29	2.55	1.95
25 year	0.759	0.759	15.71	2.55	1.95
50 year	0.744	0.743	14.48	2.55	1.95
100 year	0.741	0.741	14.30	2.55	1.95

The test statistics show that among the different return periods, the relative rank of rainfall intensity for a given duration and rain gauge location was highly statistically significant. In other words, a rain gauge location that had the highest rainfall intensity for a 2-year, 1-hour duration would likely have the highest rainfall intensity for a 2-year, 24-hour duration. The same would be true for a longer return period. The tabular values of the relative rank of individual rain gauge locations for the six return periods are listed in Appendix D (Tables D1 to D6).

The relative ranks of the rain gauges averaged over the durations and return periods are shown in Table 12.

Table 12. Values for the relative rank of each rain gauge averaged over all durations and return periods.

Gauge	Duration	Return Period
South Creek	1	1
Indian Creek	2	2
Sweet Creek	3	3
Thompson Creek	4	4
Panther Creek	5	5
Wassen Creek	6	6
Ryder Creek	7	8
Lobster Creek	8	9
Smith Creek	9	7
Cascade Creek	10	10
Mill Creek	11	11
Johnson Creek	12	13
Kirk Creek	13	12

The four rain gauge locations with the highest rainfall intensities are South Creek, Indian Creek, Sweet Creek, and Thompson Creek. The four rain gauges locations with the lowest rainfall intensities are Cascade Creek, Mill Creek, Johnson Creek, and Kirk Creek. The remaining five rain gauge locations are intermediate in rainfall intensities. While these relative rankings hold in general, they may change subtly for individual durations and return periods. For example, at the durations of 6, 12, and 24-hours, Indian Creek is ranked as the number one rain gauge location however, for the 30-minute duration, Thompson Creek is the highest ranked rain gauge

location and Indian Creek is ranked fourth. For the 1-hour duration, South Creek is ranked as the number one rain gauge location, Thompson Creek is ranked as the second, and Indian Creek is ranked third. While the relative rank for any rain gauge location may change slightly from duration to duration, the general pattern is consistent.

Results from the Spearman Rank Correlation show that there are distinct and statistically significant trends in the distribution of rainfall across the central Oregon Coast Range. Rain gauge locations with high rainfall intensities tend to be high regardless of rainfall duration or return period. Conversely, rain gauges with low rainfall intensities tend to be low across durations and return periods.

Rainfall Frequency Analysis

The results reported and verified using the Spearman Rank Correlation method can, to some degree, be verified visually, at least for the different rainfall durations, by observing the graphs of the frequency analyses shown in Figure 13 to Figure 18. These figures show rainfall intensity versus return period for all 13 rain gauges by rainfall duration. The longer durations, 6, 12, and 24-hours show a clearly different pattern than the shorter duration, 30-mintues, 1, and 2-hours. For the longer durations, the cumulative frequency distributions have almost identical slopes and the lines appear to be parallel to each other. The lines very

rarely cross meaning that the rank of the rain gauge locations for low return periods is the same as the rank for the high return periods or, the rankings don't change across return periods.

Conversely, at the shorter durations the cumulative frequency distribution lines do not necessarily have the same slope and they do cross. This means that the rankings at a low return period will not necessarily be the same rankings at the high return period. But while there is some shifting in rank for different durations, the rain gauge locations stay within their relative rankings. In other words, the top four rain gauge locations stay in the top four rankings as do the bottom four and the middle five. A rain gauge location did not move from a bottom four ranking at low return periods to a top four ranking at high return periods or vice versa. The relative rankings of the groups of rain gauge locations remained consistent. This behavior can also be observed in Figures 13 to 18.

The behavior described above can be easily viewed by observing the relative rank of the Indian Creek rain gauge location in the frequency analysis graphs. In Figures 13 to 18 at longer duration the Indian Creek location is easily and clearly ranked at the number one rain gauge location with the highest rainfall intensities at each return period. Recall that the Indian Creek rain gauge location was also the highest ranked rain gauge for the very long durations that included monthly and annual rainfall. At the shorter durations, the Indian Creek rain gauge location is no longer the

highest ranked rain gauge location and in each case the top ranking shifts between two rain gauge locations between the low return periods and the high return periods. For the 30-minute and 1-hour durations the top ranking shifts from the South Creek rain gauge location to the Thompson Creek rain gauge location. For the 2-hour duration the shift is from the Indian Creek rain gauge location to the South Creek rain gauge location.

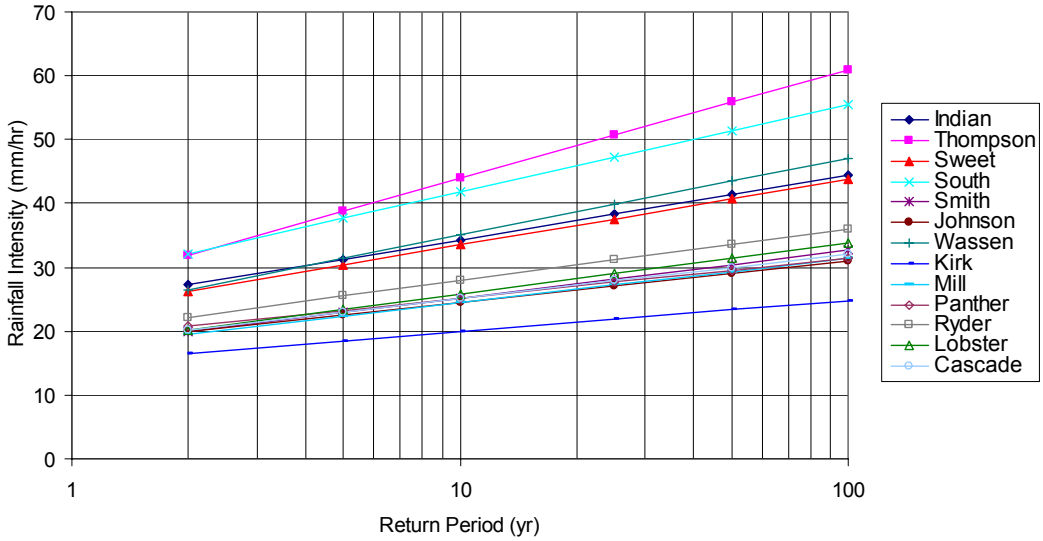

Figure 13. Rainfall intensity (mm/hr) versus return period for all 13 rain gauge locations for the 30-minute duration.

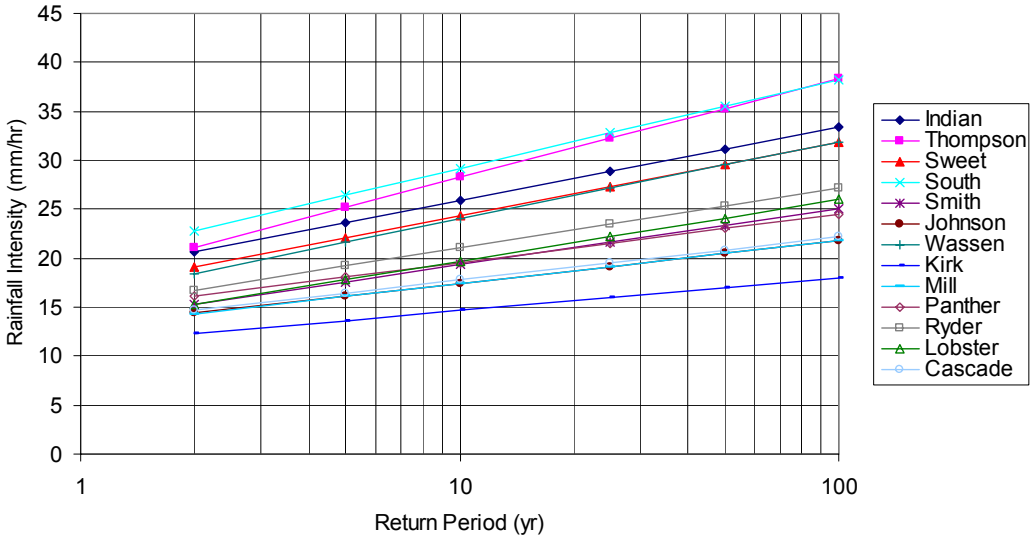

Figure 14. Rainfall intensity (mm/hr) versus return period for all 13 rain gauge locations for the 1-hour duration.

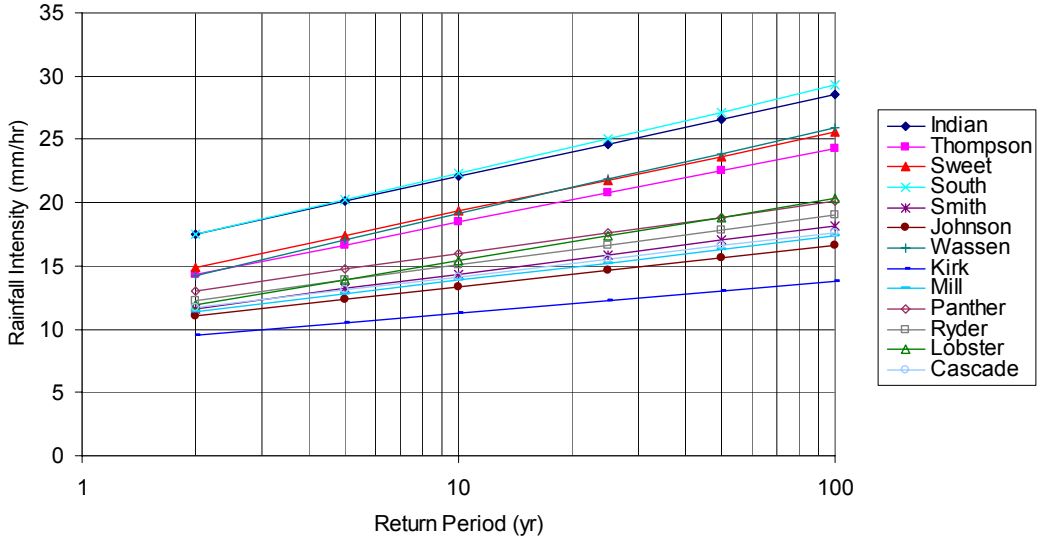

Figure 15. Rainfall intensity (mm/hr) versus return period for all 13 rain gauge locations for the 2-hour duration.

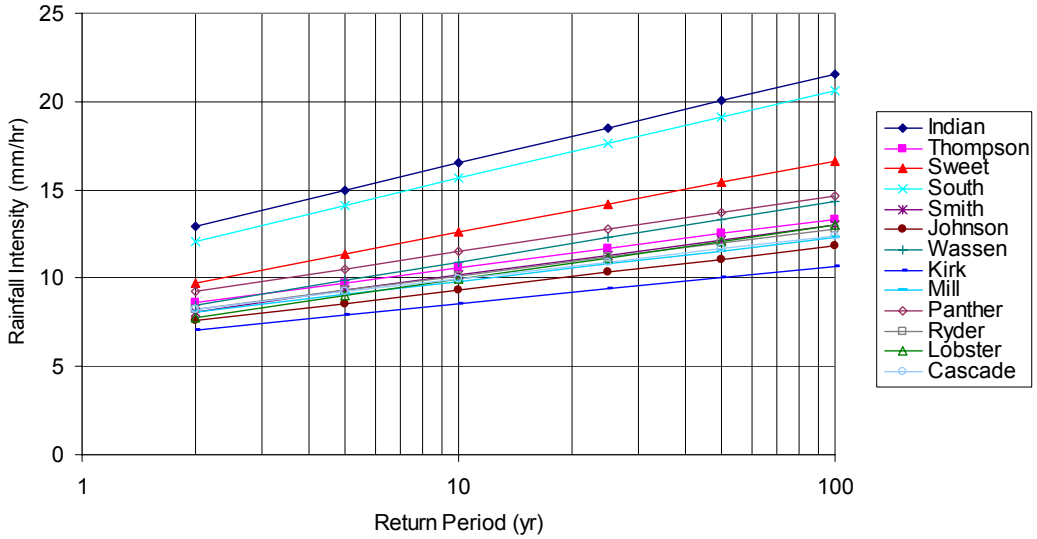

Figure 16. Rainfall intensity (mm/hr) versus return period for all 13 rain gauge locations for the 6-hour duration.

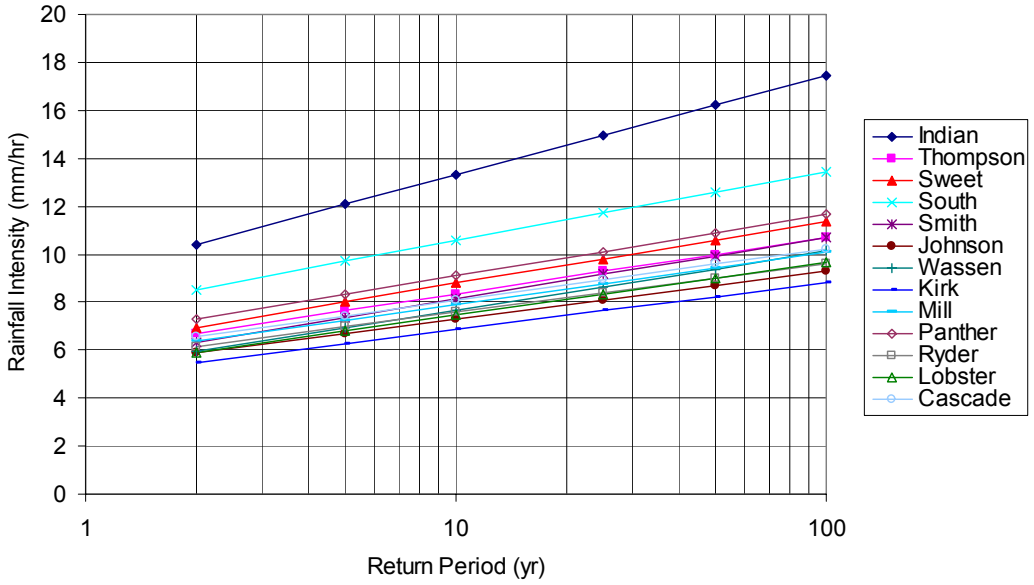

Figure 17. Rainfall intensity (mm/hr) versus return period for all 13 rain gauge locations for the 12-hour duration.

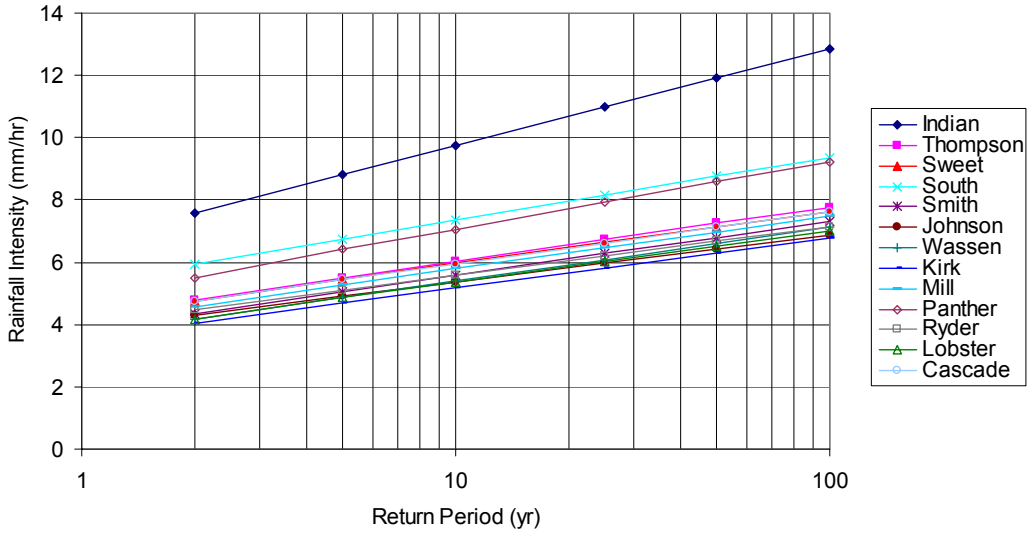

Figure 18. Rainfall intensity (mm/hr) versus return period for all 13 rain gauge locations for the 24-hour duration.

Rainfall Intensity versus Elevation

There has always been an interest in trying to explain the cause of the variability that has been observed in the rainfall intensity data across the study area at the different durations and intensities. In mountainous terrain, elevation has long been shown to be and is considered to be a primary explanatory parameter for this variability (Daly et al. 1998). In the first, preliminary analysis of these data, Surfleet (1997) showed that elevation was not a good predictor of rainfall intensity, especially at shorter durations. This result has been observed in other studies (Cooper 1967) and therefore was not unexpected in this one. The relationship between rainfall and elevation was also investigated in this study to take advantage of the more robust data set available now as opposed to when Surfleet

(1997) made the same investigations. The lack of a relationship between elevation and MAP has already been reported.

To investigate the relationship between rainfall intensity and elevation, scatter diagrams were prepared and least squares regression was performed on rainfall intensity and elevation for each unique combination of duration, and return period, which resulted in 36 separate analyses. In all 36 of the analyses, there is not a single statistically significant relationship. In addition, the R^2 for all of the relationships ranged from a low of 0.5 percent to a high of 11 percent, which means that even if the relationships were statistically significant they would not be statistically meaningful. These results indicate that for the 13 rain gauge locations studied for durations less than 24 hours there was no relationship between rainfall intensity and elevation.

Figure 19 and Figure 20 were included to show the nature of the scatter diagrams and least squares regressions for the rainfall intensity versus elevation data. Figure 19 shows the relationships for the 2-year return period rainfall intensities for short duration, 1-hour, and long duration, 24-hour. Figure 20 shows the relationships for the 25-year return period rainfall intensities for the same durations, 1-hour and 24-hour. These graphs are representative of the rainfall intensity versus elevation data for all return periods and durations.

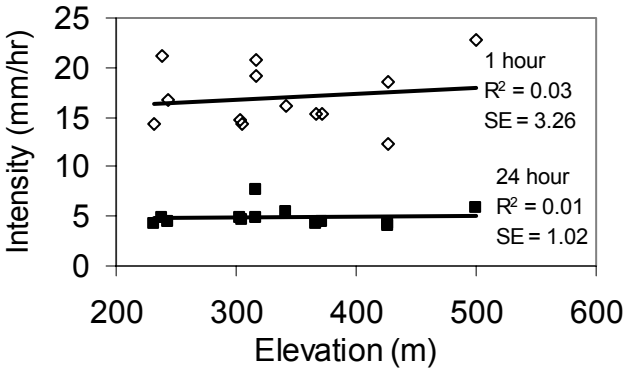

Figure 19. Relationship between elevation (m) and rainfall intensity (mm/hr) for the 2-year, 1-hour and 24-hour durations.

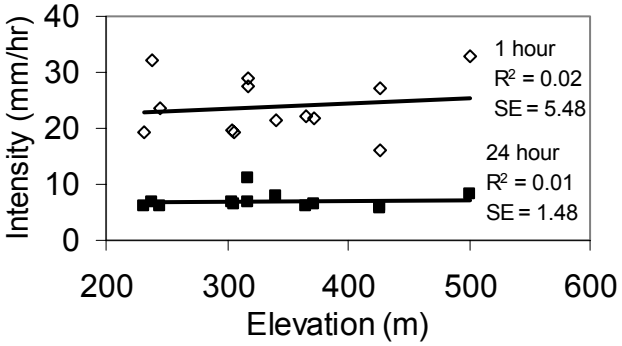

Figure 20. Relationship between elevation (m) and rainfall intensity (mm/hr) for the 25-year, 1-hour and 24-hour durations.

Isohyetal Maps of Rainfall Intensity

The rainfall intensity data that has been analyzed, graphed, and reported in this thesis is presented as a series of isohyetal maps shown in Appendix E (Figures E1 to E36). The maps show lines of constant rainfall

intensity across the study area represented by the 13 rain gauges. There is an isohyetal map for every unique combination of rainfall duration and return period. The maps show the same trend in results that was observed using the Spearman Rank Correlation method and the graphs showing frequency analysis, however in this case the data is presented in a spatial form.

To investigate the spatial patterns of rainfall intensity in a little more detail, low return period and high return period rainfall as well as short duration and long duration rainfall will be presented and discussed. Low return period rainfall is characterized by the 2-year return period and high return period rainfall by the 25-year return period. The short duration rainfall will be for 1-hour and the long duration rainfall will be for 24-hours thus hourly and daily rainfall will be observed in more detail.

For all return periods (2 to 100-years) at longer durations (24-hours) the isohyetal maps are dominated by a high value of rainfall intensity for the Indian Creek rain gauge. This is shown for the 25-year return period in Figure 21. Again, this result is consistent with what was observed in the frequency analysis graphs (Figure 13 to 18). The maximum estimated rainfall intensity for the 25-year, 24-hour storm for Indian Creek is 11 mm/hr. For the same duration and return period, all of the other rain gauge locations have rainfall intensities estimated at 6, 7, or 8 mm/hr. One of the rain gauge locations with the minimum rainfall intensity, 6 mm/hr, is the

Lobster Creek rain gauge, which is directly adjacent to the Indian Creek rain gauge. The Lobster Creek rain gauge is located approximately 15 km to the north and east of Indian Creek and is 49 m higher in elevation (see Figure 2).

These results illustrated on the isohyetal map in Figure 21 indicate that for a 25-year return period, 24-hour storm in the Oregon Coast Range the daily intensity, or total daily rainfall, can decrease by 50 percent within a distance of approximately 15 km. This is illustrated by the pattern of concentric rings of constant rainfall intensity around the Indian Creek rain gauge location. This effect can be roughly translated to return period terms. The frequency analysis for the 24-hour rainfall is show in Figure 18. If the Indian Creek frequency analysis is used as an index, then the data show that the rainfall can go from a 25-year return period storm to a sub annular storm over the distance of 15 km. Conversely, if the Lobster Creek frequency analysis is used as an index, the rainfall can go from a 25-year return period event to well over a 100-year return period event, again, within 15 km. This is an index of how variable the rainfall intensities are in space.

The isohyetal map showing the 2-year return period, 24-hour rainfall (Figure 22), or the more commonly occurring rainfall, shows the same pattern as the 25-year return period, 24-hour rainfall with a high value of rainfall intensity at the Indian Creek rain gauge location. The maximum

intensity estimated for the Indian Creek location for the 2-year, return period 24-hour duration is 8 mm/hr. Two other rain gauge locations have an estimated maximum intensity of 6 mm/hr and the remaining rain gauges are either 5 or 4 mm/hr. One of the rain gauge locations that has an estimated maximum rainfall intensity for the 2-year, 24-hour rainfall of 4 mm/hr is the Lobster Creek rain gauge location, which is directly adjacent to the Indian Creek location. Thus, at the 2-year return period level, the rainfall intensity can decrease by half (or double depending on your frame of reference) within 15 km. Again, these values can be translated into effects on return period. If the Indian creek frequency analysis is used as an index, the rainfall intensity goes from a 2-year return period event to a very common sub annular event within 15 km. Conversely, if the Lobster Creek frequency analysis is used as an index the rainfall intensity goes from a 2-year return period event to approximately a 100-year return period event within 15 km. Again, these values index how variable rainfall intensity is in space even for regularly occurring storms.

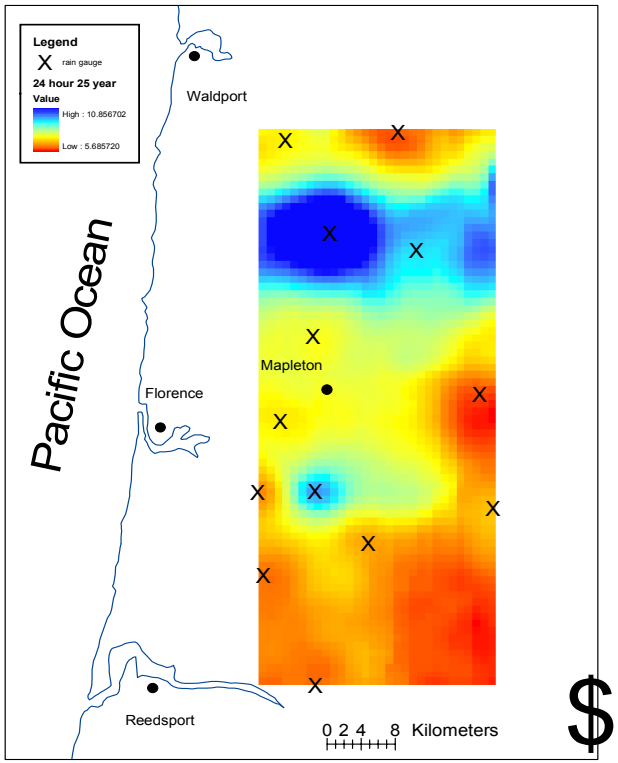

Figure 21. Isohyetal map of the 25-year return period, 24-hour rainfall in mm/hr.

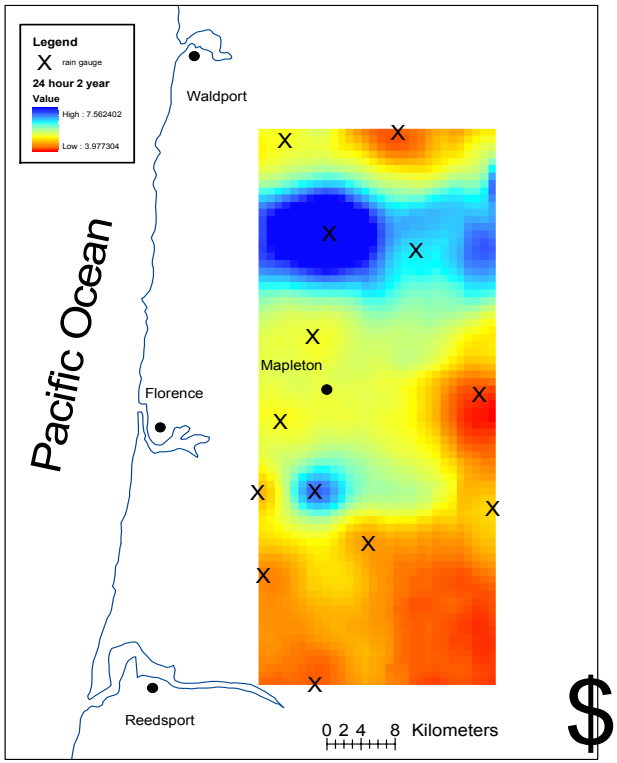

Figure 22. Isohyetal map of the 2-year return period, 24-hour rainfall in mm/hr.

These same observations can be made for the shorter duration rainfall (30-minutes and 1-hour). The isohyetal maps that illustrate these durations are dominated by a high value at the South Creek rain gauge location. This rainfall intensity pattern around the South Creek rain gauge is not as pronounced as the rainfall intensity pattern around the Indian Creek rain gauge for the longer durations (i.e. 24-hours). However, it is a consistent pattern and it is evident throughout the return periods (2-year to 100-year). For the 25-year, 1-hour rainfall (Figure 23) the maximum intensity estimated is for the South Creek rain gauge location and is approximately 33 mm/hr. The 25-year, 1-hour rainfall intensities estimated for the balance of the rain gauge locations ranged from 16 to 32 mm/hr. The minimum is 16 mm/hour and it is estimated for the Kirk Creek rain gauge location; however Kirk Creek is approximately 24 km northeast of the South Creek location. Thus the difference in the rainfall intensities could be due to a significant rain shadow effect. Another rain gauge that is directly adjacent to the South Creek rain gauge is the Ryder Creek rain gauge that is approximately 8 km west of the South Creek rain gauge and is 256 m lower in elevation. The 25-year, 1-hour rainfall intensity estimated for the Ryder Creek rain gauge location is 24 mm/hour, which is representative of the balance of the rain gauges in the study area. Thus, the value of the 25-year, 1-hour rainfall is reduced by one forth over the distance of approximately 8 km. Once again, if this difference in rainfall

intensity is expressed in terms of return period, the difference is substantial. If the South Creek rain gauge frequency analysis is used as an index, the estimated rainfall intensity goes from a 25-year return period rainfall at the South Creek rain gauge to about a 2-year return period rainfall at the Ryder Creek rain gauge. Conversely, if the Ryder Creek rain gauge frequency analysis is used as an index then the estimated rainfall intensity goes from a 25-year return period rainfall at the Ryder Creek rain gauge to a significantly greater rainfall at the South Creek rain gauge well in excess of a 100-year return period rainfall.

The pattern for the estimated rainfall intensity for the 2-year, 1-hour rainfall (Figure 24) is very similar to the pattern for the 25-year, 1-hour rainfall (Figure 23). The rain gauge location with the highest value of estimated rainfall intensity with the concentric circles a bit broader, but the basic pattern is still very much in evidence. The maximum estimated rainfall intensity at the South Creek rain gauge is 23 mm/hour. The minimum value is 12 mm/hour and again that is at the Kirk Creek rain gauge location that is northeast of the South Creek rain gauge. The Ryder Creek rain gauge location, which is directly adjacent to the South Creek rain gauge, had an estimated rainfall intensity of 17 mm/hour. This value is representative of the values estimated for the balance of the rain gauge locations that ranged from 12 to 21 mm/hour. The Ryder Creek rain gauge location is approximately 7.5 km west of the South Creek rain gauge

location. The Ryder Creek rain gauge location is 256 m lower in elevation than the South Creek rain gauge location. In this comparison the estimated rainfall intensity is reduced by about one third over a distance of 7.5 km. On the South Creek frequency analysis, 17 mm/hour is a very common, sub annular event while on the Ryder Creek frequency analysis, 23 mm/hour becomes a 25-year return period rainfall. So, like the other comparisons discussed above even for a common, hourly rainfall, the rainfall intensity can change rather dramatically over a short distance.

In summary, the presentation of previous results has pointed out the variability of the rainfall intensity values. They are highly variable for any given unique combination of return period and duration. The isohyetal maps are of value to illustrate the spatial scale of that variability. The maps and the accompanying discussion show that the rainfall intensity values can be highly variable within short distances. Rainfall intensity values can be roughly doubled or cut in half over a distance of 10 to 15 km. This generalization is true for low or high return period rainfall intensities and for short and long durations. This observation can have significant consequences for how we think about rainfall intensity and the occurrence of landslides.

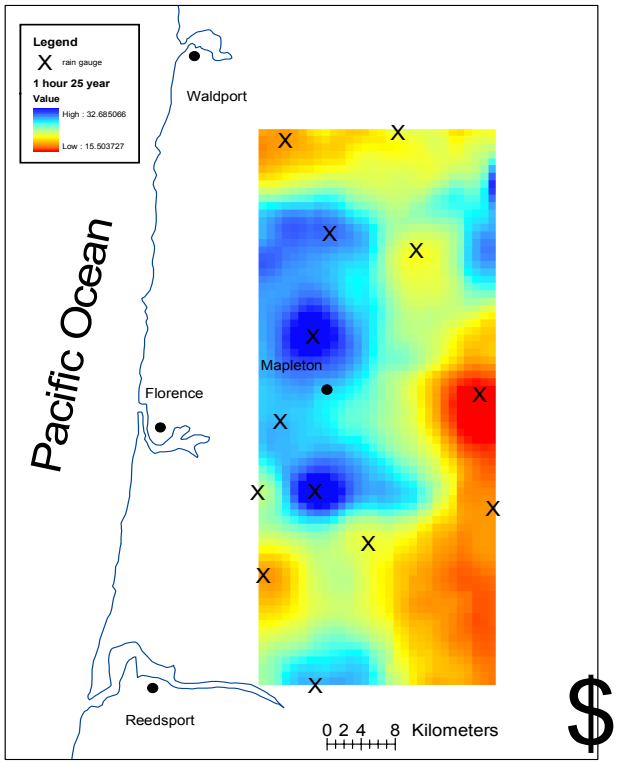

Figure 23. Isohyetal map of the 25-year return period, 1-hour rainfall in mm/hr.

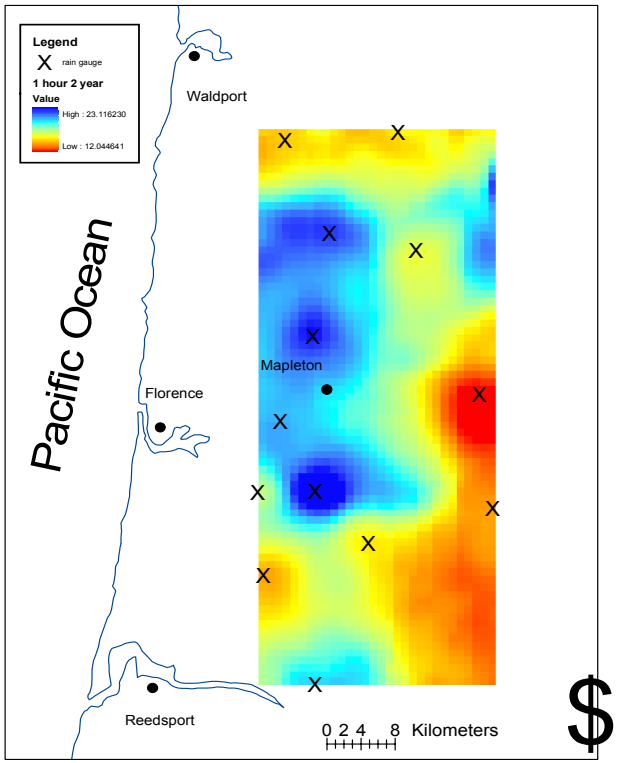

Figure 24. Isohyetal map of the 2-year return period, 1-hour rainfall in mm/hr.

Antecedent Precipitation Index

In addition to the values of rainfall intensity that were estimated for each unique combination of return period, duration, and rain gauge location, API values were also estimated for each return period and rain gauge location. Values of API were calculated for all of the storms that were included in the partial series frequency analysis for rainfall intensities. Then partial series frequency analysis was completed for the API for all of the rain gauge locations. The data from these partial series analysis are listed in Table 13 and the frequency analysis for API for all the rain gauge locations is shown in Figure 25.

Table 13. Values of the estimated, average, and coefficient of variation for antecedent precipitation index (mm) for all gauges for all return periods.

Gauge	2 year	5 year	10 year	25 year	50 year	100 year
Indian Creek	112	147	174	209	235	262
Thompson Creek	114	139	157	181	200	218
Sweet Creek	109	128	143	162	176	190
South Creek	85	113	134	162	183	204
Smith Creek	57	76	91	110	125	139
Johnson Creek	80	99	113	132	147	161
Wassen Creek	76	96	111	132	147	162
Kirk Creek	84	103	117	136	150	165
Mill Creek	99	118	132	151	165	179
Panther Creek	123	146	164	188	206	223
Ryder Creek	84	102	115	133	147	161
Lobster Creek	77	96	110	129	143	158
Cascade Creek	76	98	115	137	154	171
Average	91	112	129	151	167	184
CV (%)	21	19	18	18	18	18

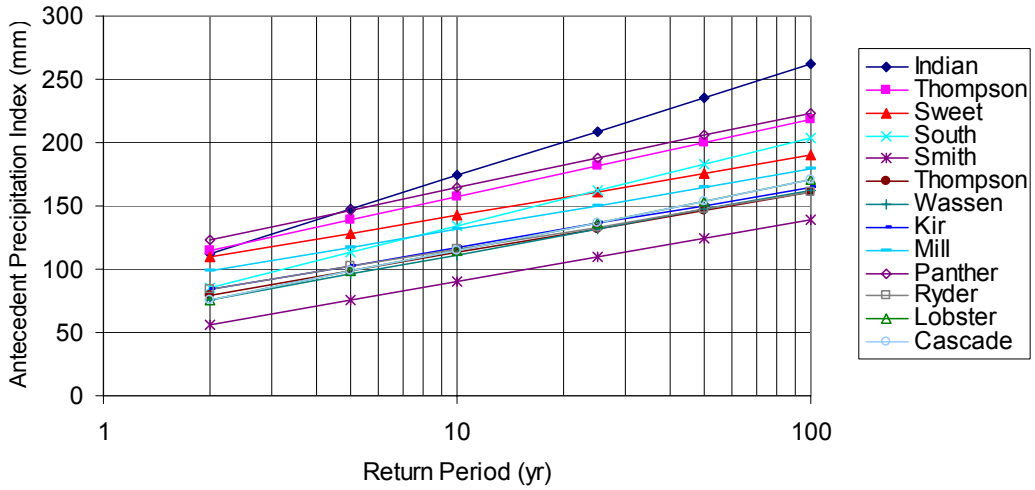

Figure 25. Gumbel distribution for trends in the antecedent precipitation index (mm) for all gauges.

API values were averaged across all 13 rain gauge locations for the study site. The average estimated API value for the 2-year return period is 91 mm (3.6 inches) and ranges from a high of 123 mm (4.8 mm) at the Panther Creek rain gauge location to a low of 57 mm (2.2 inches) at the Smith Creek rain gauge location. For the 25-year return period, the average estimated API value is 151 mm (5.9 inches) and ranges from a high of 209 mm (8.2 inches) at the Indian Creek rain gauge location to a low of 110 mm (4.3 inches) at the Smith Creek rain gauge location. The coefficient of variation for the average API values is approximately 20 percent across all of the return periods and is remarkably consistent (18 to 21 percent).

The Spearman Rank Correlation method was used to investigate if there were consistent patterns across the return periods in the estimated API values. The results indicate that there is a pattern in API values across the study site (Table 14) and the pattern is considered highly statistically significant (Table 15.).

Table 14. Spearman Rank Correlation of the antecedent precipitation index (mm) for all 13 rain gauges.

	Gauge												
Return Period	Indian	Thompson	Sweet	South	Smith	Johnson	Wassen	Kirk	Mill	Panther	Ryder	Lobster	Cascade
2 year	3	2	4	6	13	9	12	7.5	5	1	7.5	10	12
5 year	1	3	4	6	13	9	12	7	5	2	8	12	10
10 year	1	3	4	5	13	10	11	7	6	2	8.5	12	8.5
25 year	1	3	4.5	4.5	13	11	11	8	6	2	9	12	7
50 year	1	3	5	4	13	10	10	8	6	2	10	12	7
100 year	1	3	5	4	13	11	9	8	6	2	11	12	7
Sum	8	17	27	30	78	59	64	46	34	11	54	70	51
Rank	1	3	4	5	13	10	11	7	6	2	9	12	8

Table 15. Values of Coefficient of Concordance (W), and F-statistics as a result of the Spearman Rank Correlation method for antecedent precipitation index for all rain gauges.

Return Period	W	W_{adj}	F_{Sn}	$F_{1\%}$	$F_{5\%}$
All	0.951	0.951	96.30	2.55	1.95

These results can also be seen in the frequency analysis for API in Figure 25. Figure 25 also shows how the rain gauge locations are distributed relative to each other for all the return periods. For the most part, the results of the API analysis mimic the results of the analysis with the rainfall intensities. The rain gauge locations with the highest API values, (Indian, Panther, Sweet, and South, and Thompson Creek), are the rain gauge locations that had the highest rainfall intensities. Conversely, those rain gauge locations that had the lowest rainfall intensities (Kirk, Mill, Johnson, and Cascade Creek) also had the lowest API values. However, the overlap is not 100 percent.

As might be expected, the spatial patterns of API across the study site are also similar to the spatial pattern of rainfall intensity. Isohyetal maps for API are in Appendix E (Figures E1 to E6). At high return periods (25 year) the map of API (Figure 26) is dominated by a high value at the Indian Creek rain gauge location. This high value decreases within the first set of adjacent rain gauges within 10 to 15 km of the Indian Creek rain gauge. For the 25-year return period, the majority of the rain gauge locations have an API between 130 and 160 mm. Thus the high value of 209 mm at the Indian Creek rain gauge falls off to an average background value of 130 to 160 mm within 10 to 15 km.

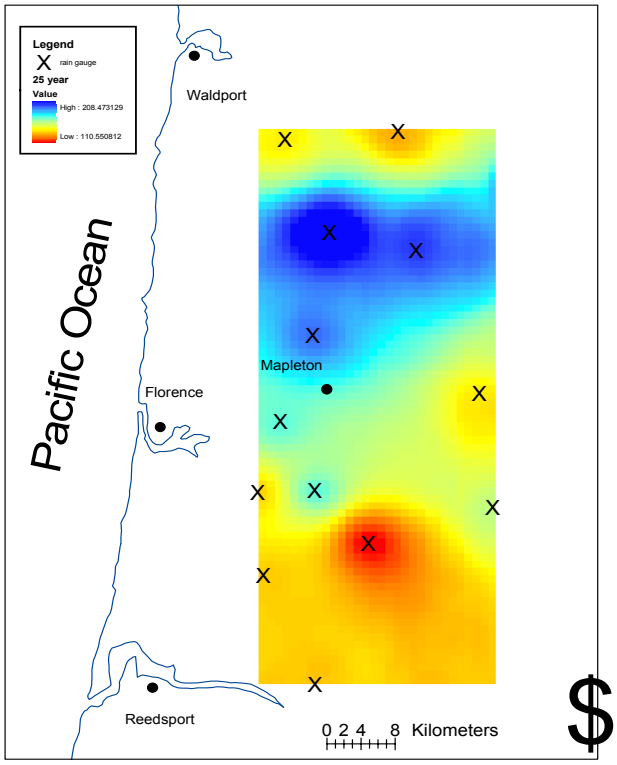

Figure 26. Isohyetal map of the 25 year return period antecedent precipitation index (mm).

Unlike the pattern for low return period rainfall intensities, the pattern for low return period API mimics the pattern for the high return period API. Figure 27 shows the spatial distribution of the 2-year return period API values. These values are centered in the north part of the study area except in this case the high value of API is at the Panther rain gauge location. The API values decrease to a background value of between 70 and 90 mm for the rest of the rain gauge network with 10 to 15 km of the Panther Creek rain gauge location.

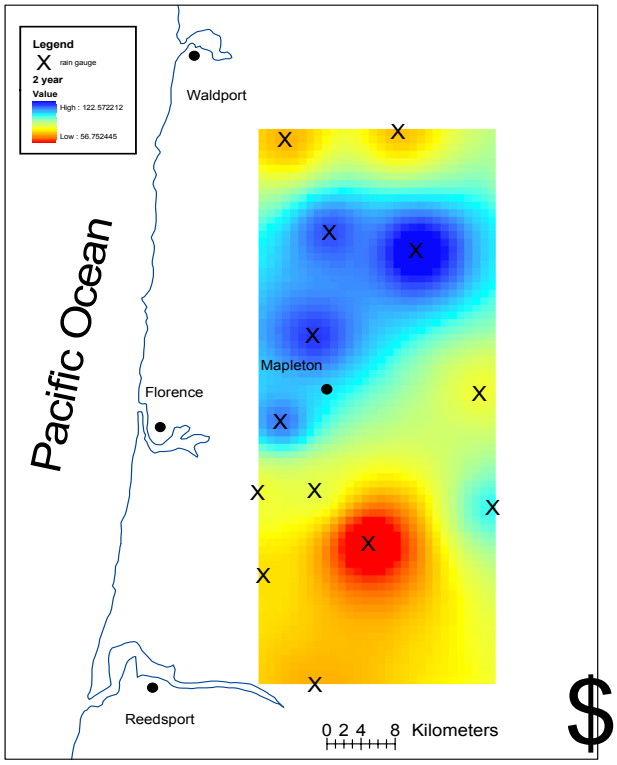

Figure 27. Isohyetal map of the 2 year return period antecedent precipitation index (mm).

Thus, API values, like the rainfall intensity values, are highly variable across the landscape with a coefficient of variation of approximately 20 percent across the study area at any given return period. There is a definite spatial pattern of API that is consistent and statistically significant. The spatial pattern is dominated by a high value in the north of the study area at either the Indian Creek or the Panther Creek rain gauge location, and decreases to an average value over the rest of the study area. The decrease in API values take place over the distance of 10 to 15 km.

Effect of the February 1996 Storm

During the 14 years of record that rainfall data was collected for this study area there were three large storms. The statistics for these three storms were reported earlier. Without a doubt the largest storm during the period of record was the February 3-9th, 1996. This storm caused widespread, regional flooding and was the dominant landslide producing storm during the period of record.

The primary data analysis method for the rainfall intensity data is frequency analysis. All observations and results from the data follow the frequency analysis of the data and frequency analysis can be susceptible to influence by extreme outliers. Thus, it is worthwhile to consider whether the pattern of the rainfall data that has been observed and reported in this thesis is in fact a regional pattern that could be expected to be replicated over time or whether it represents the pattern of rainfall that occurred during the February 1996 storm.

The pattern of rainfall intensities observed is, most likely, a regional pattern and it should be and will be replicated over time. The evidence for such a supposition is twofold. The first evidence is that the pattern of rainfall intensities that occurs at low return period events is identical to the pattern that occurs at the high return periods. Recall that the Spearman Rank Correlation results showed that the pattern of rainfall intensity that occurred for a given rainfall duration was consistent across return periods.

The patterns changed for durations but not for return periods. Thus, for the 24-hour duration the pattern of rainfall intensities for the 5 and 100-year return periods was the same pattern as for the 2 and 5-year return periods. This same observation holds for the rainfall intensity patterns observed for the 1-hour duration at the 5- and 100-year return periods as well as the 2 and 5-year return periods.

A case can be made that for the extreme or high return periods, such as the 50 and 100-year return periods, rainfall intensities are undoubtedly affected and perhaps dominated by the rainfall intensities during the extreme events, i.e. the 1996 storm. The same case can not be made for the rainfall intensities associated with the more common, or lower, 2 and 5-year return period rainfall intensities. With 14 years of rainfall data, the rainfall intensities estimated for the 10-year and less return period rainfall should represent the regional pattern of rainfall intensity. Because the high return period rainfall intensities reflect this same pattern, there is no reason, at this time, to expect the high return period rainfall intensities will change with a larger data set and more extreme rainfall events.

The second reason is the spatial pattern of rainfall accumulation for two of the largest storms during the period of record. There is no doubt that the spatial pattern of rainfall accumulation for the 1996 storm looks very much like the spatial patterns of rainfall intensity that have been

developed (Figure 28). However, the spatial pattern for the December 1995 storm (Figure 29) also looks very much like the spatial pattern of rainfall accumulation for the 1996 storm and the spatial patterns of rainfall intensity. Thus, the February 1996 and the December 1995 storms had spatial patterns of rainfall accumulation that looked the same. So the spatial pattern is not a product of a single extreme event but of at least two large events. There is no reason to believe that the patterns that caused these two extreme events in the 1990's won't cause future extreme events to behave in a similar manner.

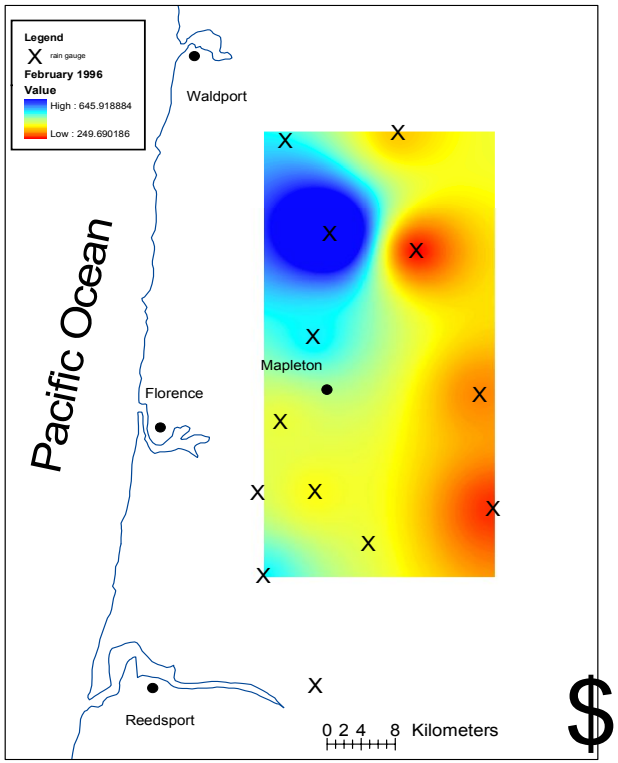

Figure 28. Isohyetal map of the February 1996 storm rainfall totals (mm).

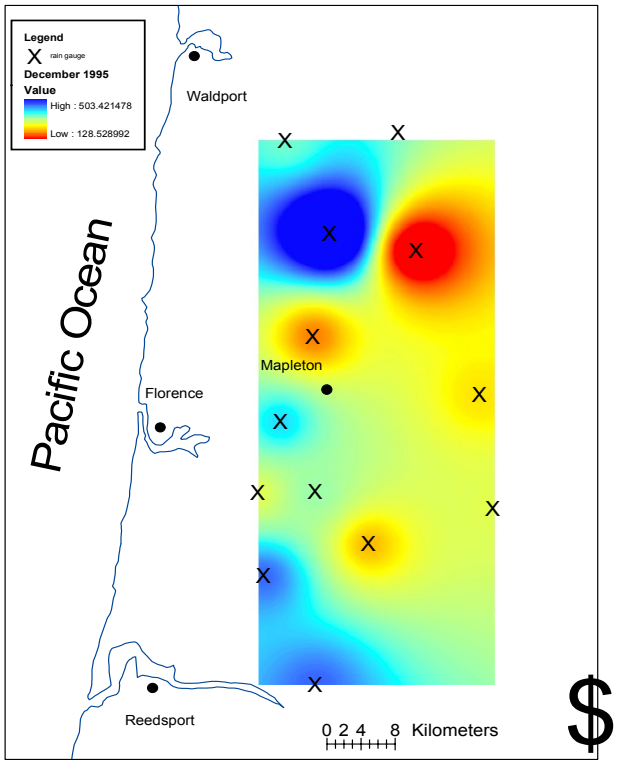

Figure 29. Isohyetal map of the December 1995 storm rainfall totals (mm).

CONCLUSIONS

Rainfall intensity data was collected for the last 14 years from 13 rain gauge locations in the central Oregon Coast Range. A description of the temporal and spatial variability of rainfall intensity is the result of the analysis of these data.

The central Oregon Coast Range has an average MAP of 2049 mm ranging from a high of 2826 mm to a low of 1668 mm. The month with the highest average rainfall is November (375 mm) and 51 percent of the MAP occurs during the months of December, January, and February. Throughout the fourteen year rainfall record three large storms were recorded. In all of these three storms the Indian Creek rain gauge had the largest amount of rainfall and two of the storms have remarkably similar patterns of rainfall distribution.

Rainfall intensity increased with increasing return periods and decreased duration. Rainfall intensities range from a high of 61 mm/hour for the 100-year return period, 30-minute rainfall intensity to a low of 4 mm/hour for the 2-year return period, 24-hour rainfall intensity. The average rainfall intensity for an average regularly occurring daily rainfall intensity (2-year return period, 24-hour duration) was 5 mm/hour, while the average rainfall intensity for an extreme event (25-year return period, 24-hour duration) increased to 7 mm/hour. The average rainfall intensity for a

regularly occurring (2-year return period) hourly rainfall was 17 mm/hour, and increased to 25 mm/hour for an average rainfall intensity for a more extreme event (25-year return period). The variability in rainfall intensity across the study site was remarkably stable with a coefficient of variance of 20 to 25 percent.

Compared to the values for rainfall intensity determined by NOAA (see literature review), the values for rainfall intensities noted in this thesis are higher and have a larger range in values. These new values have the advantage of including several large storms, such as February 1996 and December 1995 and 1998 storms, and allow for an updated data set to be used in areas such as road and drainage design.

The relative rank of the estimated rainfall intensities across all six durations and six return periods was analyzed nonparametrically using the Spearman Rank Correlation method. For duration and return period the relative rank of the rain gauge locations is statistically significant. Thus, there is a definite pattern of rainfall across the study site. The rain gauge locations that receive the most rainfall have the highest rainfall intensities regardless of duration or return period. The top four ranked rain gauge locations are South Creek, Indian Creek, Sweet Creek, and Thompson Creek.

In an attempt to understand the cause for the variability in rainfall across the study area, relationships between rainfall intensity and elevation

were developed. This was a second look at the relationship for data from the rain gauge network. Previously, Surfleet (1997) found there was no significant relationship between rainfall intensity and elevation. The work in this thesis verified these results and found there was no significant relationship between rainfall intensity and elevation for any duration or return period. While values for R^2 increased slightly and ranged from a low of 0.5 percent to a high of 11 percent, the numbers still show that almost none of the variability in rainfall intensity across the study area is explained by elevation.

The spatial distribution of rainfall intensity across the study area for each duration and return period was shown using isohyetal maps. The results mimic the findings of the Spearman Rank Correlation method. The spatial patterns show that at short durations the maximum rainfall intensities occur at the South Creek rain gauge and at long durations the maximum rainfall intensities occur at the Indian Creek rain gauge, and this pattern persists for all return periods. The maximum rainfall intensities (e.g. those surrounding the Indian Creek rain gauge) decline to background values within a distance of 10-15 km.

These findings for the spatial distribution of rainfall intensity are similar to those found by Surfleet (1997). Surfleet (1997) found that for the durations of 2-hours and less, the highest rainfall intensities were at the South Creek and Thompson Creek rain gauge locations, while at durations

of 6-hours and more the highest rainfall intensities were found to be at the Indian Creek and South Creek rain gauge locations. For this thesis, these results remain true. However, the highest rainfall intensities were at the South Creek and the Thompson Creek rain gauge for durations of 30-minute and 1-hour, while the highest rainfall intensities were at the Indian Creek and the South Creek rain gauge locations for durations of more than 2-hours.

In addition to rainfall intensity, API was also analyzed. The Spearman Rank Correlations method shows that there is a statistically significant agreement in rank for API across the return periods. API ranges from a high of 262 mm at the 100-year return period to a low of 57 mm at the 2-year return period. As with rainfall intensity, the coefficient of variance is stable across the study area at 18 to 21 percent. The graph of the frequency analysis and the isohyetal map of API confirm the results of the statistical analysis. The five rain gauge locations with the highest API are Indian Creek, Panther Creek, Sweet Creek, South Creek, and Thompson Creek. These are the same five rain gauge locations that were the top five for rainfall intensity. The Indian Creek rain gauge had the highest value for API for all but the 2-year return period and, as with rainfall intensities, this value dropped off to a background level within 10 to 15 km.

A comparison of the spatial distribution of API between this study and the study by Surfleet (1997) shows that the areas of highest API are

similar. Surfleet (1997) found the highest values of API at Thompson Creek and South Creek. These two areas also have the highest values of rainfall intensities. In this study, the highest values of API were found at the Indian Creek rain gauge. While the positions have changed slightly, the pattern of the highest API values corresponding with the areas with the highest rainfall intensities still holds true.

Through data collected from a rain gauge network in the Central Oregon Coast Range, the temporal and spatial distribution of short duration, high intensity rainfall was calculated and characterized. The spatial distribution of short duration, high intensity rainfall across the central Oregon Coast Range is remarkably similar in values and stable in variance across all durations and return periods. In addition, the spatial distribution of the antecedent precipitation index was determined and again, is similar is pattern across return periods.

The characterization of the spatial distribution of short duration, high intensity rainfall events and API can be a useful management tool. These data are now available to help fill the gap in missing rainfall data for ridgetop and higher elevation locations in landslide prone terrain in the central Oregon Coast Range. First of all, this data can update estimates of mean annual precipitation and rainfall intensities used throughout the central Oregon Coast Range for management purposes. Secondly, this information can be compared to locations with known landslides in the

central Oregon Coast Range. By comparing landslide sites to the isohyetal maps of rainfall intensities and API, relationships may be found and it may be determined that areas with higher rainfall intensities are indeed factors for landslide occurrence in the central Oregon Coast Range. It is hoped that this information will help land managers to better manage landslide prone forested terrain.

REFERENCES

Andrieu, H, M.N. French, V. Thauvin, W.F. Krajewski. 1996. Adaptation and Application of a Quantitative Rainfall Forecasting Model in a Mountainous Region. *Journal of Hydrology*. 184: 243-259.

Arkell, R.E. and F. Richards. 1986. Short Duration Rainfall Relations for the Western United States. Conference on Climate and Water Management-A Critical Era and Conference on the Human Consequences of 1985's Climate. August 4-7 1986. Asheville, N.C. p 136-141.

Bedient, P.B. and W.C. Huber. 1992. Hydrology and Floodplain Analysis. Addison-Wesley Publishing Company, USA. 692 p.

Bishop D.M. and M.E. Stevens. 1964. Landslides on Logged Areas in Southeast Alaska. Northern Forest Experimental Station, Juneau, Alaska. USDA Forest Service Research Paper NOR-1. 18 p.

Bradley, S.G., K.N. Dirks, and C.D. Stow. 1998. High Resolution Studies of Rainfall on Norfolk Island, Part III: A Model for Rainfall Redistribution. *Journal of Hydrology*. 208: 194-203.

Bransom, M. 1997. Geohydrologic Conditions on a Steep Forested Slope: Modeling Transient Piezometric Response to Precipitation. Ph.D. Thesis, Oregon State University, Corvallis, OR. 179 p.

Brown, G.W. and J.T. Krygier. 1971. Clear-Cut Logging and Sediment Production in the Oregon Coast Range. *Water Resources Research.* 7(5): 1189-1198.

Caine, N. 1980. The Rainfall Intensity-Duration Control of Shallow Landslides and Debris Flows. *Geografiska Annaler*. 62A: 23-27.

Chow, V.T. Editor in Chief. 1964. Handbook of applied hydrology. McGraw-Hill Book Co. New York.

Cooper, C.F. 1967. Rainfall Intensity and Elevation in Southwestern Idaho. *Water Resources Research*. 3(1): 131-137.

Corradini, C. 1985. Analysis of the Effects of Orography on Surface Rainfall by a Parameterized Numerical Model. *Journal of Hydrology*. 77: 19-30.

Crozier, M.J. 1999. Prediction of Rainfall-Triggered Landslides: A Test of the Antecedent Water Status Model. *Earth Surface Processes and Landforms*. 24: 825-833.

Daly, C. and G.H. Taylor. 2002. Development of New Spatial Grids of R-factor and 10-yr EI_{30} for the Conterminous United States. Submitted to U.S. Environmental Protection Agency, Las Vegas, NV. Spatial Climate Analysis Service Oregon State University Corvallis, OR. 38 p.

Daly, C., G.H. Taylor, and W.P. Gibson. 1998. The PRISM approach to mapping precipitation and temperature. Pages 150-152 in Proc. of Modeling for Crop-Climate-Soil-Pest System and its Applications in Sustainable Crop Production, June 22-26, Nanjing, China. Jaingsu Academy of Agricultural Sciences.

Daly, C., R.P. Nelson, and D.L. Phillips. 1994. A Statistical-Topographical Model for Mapping Climatological Precipitation over Mountainous Terrain. *Journal of Applied Meteorology*. 33: 140-158.

Desert Research Institute. Western Research Climate Center. http://www.wrcc.dri.edu/cgi-bin/cliRECtM.pl?orreed. October 24, 2003.

Dietrich, W.E. 1989. Headwall Geomorphology in Steep Coast Range Terrain. Forestry and Landslides in the Oregon Coast Range. Proceedings of a C.O.P.E. Workshop. March 7-8. Newport, Oregon.

Fedora and Beschta. 1989. Storm Runoff Simulation Using An Antecedent Precipitation Index (API) Model. *Journal of Hydrology.* 112: 121-133.

Fedora, M. A. 1987. Simulation of Storm Runoff in the Oregon Coast Range. MS Thesis, Oregon State University. Corvallis, OR. 133 p.

Finlay, P.J., R. Fell, and P.K. Maguire. 1997. The Relationship between the Probability of Landslide Occurrence and Rainfall. *Canadian Geotechnical Journal*. 34: 811-824.

Gresswell, S., D. Heller, and D.N. Swanston. 1979. Mass Movement Response to Forest Management in the Central Oregon Coast Ranges. Resource Bulletin PNW-84, USDA Forest Service, Pacific Northwest Forest and Range Experiment Station, Portland OR. 26 p.

Johnson, A.C., D.N. Swanston, and K.E. McGee. 2000. Landslide Initiation, Runout, and Deposition within Clearcuts and Old-Growth Forests of Alaska. *Journal of the American Water Resources Association*. 36(1): 17-30.

Keefer, D.K., R.C. Wilson, R.K. Mark, E.E. Brabb, W.M. Brown III, S.D. Ellen, E.L. Harp, G.F. Wieczorek, C.S. Alger, and R.S. Zatkin. 1987. Real-Time Landslide Warning During Heavy Rainfall. *Science*. 23: 921-925.

Ketcheson, G. and H.A. Froelich. 1978. Hydrologic Factors and Environmental Impacts of Mass Soil Movements in the Oregon Coast Range. Water Resource Research Institute. Oregon State University. 93 p.

Kite, G.W. 1977. Frequency and Risk Analysis in Hydrology. Water Resources Publications, Fort Collins, Co. 224 p.

Kobashi, S., and M. Suzuki. 1987. The Critical Rainfall (Danger Index) for Disasters Caused by Debris Flows and Slope Failures. Erosion and Sedimentation in the Pacific Rim. Proceedings of the Corvallis Symposium, IAHS Pub. no. 165.

Loukas, A. and M.C. Quick. 1996. Spatial and Temporal Distribution of Storm Precipitation in Southwestern British Columbia. *Journal of Hydrology*. 174: 37-56.

May, C. L. 1999. Debris flow characteristics associated with forest practices in the central Oregon Coast Range. Masters Thesis. Oregon State University. Corvallis, Oregon. 121 p.

Montgomery, D.R., K.M. Schmidt, H.M. Greenberg, W.E. Dietrich. 2000. Forest Clearing and Regional Landsliding. *Geology*. 28(4): 311-314.

Moroney, M.J. 1951. Facts from Figures. Penguin Books, Baltimore, Maryland. 472 p.

NOAA. Southern Regional Climate Center. http://www.srcc.lsu.edu/7100/prcp/OR.html. October 24, 2003.

Oregon Climate Service. http://www.ocs.orst.edu/pub_ftp/reports/zone/zone1prec.htm. October 24, 2003.

Peck, E.L. and M.J. Brown. 1962. An Approach to the Development of Isohyetal Maps for Mountainous Areas. *Journal of Geophysical Research*. 67(2): 681-694.

Robison, E.G., K. Mills, J. Paul, L. Dent, and A. Skaugset. 1999. Oregon Department of Forestry Storm Impacts and Landslides of 1996: Final Report. Forest Practices Technical Report No. 4, Oregon Department of Forestry, Salem. 145 p.

Sidle, R.C. and D.N. Swanston. 1982. Analysis of a Small Debris Slide in Coastal Alaska. *Canadian Geotechnical Journal*. 19: 167-174.

Sidle R.C., A.J. Pearce, and C.L. O'Loughlin. 1985. *Hillslope Stability and Land Use*, American Geophysical Union, Washington, DC. 140 p.

Singh, P and N. Kumar. 1997. Effect of Orography on Precipitation in the Western Himalayan Region. *Journal of Hydrology*. 199: 183-206.

Surfleet, C. 1997. Precipitation Characteristics for Landslide Hazard Assessment for the Central Oregon Coast Range. Masters Thesis. Oregon State University. Corvallis, Oregon. 168 p.

Swanson, Frederick J., L. Clayton, W. F. Megahan, and G. Bush, 1989. Erosional Processes and Long -Term Site Productivity. In: Maintaining the Long-term Productivity of Pacific Northwest Forest Ecosystems p 164-184. D.A. Perry, R. Meurisse, B. Thomas, R. Miller, J. Boyle, J. Means, C.R. Perry, and R.F. Powers, ed., Timber Press, OR.

Swanson, F.J., L.E. Benda, S.H. Duncan, G.E. Grant, W.F. Megahan, L.M. Reid. 1987. Mass Failures and Other Processes of Sediment Production in Pacific Northwest Forest Landscapes. Pages 9-38 In E.O. Salo and T.W. Cundy, eds. Streamside Management: Forestry and Fishery Interactions. Institute of Forest Resources, University of Washington, Seattle, Washington, USA.

Swanston, D. N. 1969. Mass wasting in coastal Alaska. Res. Paper PNW-83. Portland, OR: Pac. NW Forest & Range Expt. Stn., Forest Service, USDA. 15 p.

Swanston, D. N., and F. J. Swanson. 1976. Timber Harvesting, Mass Erosion, and Steepland Forest Geomorphology in the Pacific Northwest: in Geomorphology and engineering. p. 199-221. D. R. Coates, ed., Dowden, Hutchinson, and Ross, Inc. Stroudsburg, PA.

Taylor, G., C. Daly, W. Gibson, J. Sibul-Weisburg. http://www.ocs.orst.edu/prism/prodep.html. October 2001.

Western Regional Climate Center. 2003. http://www.wrcc.dri.edu/pcpnfreq.html. December 3, 2003.

Wong, B. 1991. Controls on Movement of Selected Landslides in the Coast Range and Western Cascades, Oregon. Masters Thesis, Oregon State University. Corvallis, Oregon. 193p.

Wotling, G., Ch. Bouvier, J. Danloux, J.-M. Fritsch. 2000. Regionalization of Extreme Precipitation Distribution Using the Principal Components of the Topographical Environment. *Journal of Hydrology*. 233: 86-101.

Yue, S. 2001. The Gumbel Logistic Model for Representing a Multivariate Storm Event. *Advances in Water Resources*. 24: 179-185.

APPENDICES

APPENDIX A. Values of Rainfall Intensity

Table A16. Rainfall intensities for Indian Creek (mm/hr).

	30 minute	1 hour	2 hour	6 hour	12 hour	24 hour
2 year	27	21	17	13	10	8
5 year	31	24	20	15	12	9
10 year	34	26	22	17	13	10
25 year	38	29	25	19	15	11
50 year	41	31	27	20	16	12
100 year	44	33	29	22	17	13

Table A2. Rainfall intensities for Thompson Creek (mm/hr).

	30 minute	1 hour	2 hour	6 hour	12 hour	24 hour
2 year	32	21	14	9	7	5
5 year	39	25	17	10	8	5
10 year	44	28	18	11	8	6
25 year	51	32	21	12	9	7
50 year	56	35	23	13	10	7
100 year	61	38	24	13	11	8

Table A3. Rainfall intensities for Sweet Creek (mm/hr).

	30 minute	1 hour	2 hour	6 hour	12 hour	24 hour
2 year	26	19	15	10	7	5
5 year	30	22	17	11	8	5
10 year	34	24	19	13	9	6
25 year	38	27	22	14	10	7
50 year	41	30	24	15	11	7
100 year	44	32	26	17	11	8

Table A4. Rainfall intensities for South Creek (mm/hr).

	30 minute	1 hour	2 hour	6 hour	12 hour	24 hour
2 year	32	23	17	12	9	6
5 year	38	26	20	14	10	7
10 year	42	29	22	16	11	7
25 year	47	33	25	18	12	8
50 year	51	36	27	19	13	9
100 year	56	38	29	21	13	9

Table A5. Rainfall intensities for Smith Creek (mm/hr).

	30 minute	1 hour	2 hour	6 hour	12 hour	24 hour
2 year	20	15	12	8	6	4
5 year	23	18	13	9	7	5
10 year	25	19	14	10	8	6
25 year	28	22	16	11	9	6
50 year	30	23	17	12	10	7
100 year	33	25	18	13	11	7

Table A6. Rainfall intensities for Johnson Creek (mm/hr).

	30 minute	1 hour	2 hour	6 hour	12 hour	24 hour
2 year	20	14	11	8	6	4
5 year	23	16	12	9	7	5
10 year	25	17	13	9	7	5
25 year	27	19	15	10	8	6
50 year	29	20	16	11	9	6
100 year	31	22	17	12	9	7

Table A7. Rainfall intensities for Wassen Creek (mm/hr).

	30 minute	1 hour	2 hour	6 hour	12 hour	24 hour
2 year	26	18	14	8	6	4
5 year	31	22	17	10	7	5
10 year	35	24	19	11	8	5
25 year	40	27	22	12	9	6
50 year	43	30	24	13	9	7
100 year	47	32	26	14	10	7

Table A8. Rainfall intensities for Kirk Creek (mm/hr).

	30 minute	1 hour	2 hour	6 hour	12 hour	24 hour
2 year	17	12	10	7	5	4
5 year	18	14	11	8	6	5
10 year	20	15	11	9	7	5
25 year	22	16	12	9	8	6
50 year	23	17	13	10	8	6
100 year	25	18	14	11	9	7

Table A9. Rainfall intensities for Mill Creek (mm/hr).

	30 minute	1 hour	2 hour	6 hour	12 hour	24 hour
2 year	20	14	11	8	6	5
5 year	22	16	13	9	7	5
10 year	24	17	14	10	8	6
25 year	27	19	15	11	9	6
50 year	29	20	16	12	9	7
100 year	31	22	17	12	10	7

Table A10. Rainfall intensities for Panther Creek (mm/hr).

	30 minute	1 hour	2 hour	6 hour	12 hour	24 hour
2 year	21	16	13	9	7	6
5 year	23	18	15	11	8	6
10 year	25	20	16	11	9	7
25 year	28	22	18	13	10	8
50 year	30	23	19	14	11	9
100 year	31	24	20	15	12	9

Table A11. Rainfall intensities for Ryder Creek (mm/hr).

	30 minute	1 hour	2 hour	6 hour	12 hour	24 hour
2 year	22	17	12	8	6	4
5 year	25	19	14	9	7	5
10 year	28	21	15	10	8	6
25 year	31	24	17	11	8	6
50 year	34	25	18	12	9	7
100 year	36	27	19	13	10	7

Table A12. Rainfall intensities for Lobster Creek (mm/hr).

	30 minute	1 hour	2 hour	6 hour	12 hour	24 hour
2 year	20	15	12	8	6	4
5 year	23	18	14	9	7	5
10 year	26	20	15	10	7	5
25 year	29	22	17	11	8	6
50 year	31	24	19	12	9	6
100 year	34	26	20	13	10	7

Table A13. Rainfall intensities for Cascade Creek (mm/hr).

	30 minute	1 hour	2 hour	6 hour	12 hour	24 hour
2 year	20	15	12	8	7	5
5 year	23	16	13	9	7	5
10 year	25	18	14	10	8	6
25 year	28	20	16	11	9	7
50 year	30	21	17	12	10	7
100 year	32	22	18	12	10	8

APPENDIX B. Intensity-Duration-Frequency Curves

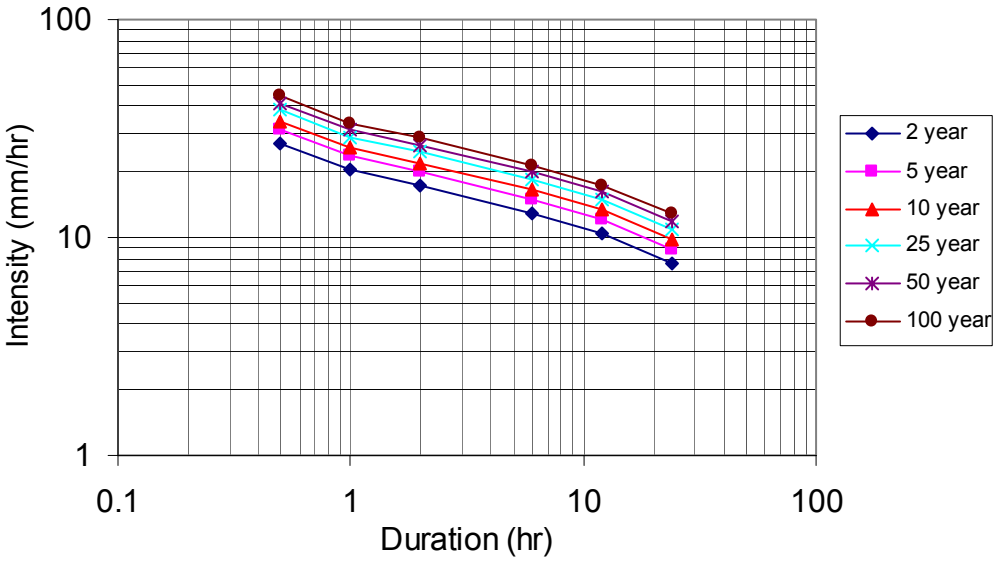

Figure B1. Intensity-Duration-Frequency curve for Indian Creek.

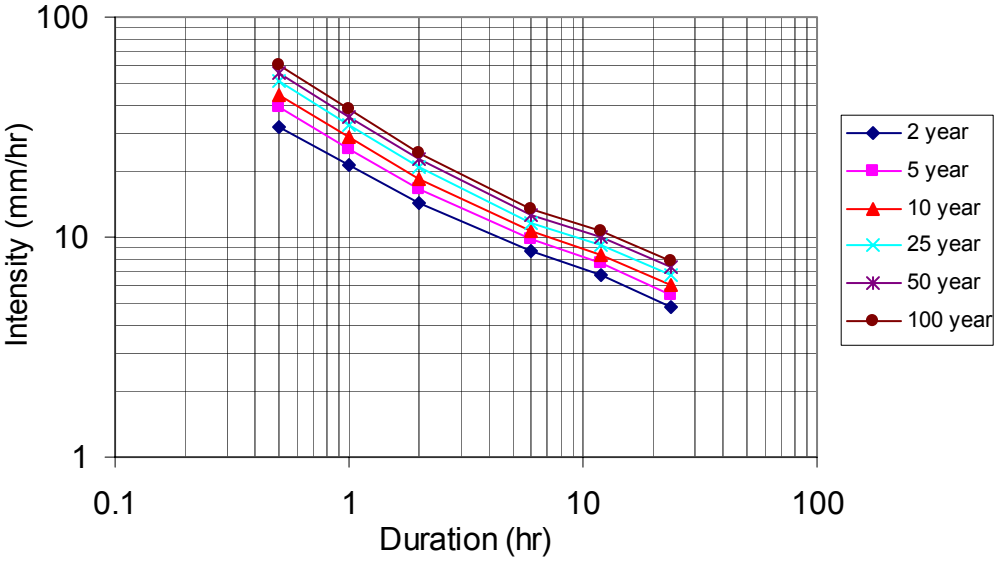

Figure B2. Intensity-Duration-Frequency curve for Thompson Creek.

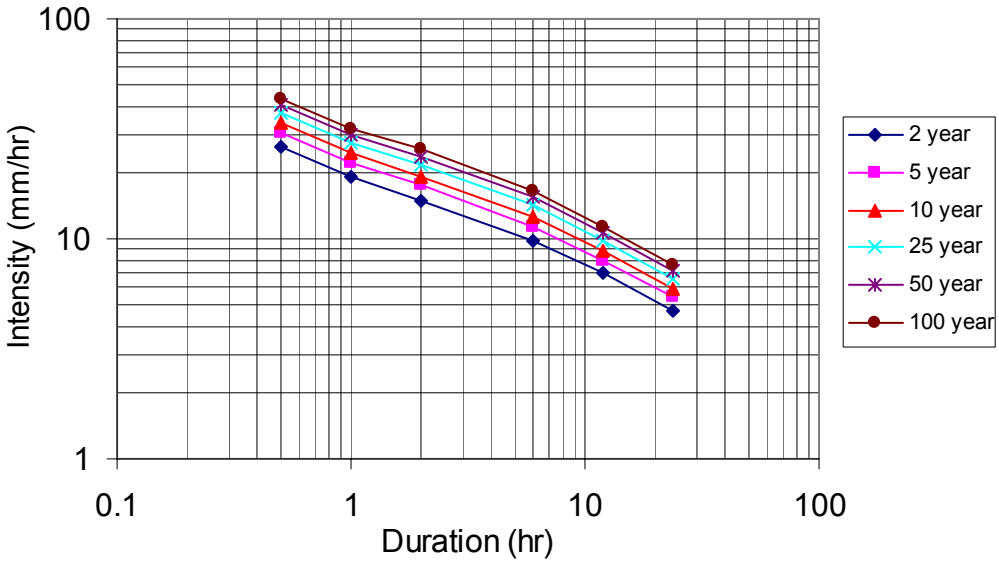

Figure B30. Intensity-Duration-Frequency curve for Sweet Creek.

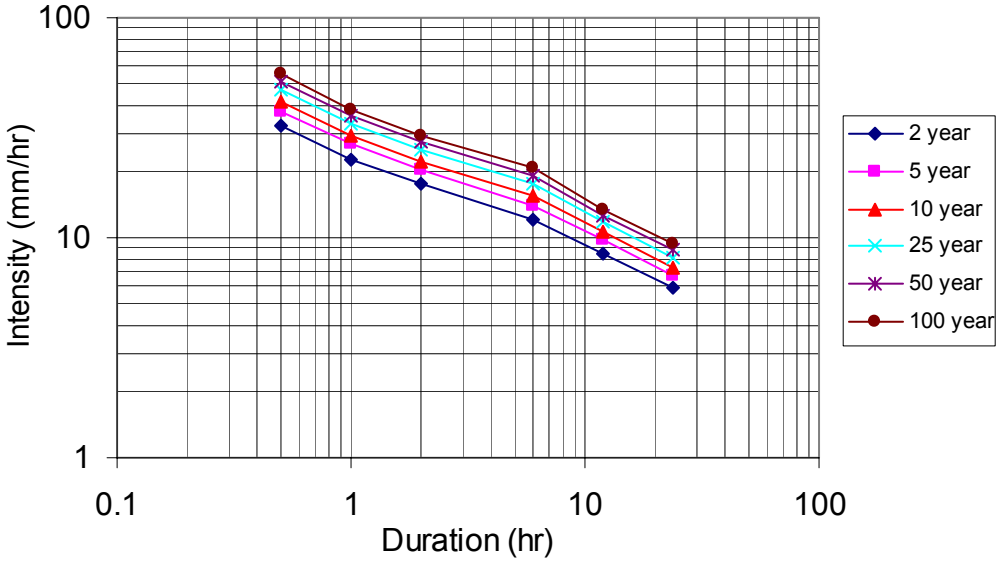

Figure B4. Intensity-Duration-Frequency curve for South Creek.

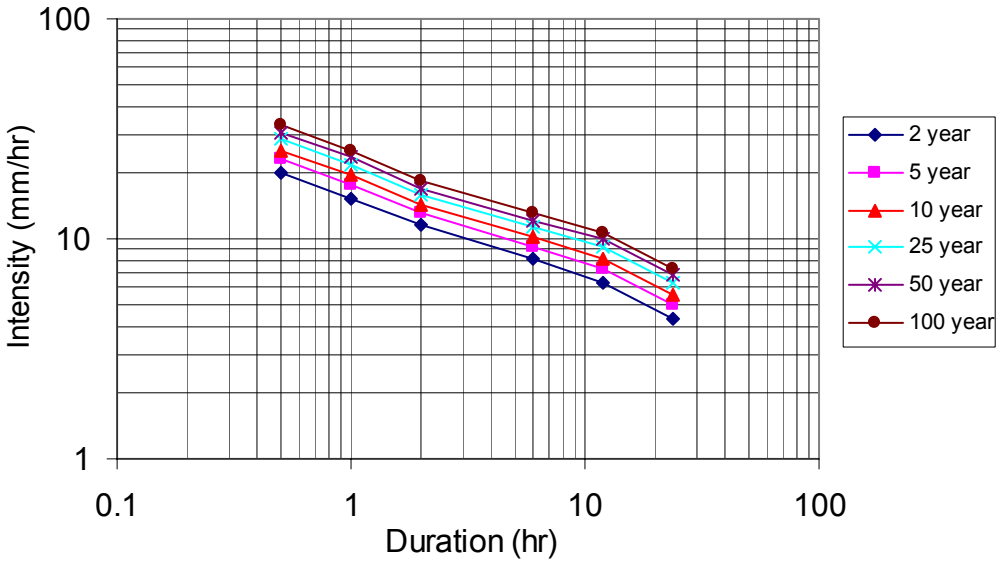

Figure B5. Intensity-Duration-Frequency curve for Smith Creek.

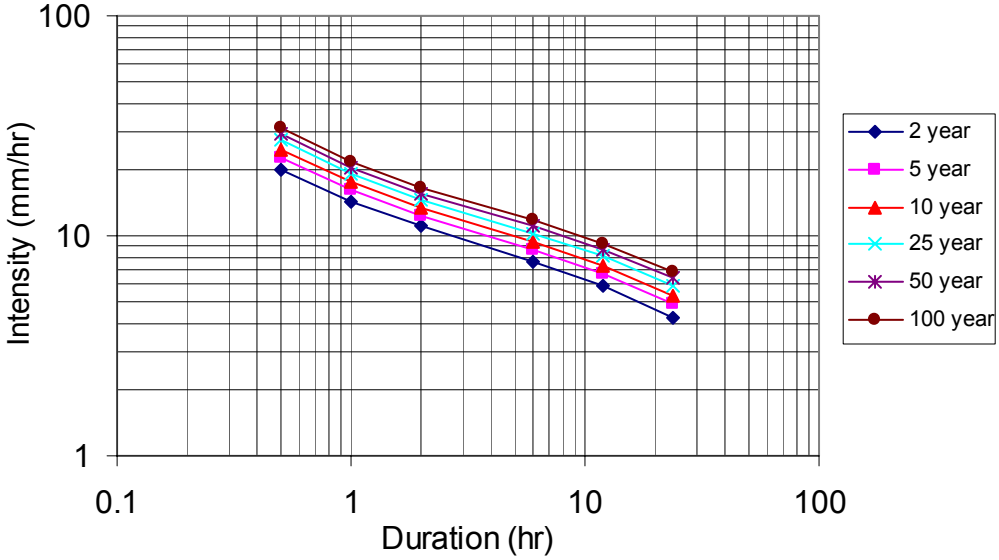

Figure B6. Intensity-Duration-Frequency curve for Johnson Creek.

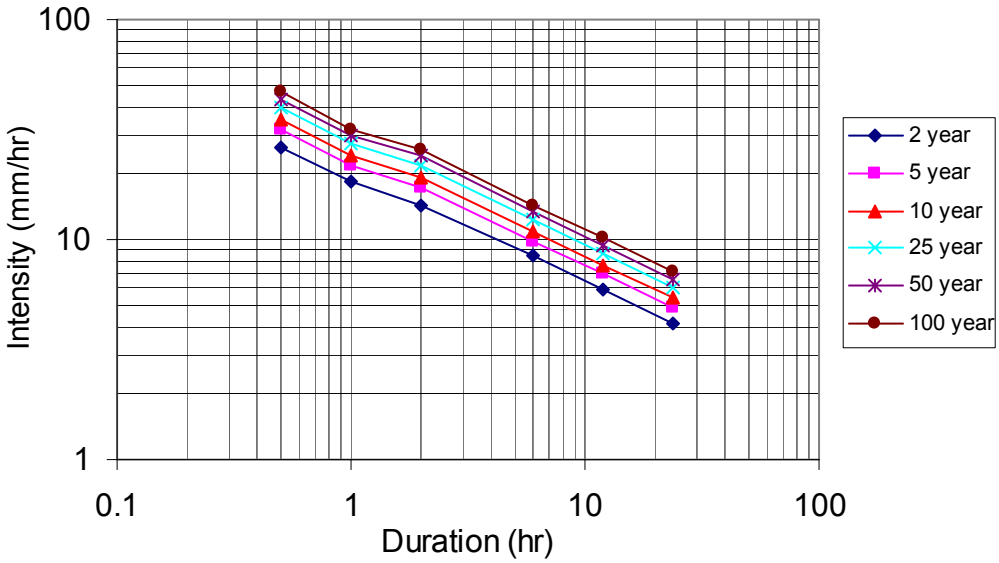

Figure B7. Intensity-Duration-Frequency curve for Wassen Creek.

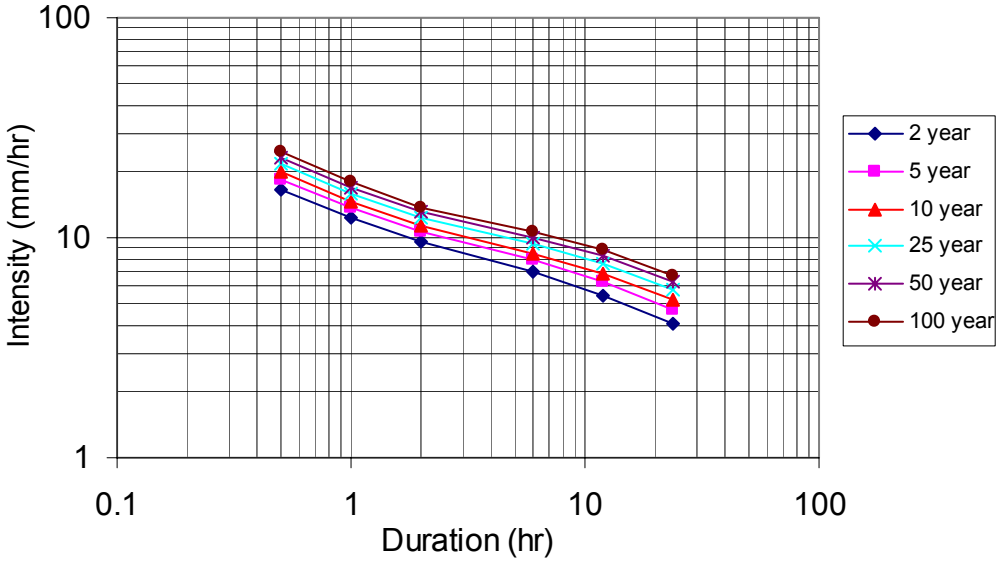

Figure B8. Intensity-Duration-Frequency curve for Kirk Creek.

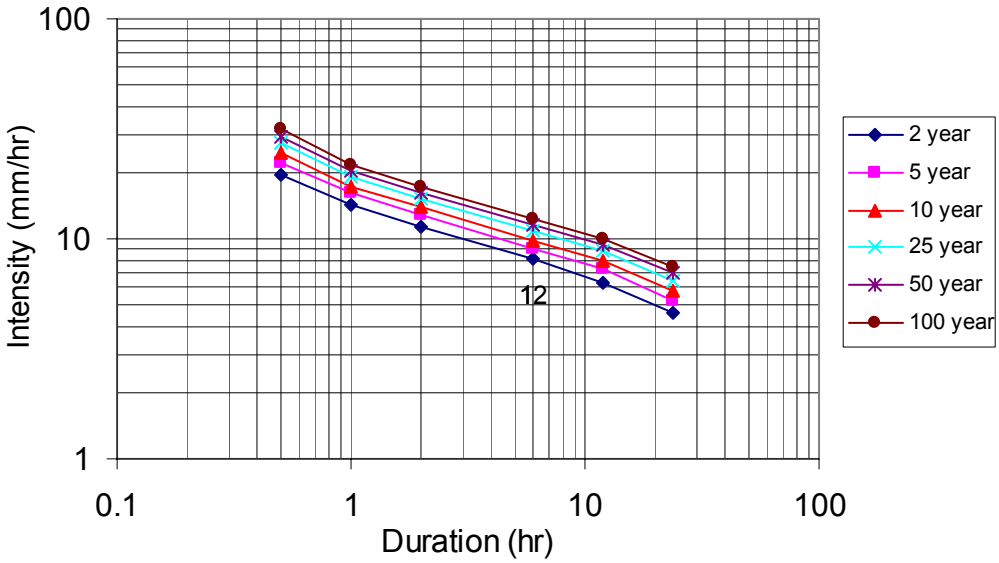

Figure B9. Intensity-Duration-Frequency curve for Mill Creek.

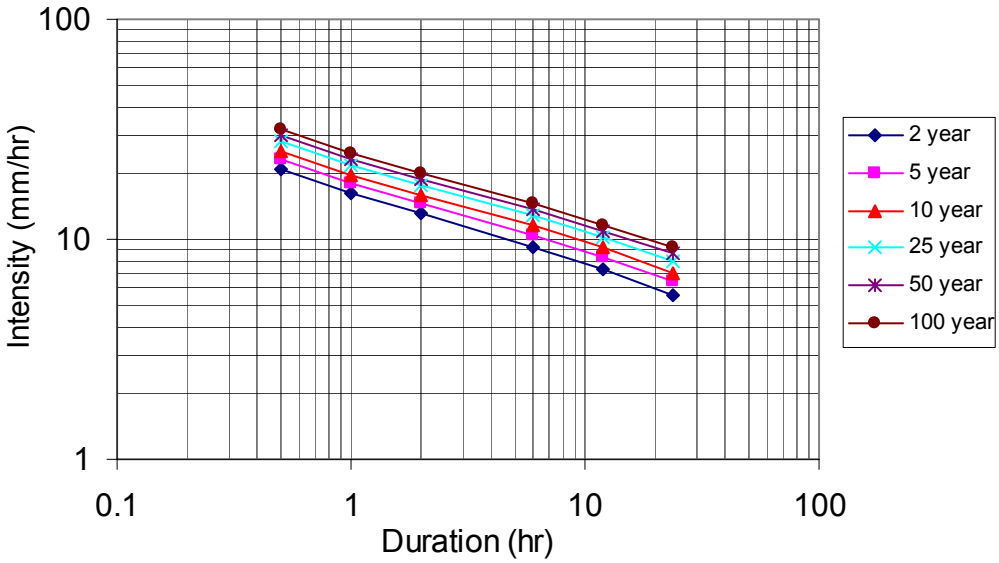

Figure B10. Intensity-Duration-Frequency curve for Panther Creek.

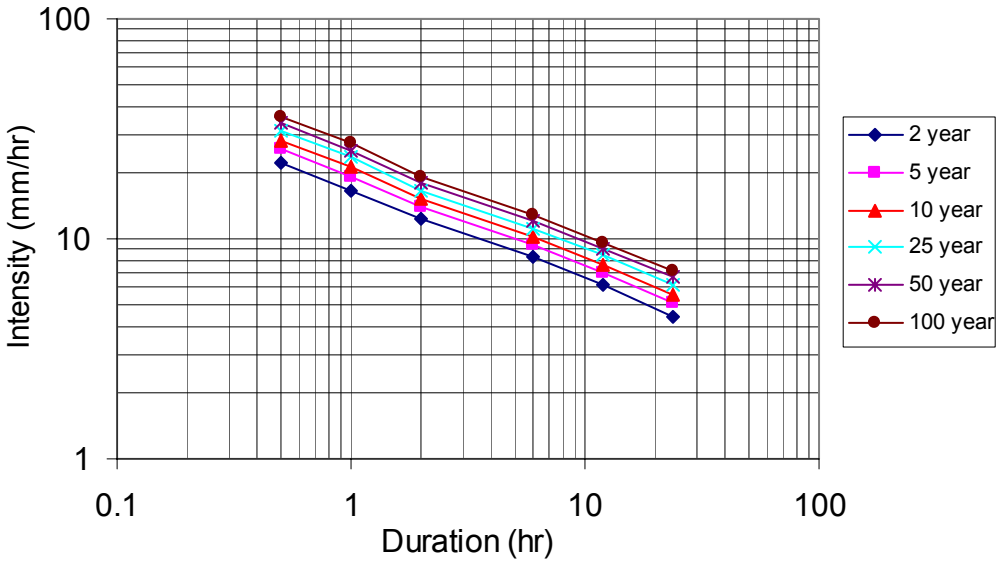

Figure B11. Intensity-Duration-Frequency curve for Ryder Creek.

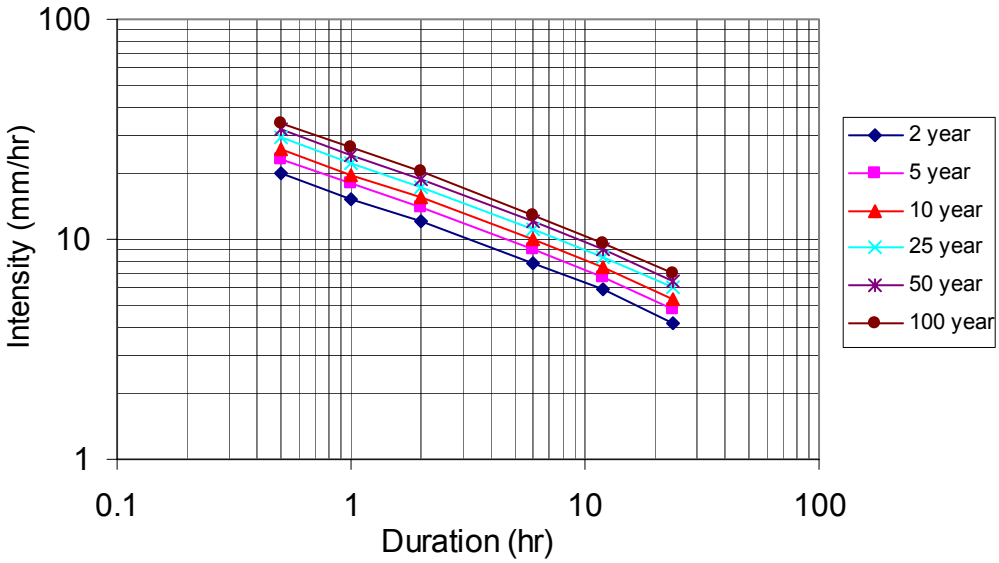

Figure B12. Intensity-Duration-Frequency curve for Lobster Creek.

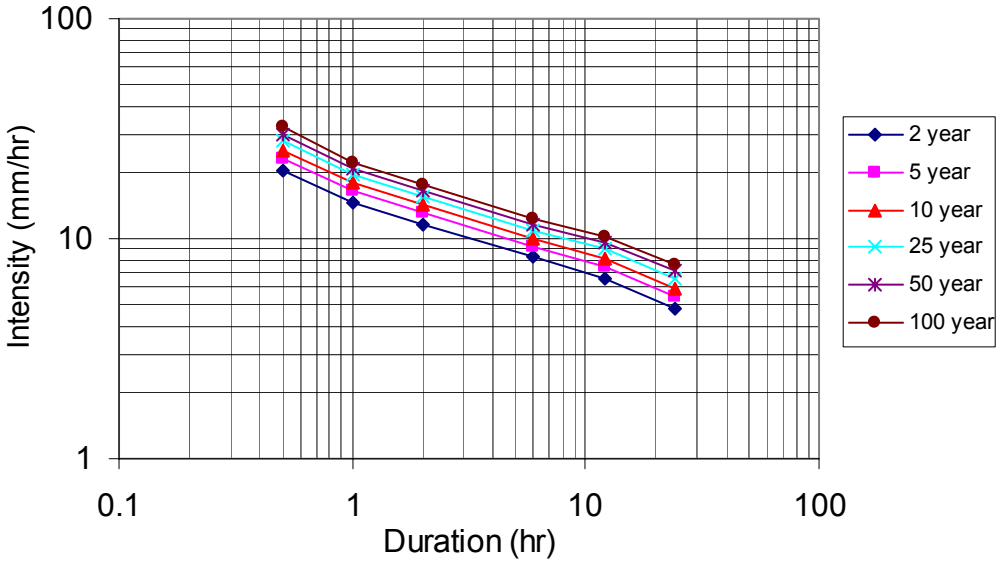

Figure B13. Intensity-Duration-Frequency curve for Cascade Creek.

APPENDIX C. Spearman Rank Tables for Duration

Table C1. Relative ranks of each rain gauge using the Spearman Rank Correlation method for the 30-minute duration rainfall intensities.

	Gauge												
Return Period	Indian	Thompson	Sweet	South	Smith	Johnson	Wassen	Kirk	Mill	Panther	Ryder	Lobster	Cascade
2 year	3	1.5	4.5	1.5	10	10	4.5	13	10	7	6	10	10
5 year	3.5	1	5	2	9	9	3.5	13	12	9	6	9	9
10 year	4.5	1	4.5	2	9.5	9.5	3	13	12	9.5	6	7	9.5
25 year	4.5	1	4.5	2	9	12	3	13	11.5	9	6	7	9
50 year	4.5	1	4.5	2	9	12	3	13	11.5	9	6	7	9
100 year	4.5	1	4.5	2	8	11	3	13	11	11	6	7	9
Sum	25	6.5	28	12	55	63	20	78	68	55	36	47	56
Rank	4	1	5	2	8.5	11	3	13	12	8.5	6	7	10

Table C2. Relative ranks of each rain gauge using the Spearman Rank Correlation method for the 1-hour duration rainfall intensities.

	Gauge												
Return Period	Indian	Thompson	Sweet	South	Smith	Johnson	Wassen	Kirk	Mill	Panther	Ryder	Lobster	Cascade
2 year	2.5	2.5	4	1	9	12	5	13	11.5	7	6	9	9
5 year	3	2	4.5	1	8	11	4.5	13	11	8	6	8	11
10 year	3	2	4.5	1	9	12	4.5	13	11.5	7.5	6	7.5	10
25 year	3	2	4.5	1	8	12	4.5	13	11.5	8	6	8	10
50 year	3	2	4.5	1	8.5	12	4.5	13	11.5	8.5	6	7	10
100 year	3	1.5	4.5	1.5	8	11	4.5	13	11	9	6	7	11
Sum	18	12	27	6.5	51	68	28	78	68	48	36	47	61
Rank	3	2	4	1	9	12	5	13	11.5	8	6	7	10

Table C3. Relative ranks of each rain gauge using the Spearman Rank Correlation method for the 2-hour duration rainfall intensities.

	Gauge												
Return Period	Indian	Thompson	Sweet	South	Smith	Johnson	Wassen	Kirk	Mill	Panther	Ryder	Lobster	Cascade
2 year	1.5	4.5	3	1.5	8.5	12	4.5	13	11.5	6	8.5	8.5	8.5
5 year	1.5	4	4	1.5	10	12	4	13	10	6	7.5	7.5	10
10 year	1.5	5	3.5	1.5	10	12	3.5	13	10	6	7.5	7.5	10
25 year	1.5	5	3.5	1.5	9.5	12	3.5	13	11.5	6	7.5	7.5	9.5
50 year	1.5	5	3.5	1.5	9.5	12	3.5	13	11.5	6.5	8	6.5	9.5
100 year	1.5	5	3.5	1.5	9.5	12	3.5	13	11.5	6.5	8	6.5	9.5
Sum	9	29	21	9	57	70	23	78	66	37	47	44	57
Rank	1.5	5	3	1.5	9.5	12	4	13	11	6	8	7	9.5

Table C4. Relative ranks of each rain gauge using the Spearman Rank Correlation method for the 6-hour duration rainfall intensities.

	Gauge												
Return Period	Indian	Thompson	Sweet	South	Smith	Johnson	Wassen	Kirk	Mill	Panther	Ryder	Lobster	Cascade
2 year	1	4.5	3	2	9	9	9	13	9	4.5	9	9	9
5 year	1	5.5	3.5	2	10	10	5.5	10	10	3.5	10	10	10
10 year	1	5	3	2	9	13	5	13	9	5	9	9	9
25 year	1	5.5	3	2	9	12	5.5	13	9	4	9	9	9
50 year	1	5.5	3	2	9	12	5.5	13	9	4	9	9	9
100 year	1	7.5	3	2	7.5	11	5	13	11	4	7.5	7.5	11
Sum	6	34	19	12	54	67	36	75	57	25	54	54	57
Rank	1	5	3	2	8	12	6	13	10.5	4	8	8	11

Table C5. Relative ranks of each rain gauge using the Spearman Rank Correlation method for the 12-hour duration rainfall intensities.

	Gauge												
Return Period	Indian	Thompson	Sweet	South	Smith	Johnson	Wassen	Kirk	Mill	Panther	Ryder	Lobster	Cascade
2 year	1	4	4	2	9.5	9.5	9.5	13	9.5	4	9.5	9.5	6
5 year	1	4	4	2	9	9	9	13	9	4	9	9	9
10 year	1	7.5	3.5	2	7.5	12	7.5	12	7.5	3.5	7.5	12	7.5
25 year	1	7	3.5	2	7	12	7	12	7	3.5	12	12	7
50 year	1	6	3.5	2	6	10	10	13	10	3.5	10	10	6
100 year	1	5	5	2	5	13	9	13	9	3	9	9	9
Sum	6	34	24	12	44	65	52	75	52	22	57	61	45
Rank	1	5	4	2	6	12	8.5	13	8.5	3	10	11	7

Table C6. Relative ranks of each rain gauge using the Spearman Rank Correlation method for the 24-hour duration rainfall intensities.

	Gauge												
Return Period	Indian	Thompson	Sweet	South	Smith	Johnson	Wassen	Kirk	Mill	Panther	Ryder	Lobster	Cascade
2 year	1	5.5	5.5	2.5	11	11	11	11	5.5	2.5	11	11	5.5
5 year	1	8.5	8.5	2	8.5	8.5	8.5	8.5	8.5	3	8.5	8.5	8.5
10 year	1	6.5	6.5	2.5	6.5	12	12	12	6.5	2.5	6.5	12	6.5
25 year	1	5	5	2.5	10	10	10	10	10	2.5	10	10	5
50 year	1	7	7	2.5	7	12	7	12	7	2.5	7	12	7
100 year	1	5	5	2.5	10	10	10	10	10	2.5	10	10	5
Sum	6	38	38	15	53	63	58	63	47.5	16	53	63	38
Rank	1	5	5	2	8.5	12	10	12	7	3	8.5	12	5

APPENDIX D. Spearman Rank Tables for Return Period

Table D1. Relative ranks of each rain gauge using the Spearman Rank Correlation method for the 2-year return period rainfall intensities.

	Gauge												
Duration	Indian	Thompson	Sweet	South	Smith	Johnson	Wassen	Kirk	Mill	Panther	Ryder	Lobster	Cascade
0.5 hour	3	1.5	4.5	1.5	10	10	4.5	13	10	7	6	10	10
1 hour	2.5	2.5	4	1	9	12	5	13	12	7	6	9	9
2 hour	1.5	4.5	3	1.5	8.5	12	4.5	13	12	6	8.5	8.5	8.5
6 hour	1	4.5	3	2	9	9	9	13	9	9	9	9	9
12 hour	1	4.5	4.5	2	9.5	9.5	9.5	13	9.5	9.5	4.5	9.5	4.5
24 hour	1	5.5	5.5	2.5	11	11	11	11	5.5	11	5.5	11	5.5
Sum	10	23	25	11	57	62	43	76	57	49	40	57	47
Rank	1	3	4	2	10	12	6	13	10	8	5	10	7

Table D2. Relative ranks of each rain gauge using the Spearman Rank Correlation method for the 5-year return period rainfall intensities.

	Gauge												
Duration	Indian	Thompson	Sweet	South	Smith	Johnson	Wassen	Kirk	Mill	Panther	Ryder	Lobster	Cascade
0.5 hour	3.5	1	5	2	9	9	3.5	13	12	9	6	9	9
1 hour	3	2	4.5	1	8	11	4.5	13	11	8	6	8	11
2 hour	1.5	4	4	1.5	10	12	4	13	10	6	7.5	7.5	10
6 hour	1	5.5	3.5	2	9.5	9.5	5.5	13	9.5	3.5	9.5	9.5	9.5
12 hour	1	4	4	2	9	9	9	13	9	4	9	9	9
24 hour	1	8.5	8.5	2	8.5	8.5	8.5	8.5	8.5	3	8.5	8.5	8.5
Sum	11	25	30	11	54	59	35	74	60	34	47	52	57
Rank	1.5	3	4	1.5	9	11	6	13	12	5	7	8	10

Table D3. Relative ranks of each rain gauge using the Spearman Rank Correlation method for the 10-year return period rainfall intensities.

	Gauge												
Duration	Indian	Thompson	Sweet	South	Smith	Johnson	Wassen	Kirk	Mill	Panther	Ryder	Lobster	Cascade
0.5 hour	4.5	1	4.5	2	9.5	9.5	3	13	12	9.5	6	7	9.5
1 hour	3	2	4.5	1	9	12	4.5	13	12	7.5	6	7.5	10
2 hour	1.5	5	3.5	1.5	10	12	3.5	13	10	6	7.5	7.5	10
6 hour	1	5	3	2	9	13	5	13	9	5	9	9	9
12 hour	1	7.5	3.5	2	7.5	12	7.5	12	7.5	3.5	7.5	12	7.5
24 hour	1	6.5	6.5	2.5	6.5	12	12	12	6.5	2.5	6.5	12	6.5
Sum	12	27	26	11	52	69	35	75	57	34	43	55	53
Rank	2	4	3	1	8	12	6	13	11	5	7	10	9

Table D4. Relative ranks of each rain gauge using the Spearman Rank Correlation method for the 25-year return period rainfall intensities.

	Gauge												
Duration	Indian	Thompson	Sweet	South	Smith	Johnson	Wassen	Kirk	Mill	Panther	Ryder	Lobster	Cascade
0.5 hour	4.5	1	4.5	2	9	12	3	13	12	9	6	7	9
1 hour	3	2	4.5	1	8	12	4.5	13	12	8	6	8	10
2 hour	1.5	5	3.5	1.5	9.5	12	3.5	13	12	6	7.5	7.5	9.5
6 hour	1	5.5	3	2	9	12	5.5	13	9	4	9	9	9
12 hour	1	7	3.5	2	7	12	7	12	7	3.5	12	12	7
24 hour	1	5	5	2.5	10	10	10	10	10	2.5	10	10	5
Sum	12	26	24	11	53	68	34	74	61	33	50	53	50
Rank	2	4	3	1	9.5	12	6	13	11	5	7.5	9.5	7.5

Table D5. Relative ranks of each rain gauge using the Spearman Rank Correlation method for the 50-year return period rainfall intensities.

	Gauge												
Duration	Indian	Thompson	Sweet	South	Smith	Johnson	Wassen	Kirk	Mill	Panther	Ryder	Lobster	Cascade
0.5 hour	4.5	1	4.5	2	9	12	3	13	12	9	6	7	9
1 hour	3	2	4.5	1	8.5	12	4.5	13	12	8.5	6	7	10
2 hour	1.5	5	3.5	1.5	9.5	12	3.5	13	12	6.5	8	6.5	9.5
6 hour	1	5.5	3	2	9	12	5.5	13	9	4	9	9	9
12 hour	1	6	3.5	2	6	11	11	11	11	3.5	11	11	6
24 hour	1	7	7	2.5	7	12	7	12	7	2.5	7	12	7
Sum	12	27	26	11	49	69	34	75	61	34	47	52	51
Rank	2	4	3	1	8	12	5.5	13	11	5.5	7	10	9

Table D6. Relative ranks of each rain gauge using the Spearman Rank Correlation method for the 100-year return period rainfall intensities.

	Gauge												
Duration	Indian	Thompson	Sweet	South	Smith	Johnson	Wassen	Kirk	Mill	Panther	Ryder	Lobster	Cascade
0.5 hour	4.5	1	4.5	2	8	11	3	13	11	11	6	7	9
1 hour	3	1.5	4.5	1.5	8	11	4.5	13	11	9	6	7	11
2 hour	1.5	5	3.5	1.5	9.5	12	3.5	13	12	6.5	8	6.5	9.5
6 hour	1	7.5	3	2	7.5	11	5	13	11	4	7.5	7.5	11
12 hour	1	5	5	2	5	13	9	13	9	3	9	9	9
24 hour	1	5	5	2.5	10	10	10	10	10	2.5	10	10	5
Sum	12	25	26	12	48	67	35	75	64	36	47	47	55
Rank	1.5	3	4	1.5	9	12	5	13	11	6	7.5	7.5	10

APPENDIX E. Isohyetal Maps for Rainfall Intensity

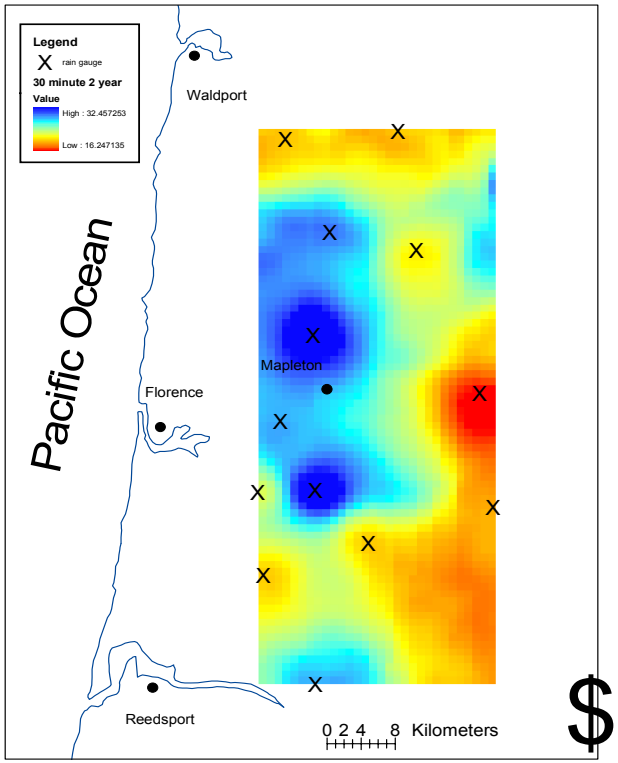

Figure E1. Isohyetal map of the 2-year return period, 30-minute rainfall intensity (mm/hr).

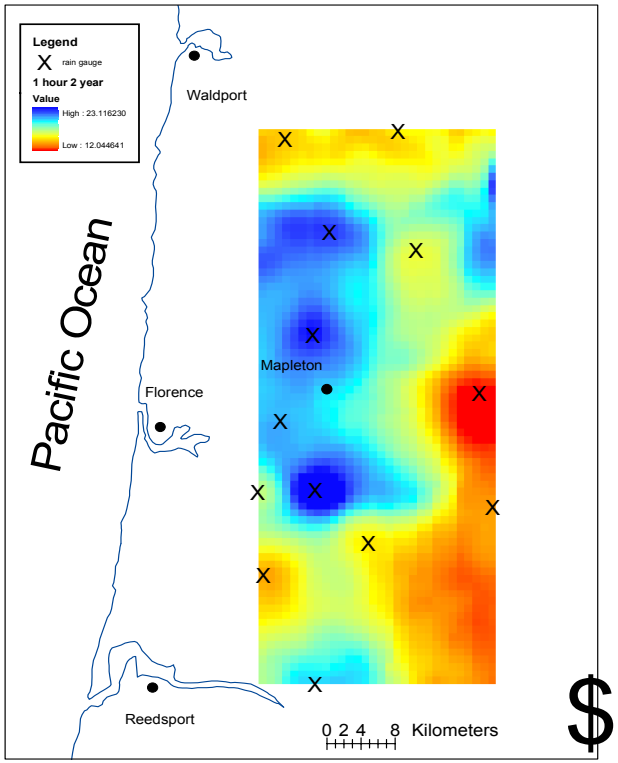

Figure E2. Isohyetal map of the 2-year return period, 1-hour rainfall intensity (mm/hr).

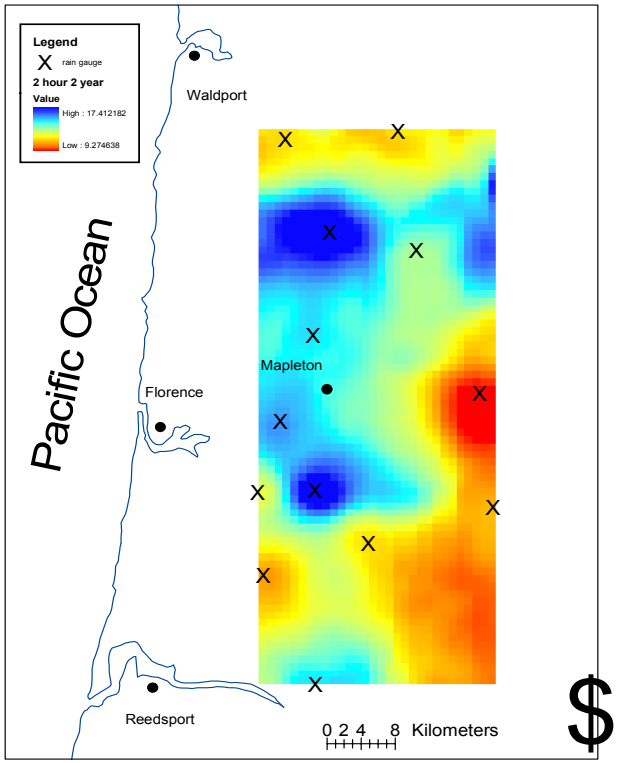

Figure E3. Isohyetal map of the 2-year return period, 2-hour rainfall intensity (mm/hr).

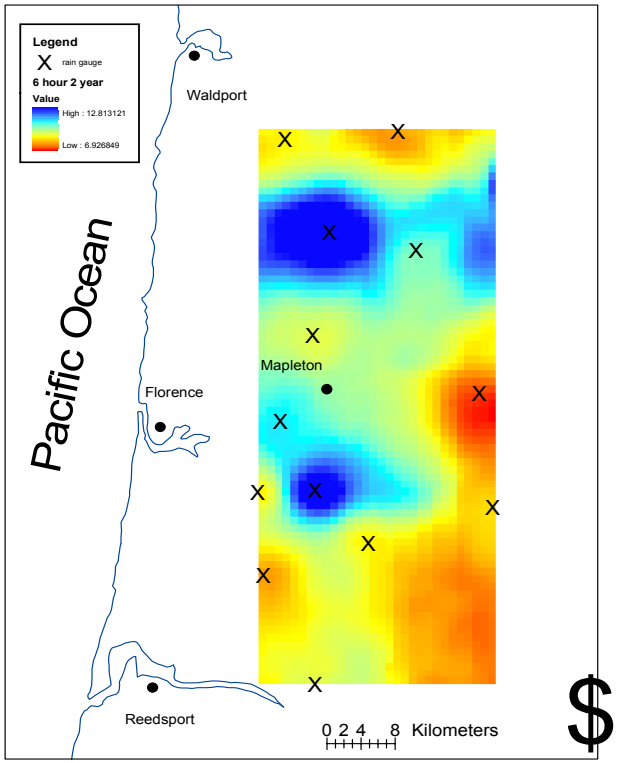

Figure E4. Isohyetal map of the 2-year return period, 6-hour rainfall intensity (mm/hr).

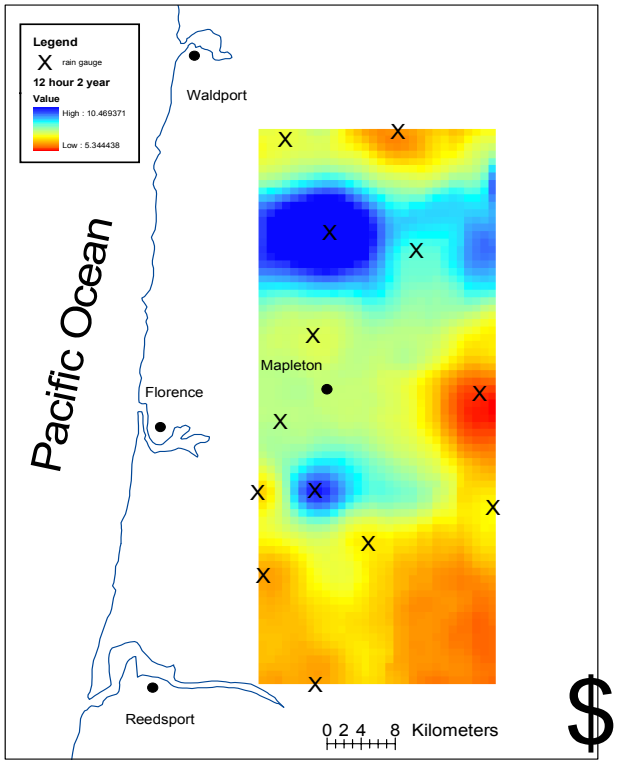

Figure E5. Isohyetal map of the 2-year return period, 12-hour rainfall intensity (mm/hr).

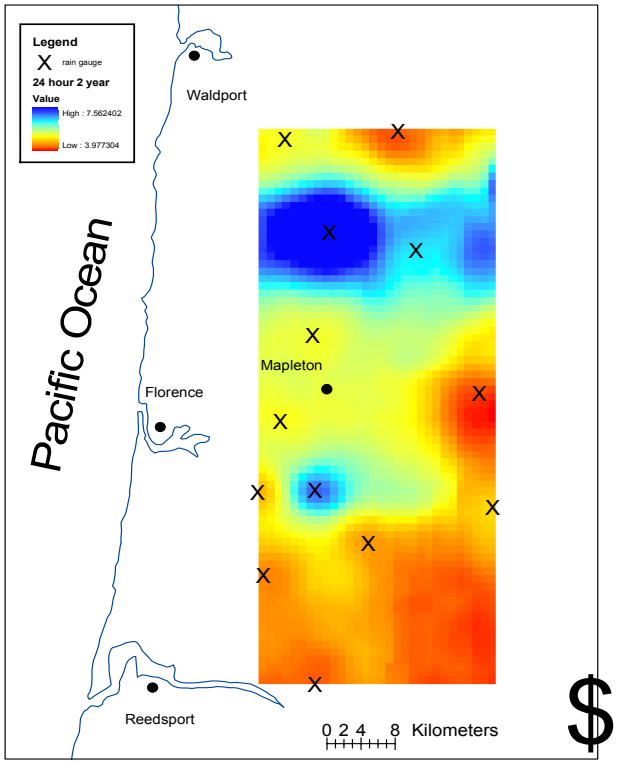

Figure E6. Isohyetal map of the 2-year return period, 24-hour rainfall intensity (mm/hr).

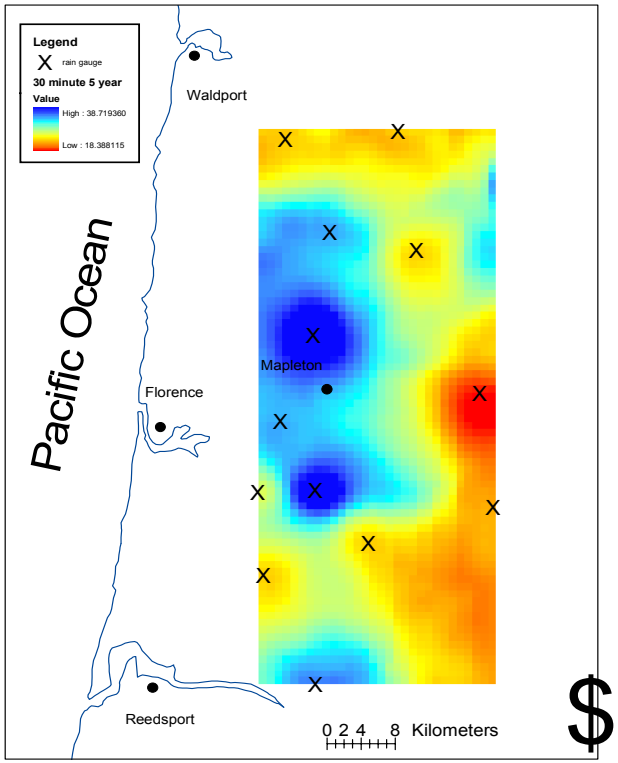

Figure E7. Isohyetal map of the 5-year return period, 30-minute rainfall intensity (mm/hr).

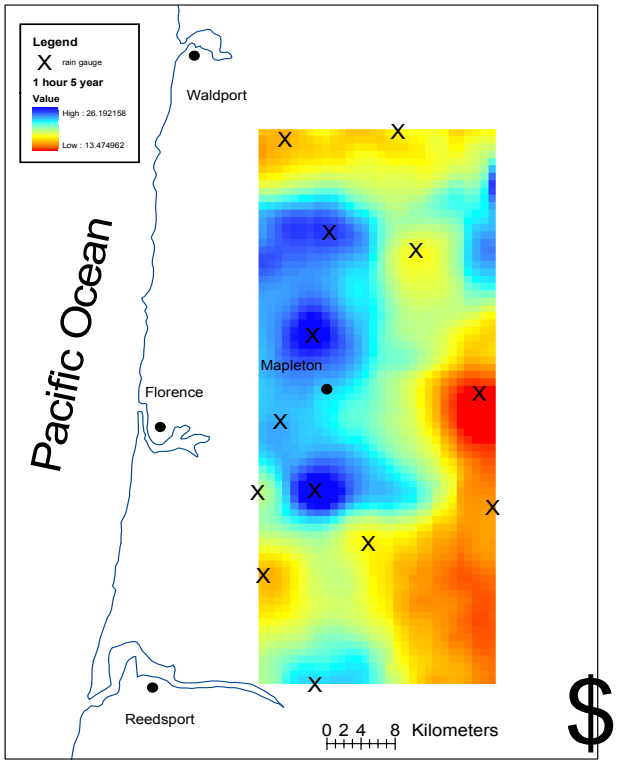

Figure E8. Isohyetal map of the 5-year return period, 1-hour rainfall intensity (mm/hr).

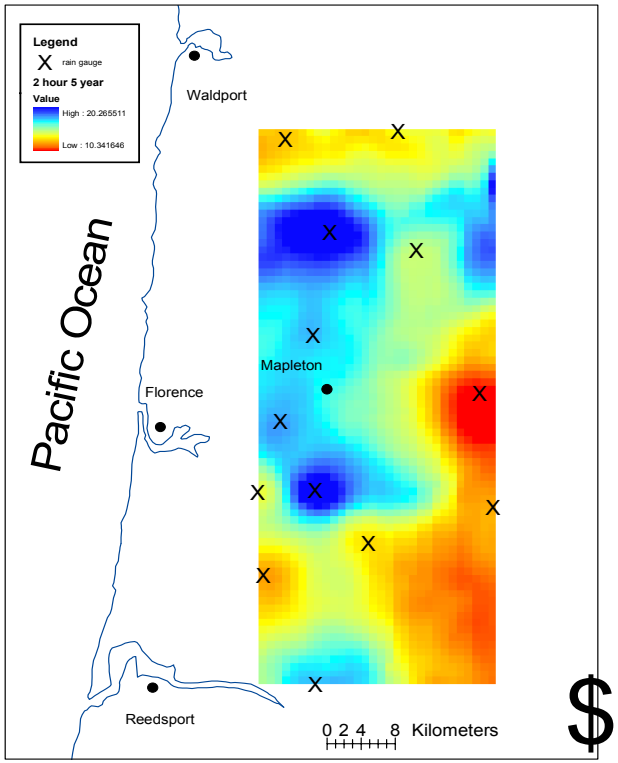

Figure E9. Isohyetal map of the 5-year return period, 2-hour rainfall intensity (mm/hr).

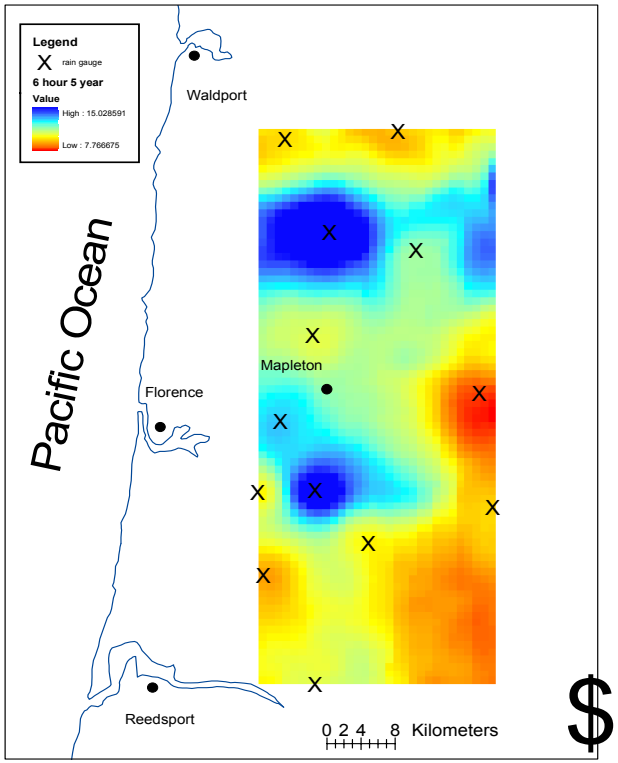

Figure E10. Isohyetal map of the 5-year return period, 6-hour rainfall intensity (mm/hr).

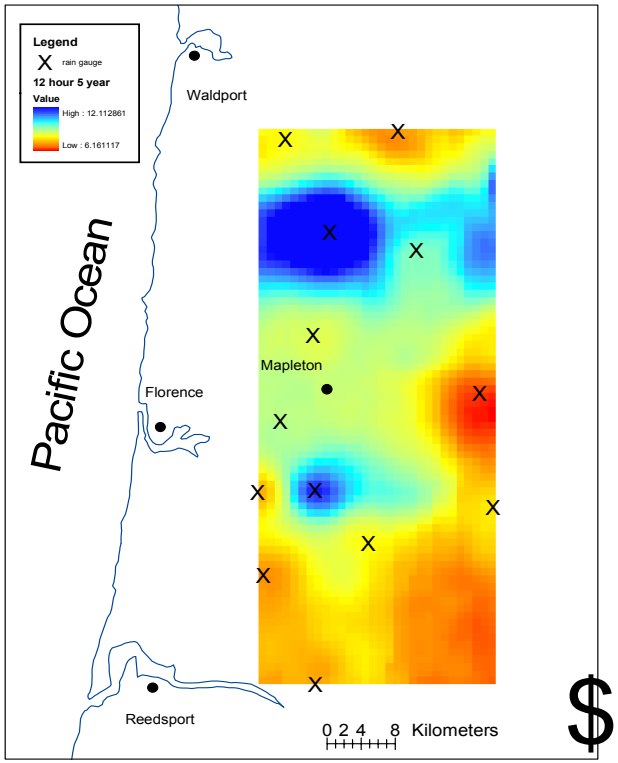

Figure E11. Isohyetal map of the 5-year return period, 12-hour rainfall intensity (mm/hr).

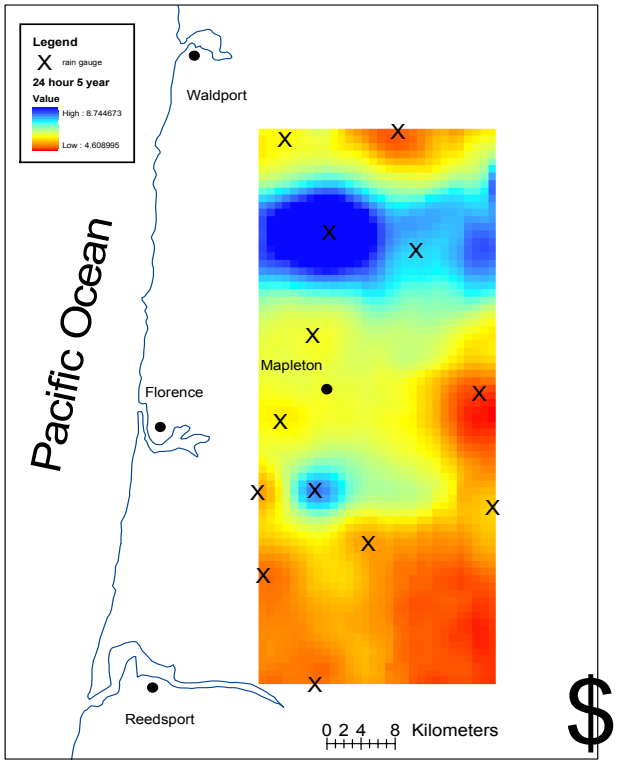

Figure E12. Isohyetal map of the 5-year return period, 24-hour rainfall intensity (mm/hr).

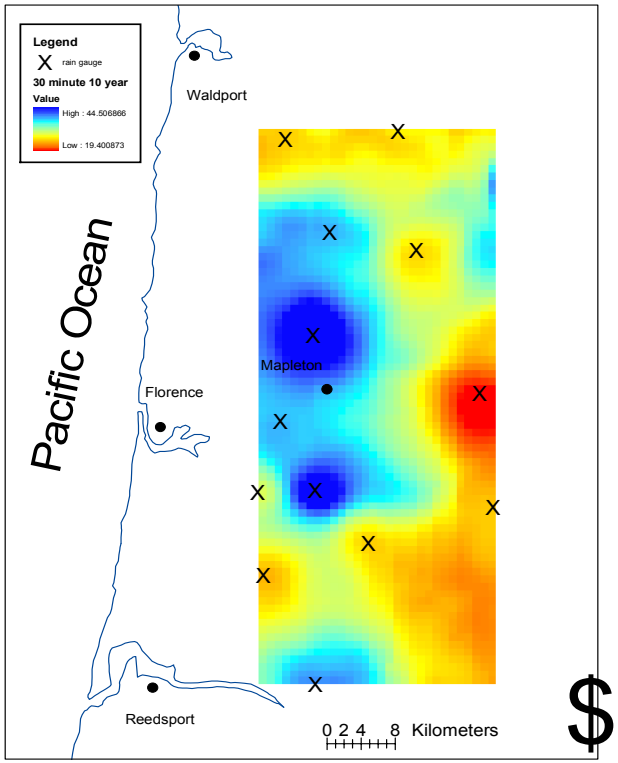

Figure E13. Isohyetal map of the 10-year return period, 30-minute rainfall intensity (mm/hr).

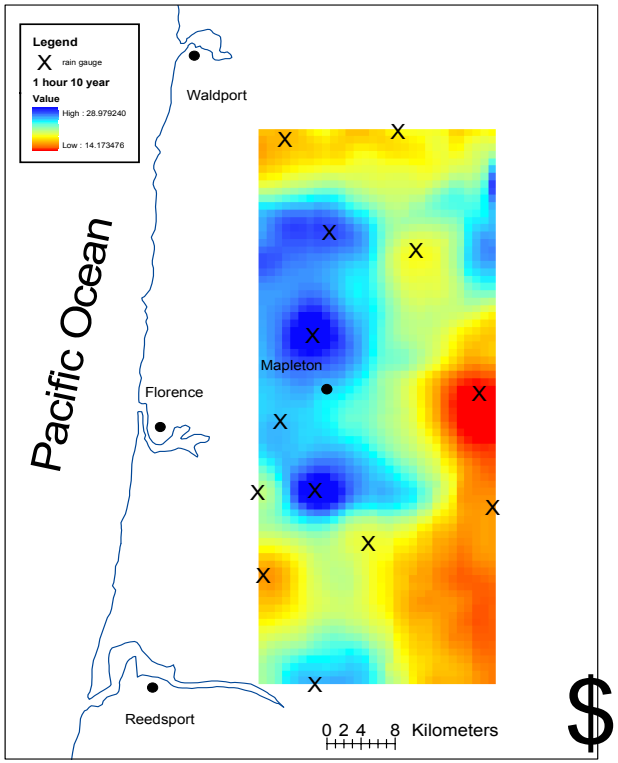

Figure E14. Isohyetal map of the 10-year return period, 1-hour rainfall intensity (mm/hr).

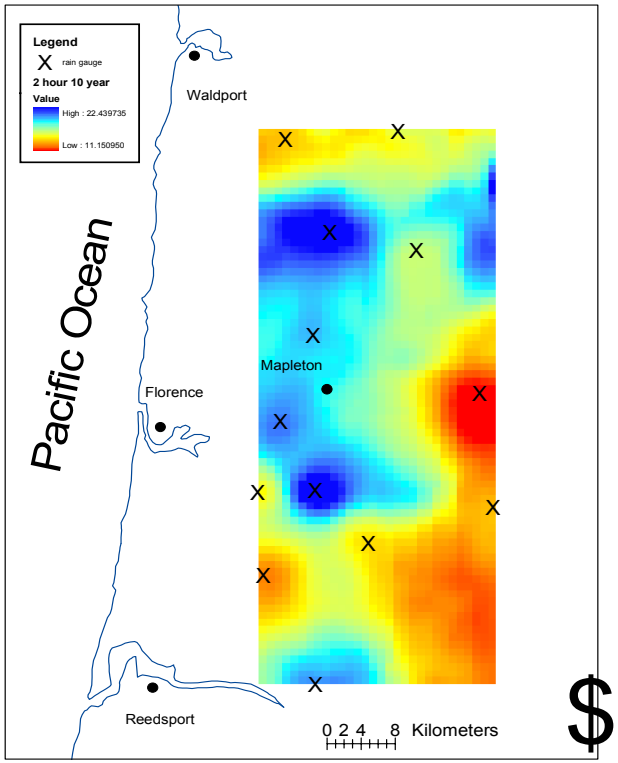

Figure E15. Isohyetal map of the 10-year return period, 2-hour rainfall intensity (mm/hr).

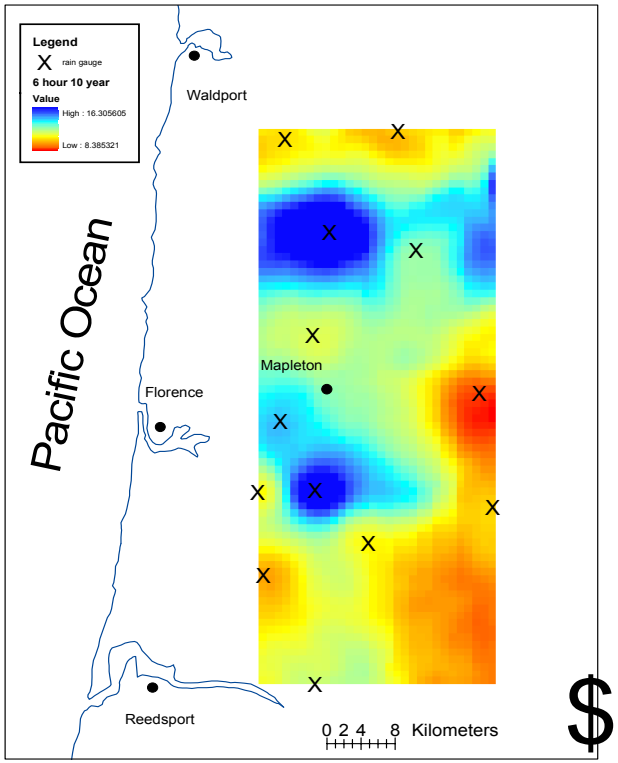

Figure E16. Isohyetal map of the 10-year return period, 6-hour rainfall intensity (mm/hr).

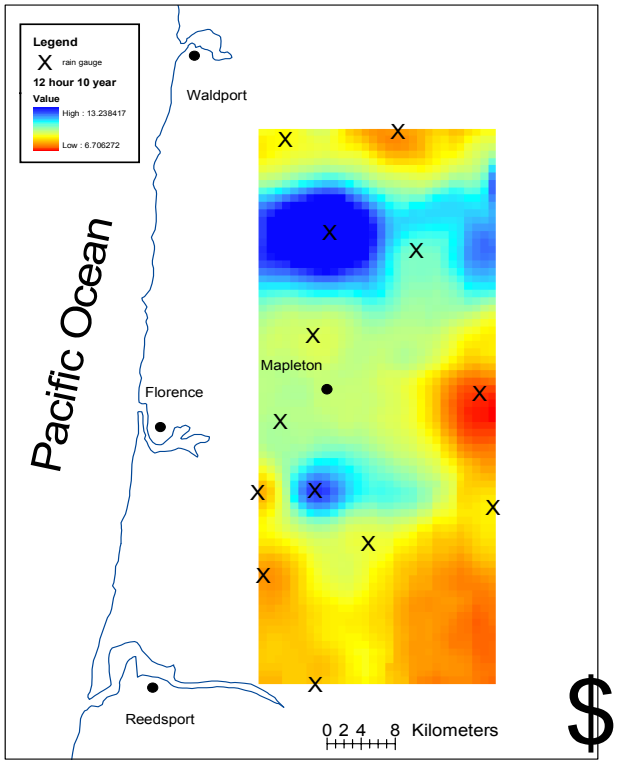

Figure E17. Isohyetal map of the 10-year return period, 12-hour rainfall intensity (mm/hr).

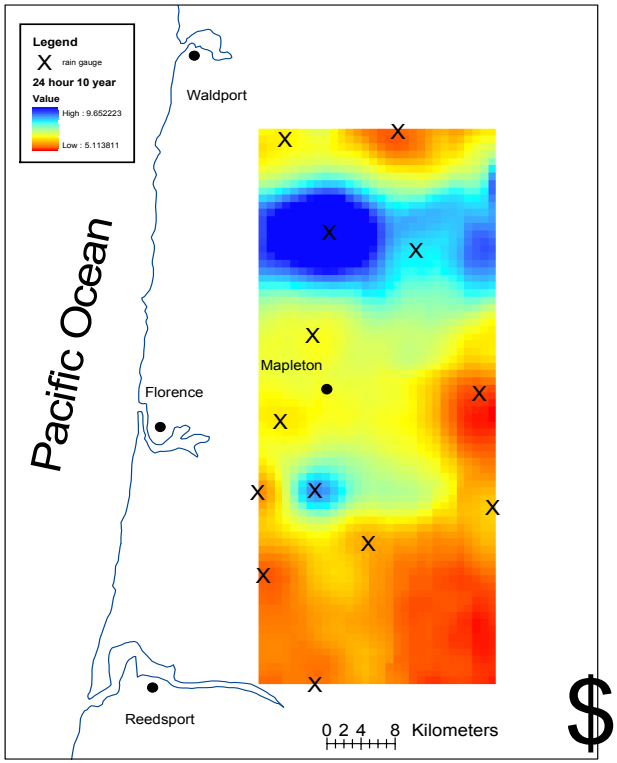

Figure E18. Isohyetal map of the 10-year return period, 24-hour rainfall intensity (mm/hr).

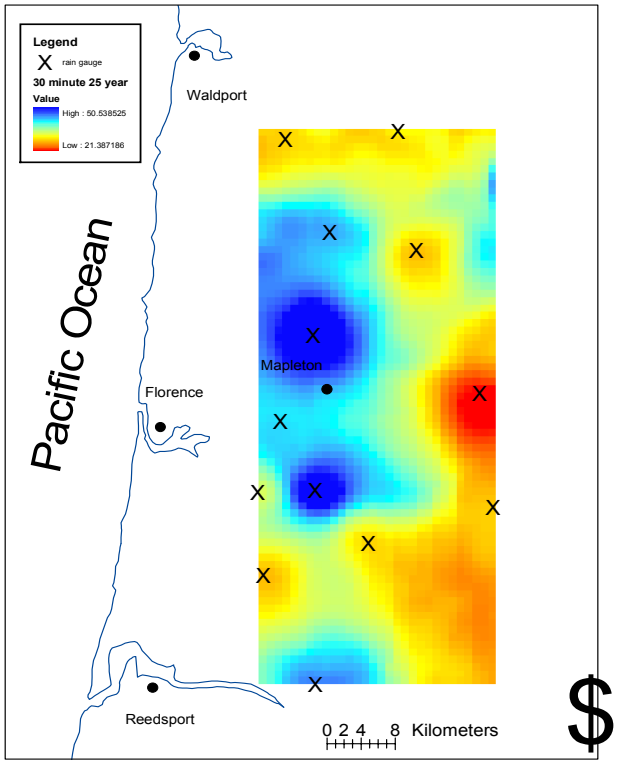

Figure E19. Isohyetal map of the 25-year return period, 30-minute rainfall intensity (mm/hr).

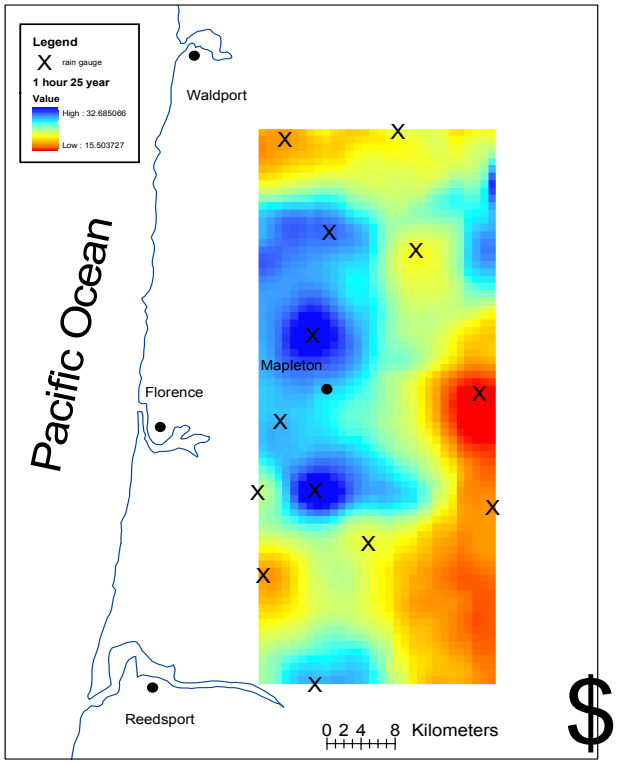

Figure E20. Isohyetal map of the 25-year return period, 1-hour rainfall intensity (mm/hr).

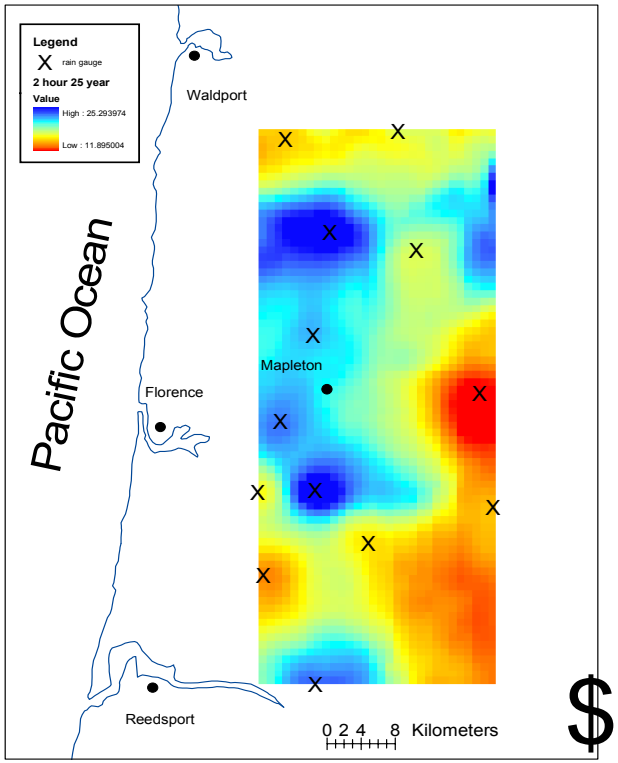

Figure E21. Isohyetal map of the 25-year return period, 2-hour rainfall intensity (mm/hr).

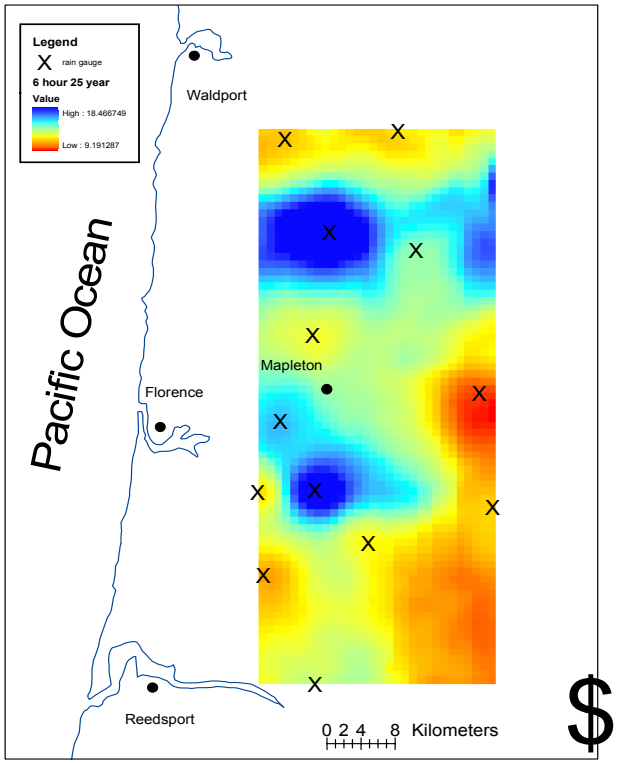

Figure E22. Isohyetal map of the 25-year return period, 6-hour rainfall intensity (mm/hr).

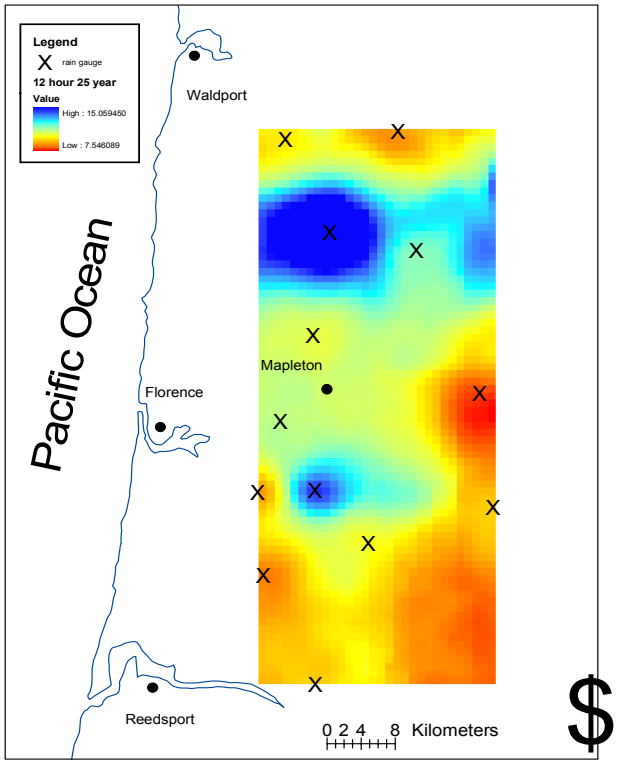

Figure E23. Isohyetal map of the 25-year return period, 12-hour rainfall intensity (mm/hr).

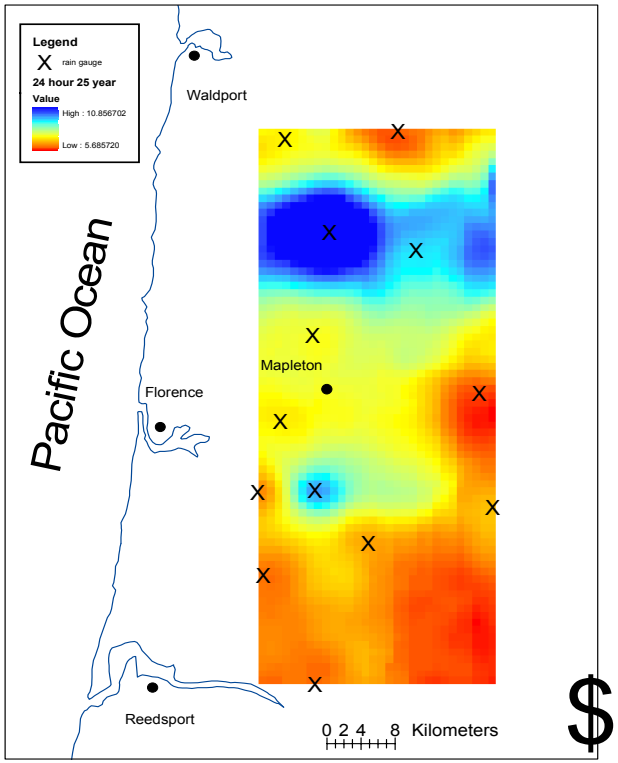

Figure E24. Isohyetal map of the 25-year return period, 24-hour rainfall intensity (mm/hr).

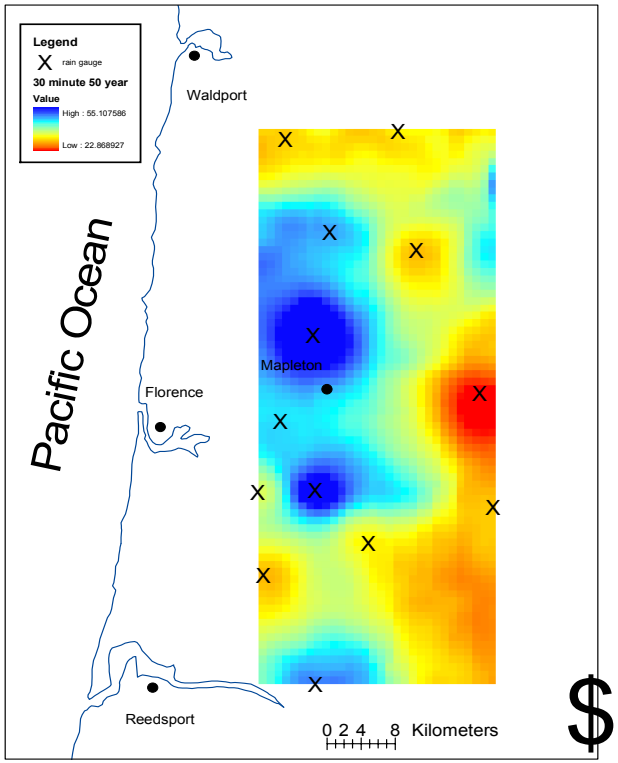

Figure E25. Isohyetal map of the 50-year return period, 30-minute rainfall intensity (mm/hr).

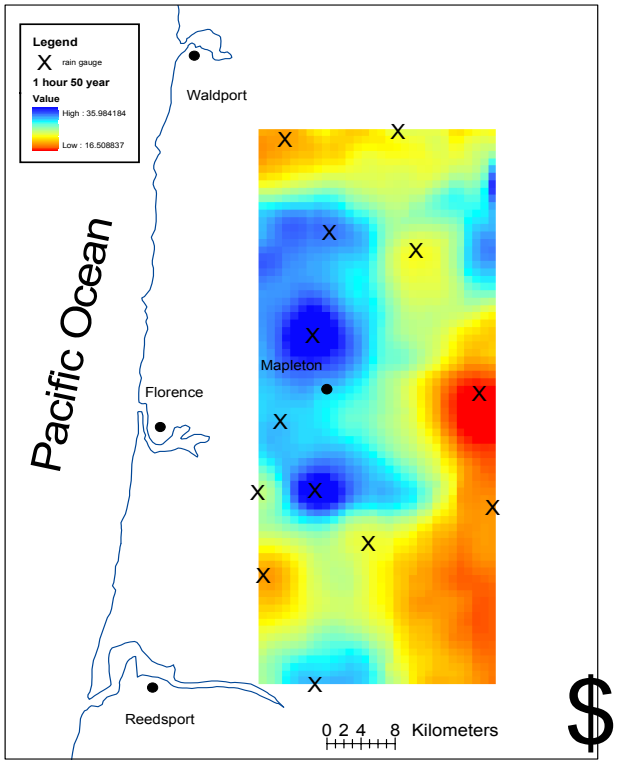

Figure E26. Isohyetal map of the 50-year return period, 1-hour rainfall intensity (mm/hr).

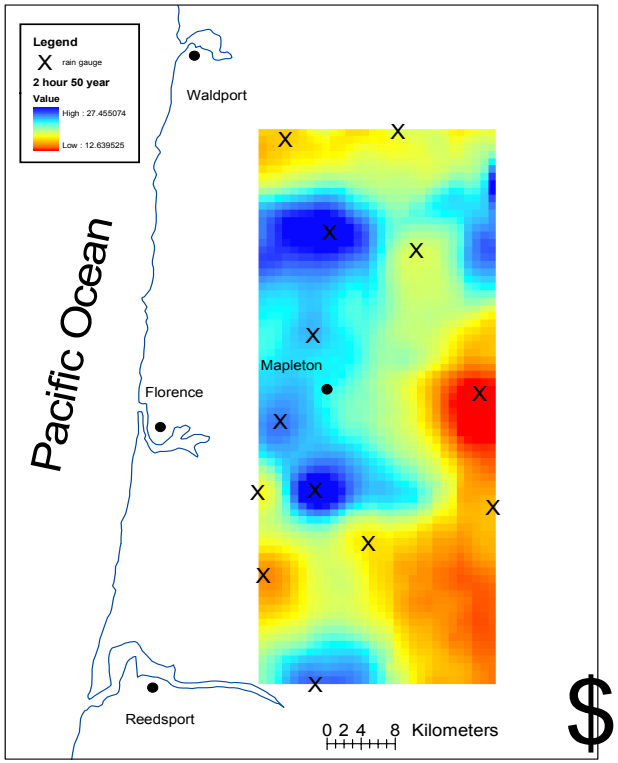

Figure E27. Isohyetal map of the 50-year return period, 2-hour rainfall intensity (mm/hr).

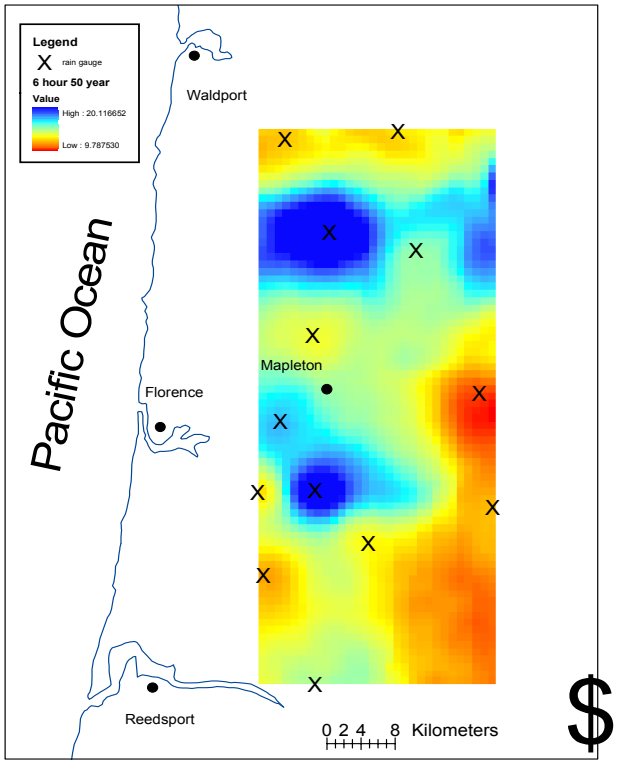

Figure E28. Isohyetal map of the 50-year return period, 6-hour rainfall intensity (mm/hr).

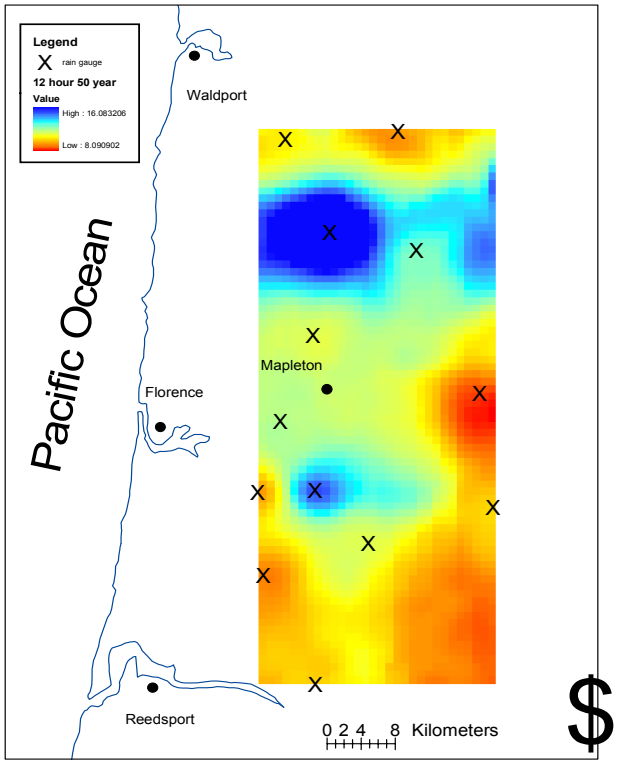

Figure E29. Isohyetal map of the 50-year return period, 12-hour rainfall intensity (mm/hr).

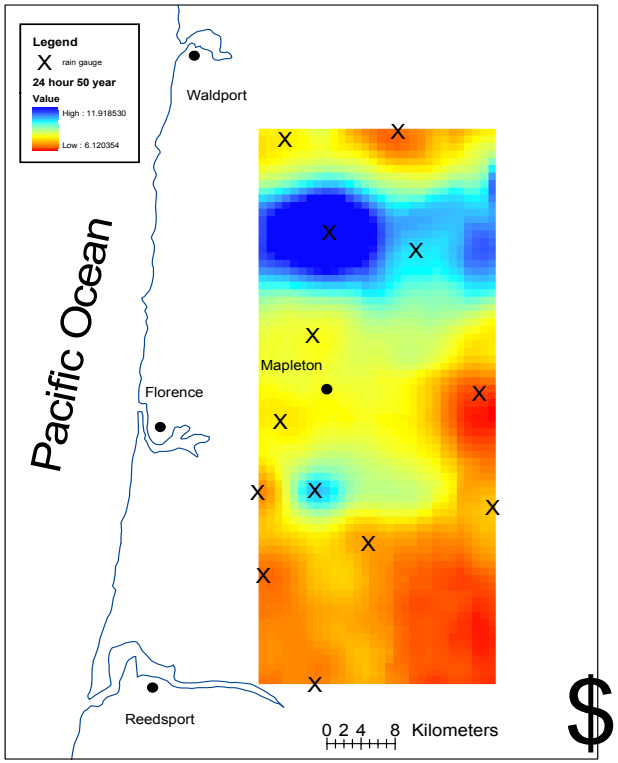

Figure E30. Isohyetal map of the 50-year return period, 24-hour rainfall intensity (mm/hr).

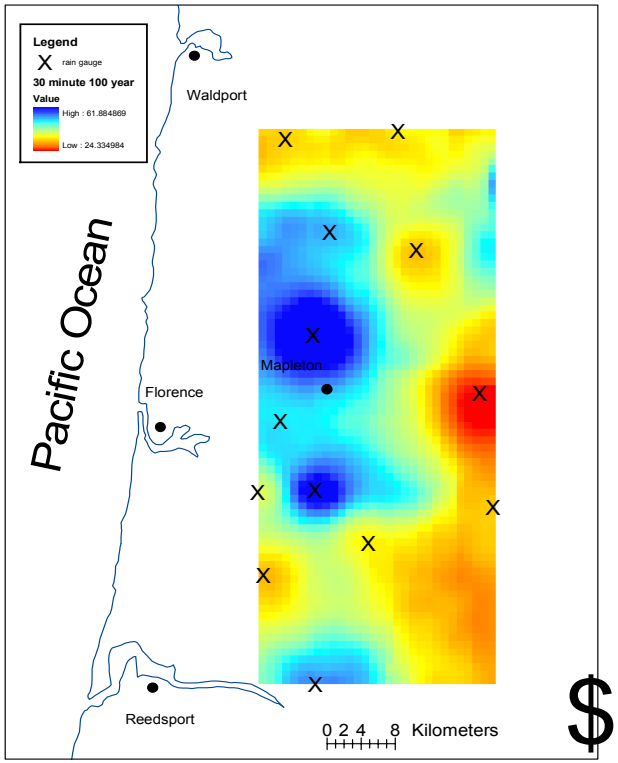

Figure E31. Isohyetal map of the 100-year return period, 30-minute rainfall intensity (mm/hr).

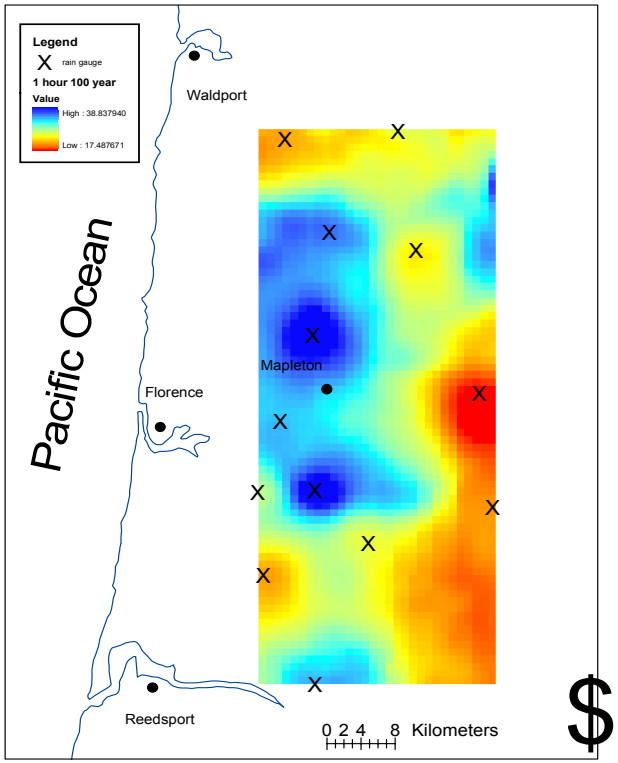

Figure E32. Isohyetal map of the 100-year return period, 1-hour rainfall intensity (mm/hr).

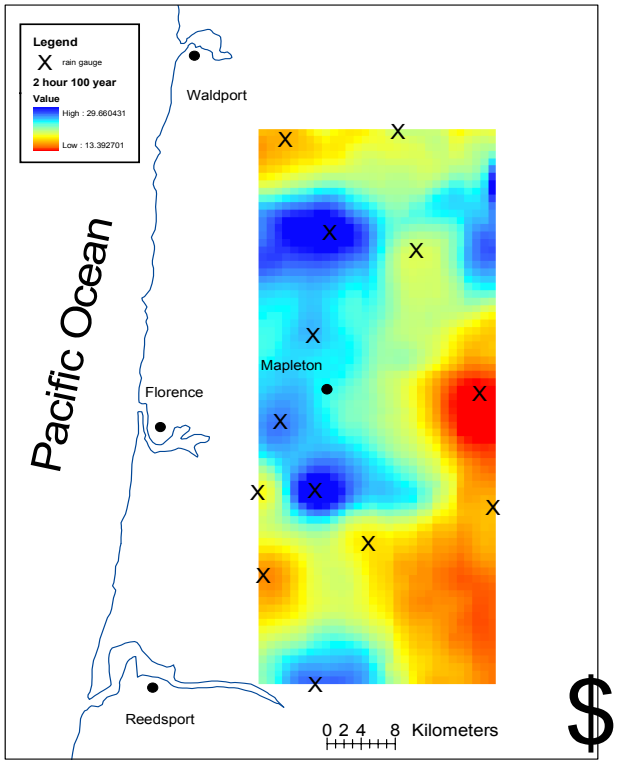

Figure E31. Isohyetal map of the 100-year return period, 2-hour rainfall intensity (mm/hr).

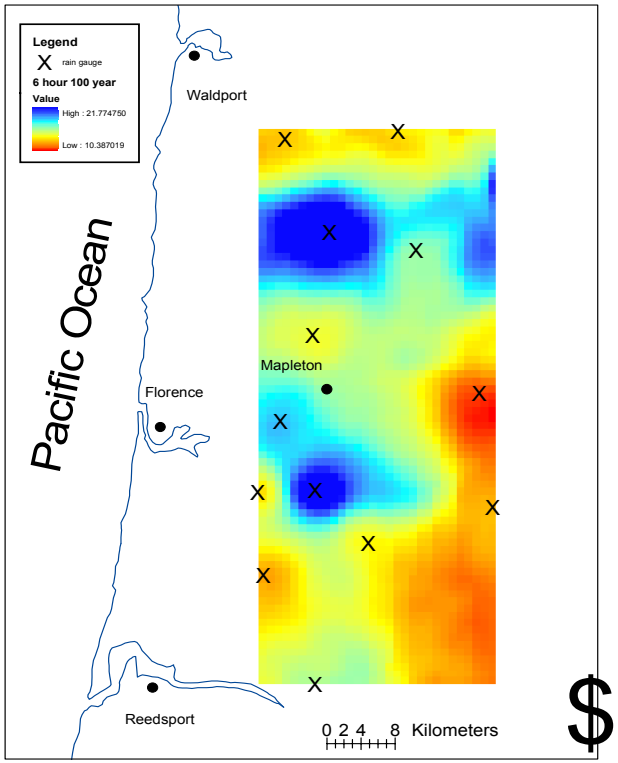

Figure E34. Isohyetal map of the 100-year return period, 6-hour rainfall intensity (mm/hr).

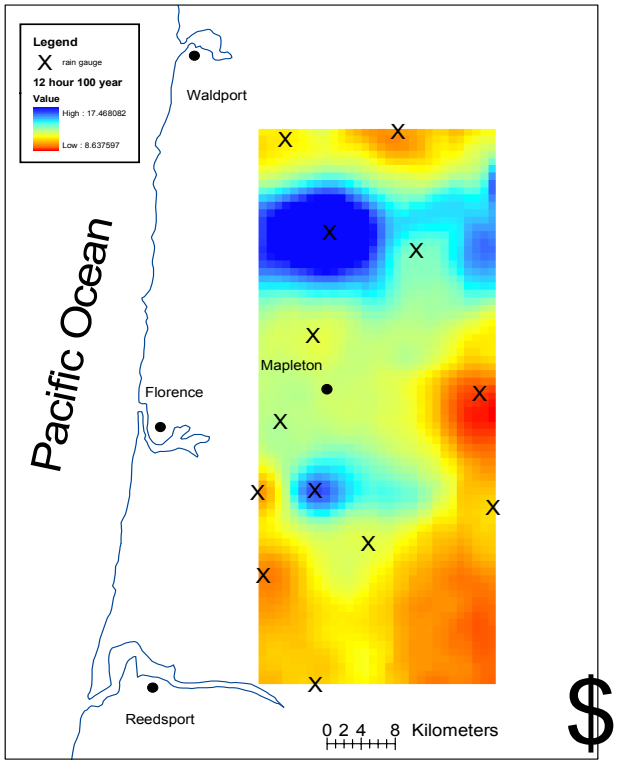

Figure E35. Isohyetal map of the 100-year return period, 12-hour rainfall intensity (mm/hr).

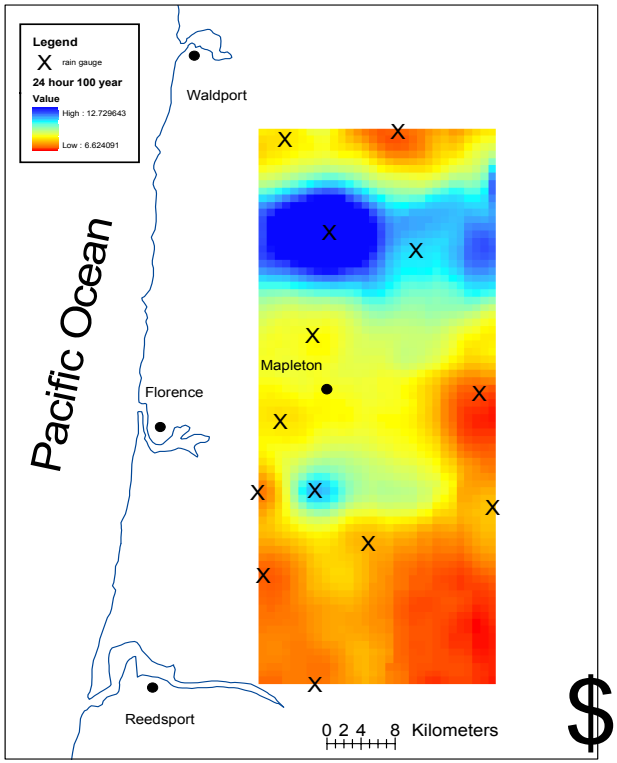

Figure E36. Isohyetal map of the 100-year return period, 24-hour rainfall intensity (mm/hr).

APPENDIX F. Isohyetal Maps for Antecedent Precipitation Index

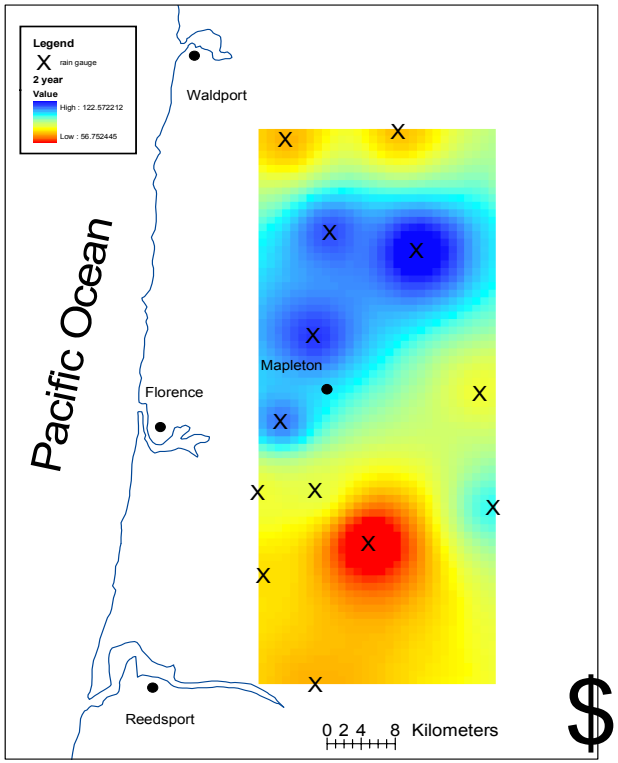

Figure F1. Isohyetal map of the 2-year return period for the antecedent precipitation index (mm).

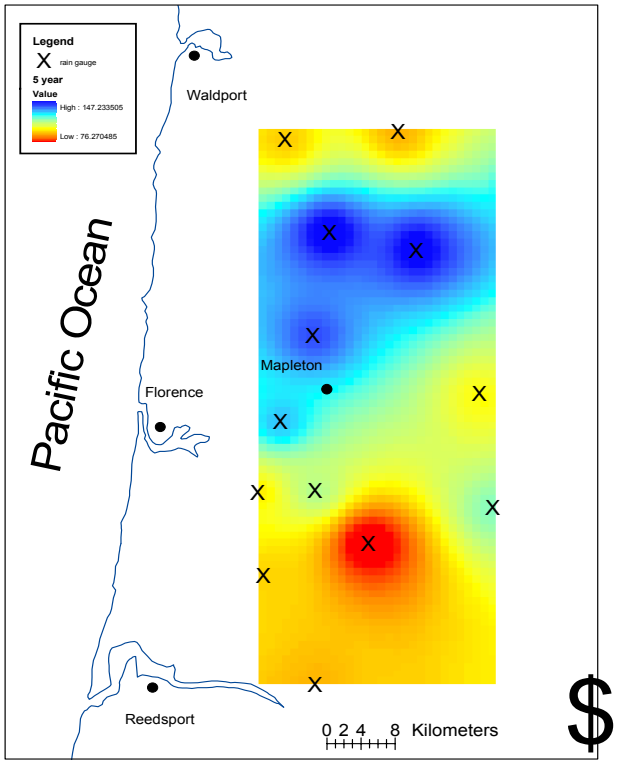

Figure F2. Isohyetal map of the 5-year return period for the antecedent precipitation index (mm).

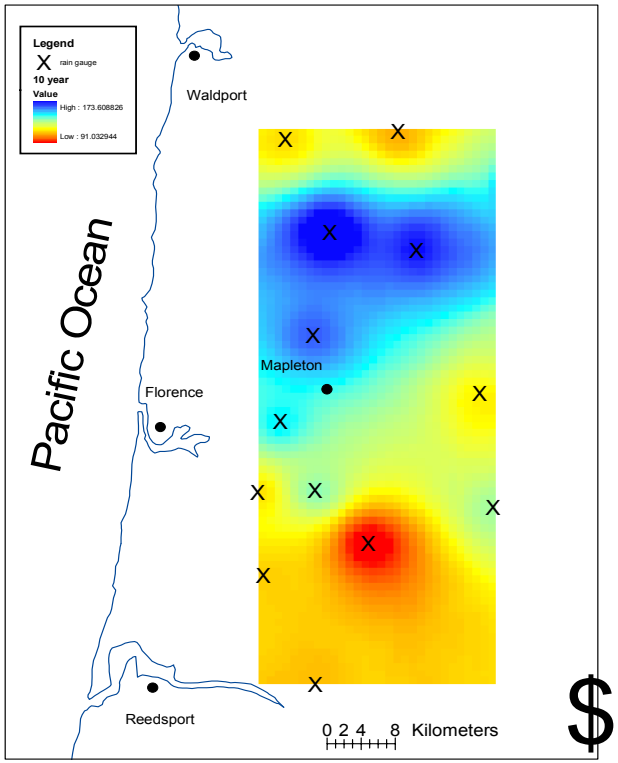

Figure F3. Isohyetal map of the 10-year return period for the antecedent precipitation index (mm).

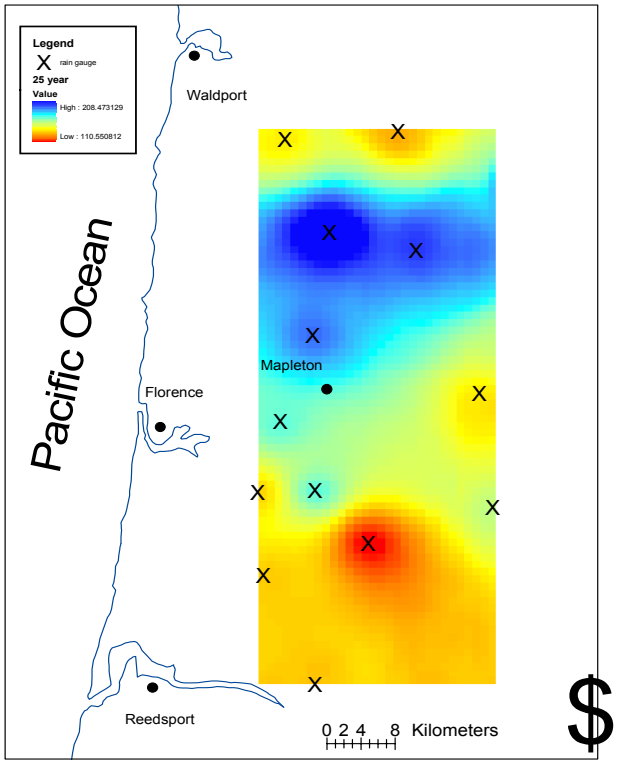

Figure F4. Isohyetal map of the 25-year return period for the antecedent precipitation index (mm).

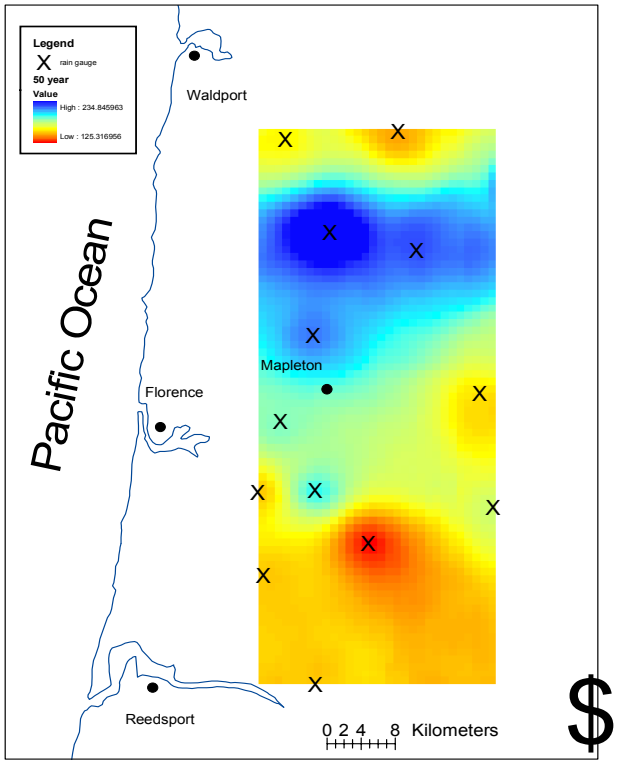

Figure F5. Isohyetal map of the 50-year return period for the antecedent precipitation index (mm).

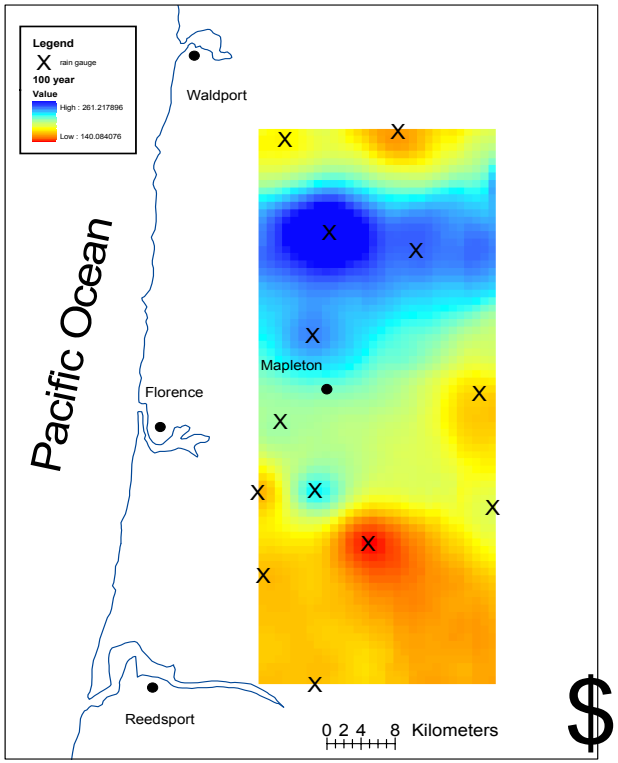

Figure F6. Isohyetal map of the 100-year return period for the antecedent precipitation index (mm).